UAB
Universitat Autònoma de Barcelona

Targeting aldehyde dehydrogenases in combined therapy against glioblastoma

RAFAEL JIMÉNEZ AGUILAR

Universitat Autònoma de Barcelona

Targeting aldehyde dehydrogenases in combined therapy against glioblastoma

Memòria presentada per

RAFAEL JIMÉNEZ AGUILAR

per optar al Grau de Doctor en Bioquímica, Biologia Molecular i Biomedicina

Treball realitzat al Departament de Bioquímica i Biologia Molecular de la Universitat Autònoma de Barcelona, sota la direcció dels Doctors

JAUME FARRÉS VICÉN, JULIA LORENZO RIVERA I RAQUEL PEQUERUL PAVÓN

Bellaterra, 02 de juny de 2023

AGRADECIMIENTOS

En primer lugar, me gustaría dar las gracias a mis directores de tesis, Jaume Farrés, Julia Lorenzo y Raquel Pequerul, por brindarme la oportunidad de realizar mi tesis doctoral en su grupo de investigación, por prestarme su ayuda siempre que lo he necesitado y guiarme durante todo el camino. También, por supuesto, a Xavier Parés, por estar siempre ahí para darme consejos, y por confiar en mí y hacer que pudiese entrar en el grupo desde el máster. Muchas gracias a los cuatro por vuestra cercanía, por vuestras sabias y buenas palabras, y por la experiencia tan enriquecedora que he podido vivir aquí.

Quiero agradecer también a Ana Paula Candiota, por su valiosa ayuda en todos mis experimentos *in vivo*, además de a Josep Antoni Biosca y Fernando Novio, que, junto a ella, han formado mi comisión de seguimiento, evaluando mi progreso a lo largo de estos años. Gracias en especial a Biosca por, además, compartir conmigo las prácticas de Biocatálisis, ayudarme en todo lo que hiciera falta y tener siempre buenas palabras para mí. Tampoco me olvido del resto de compañeros del departamento, que han hecho que todo este tiempo me sienta como en casa: Alicia, Inma, Esther, Mohammed, Irantzu, Pep Vendrell, Chari, Natàlia, Marc Torrent, Jordi Moreno y Salva; los técnicos, Helena, Santi y Magda, no sé qué haríamos sin vosotros, y en especial, gracias Helena por prepararme tantos geles y reactivos, por tener siempre ese trato tan cercano y hacer que me sienta casi como un hijo; Juan Carlos y Silvia, gracias por todas las gestiones administrativas y tramitar tantos pedidos con tanta eficiencia, sois siempre de gran ayuda. Y los demás doctorandos, gracias por la complicidad, los favores y el buen ambiente que se respira entre nosotros: Dani, Marta y Jordi, de DNAs; Guillem, Raúl, Li y Lu, de Ribos; Pilar, Shuang y Lucía, de RMNs; Francisca, Samu, Jaime, Jordi, Marc y Zoe, de PROs; Jofre, de SELFIEs; Gabri, Alejandro y Paula, de PFs; Núria, Valen, Daniel y Roberto, de SysBio. Especialmente, me gustaría agradecer a Dani y a Jofre por el buen rollo entre nosotros en la sala de cultivos, por ser comprensivos cuando acaparaba con la cabina de seguridad biológica 2 y que nunca hubiese problemas para repartírnosla; a Marta y Francisca por ser las compañeras de prácticas más perfeccionistas y comprometidas que he podido tener; y a Pilar, por ayudarme desinteresadamente con mis experimentos con ratones, te estoy muy agradecido y aprendí mucho de ti. También quiero dar las gracias por ello a Marta y a Paula, del grupo de Enzimo del IBB, así como al resto del grupo: David, Eddi, Pau, Sergi Montané y Sergi Rodríguez. Gracias de verdad a todos vosotros por echarme un cable en literalmente cualquier cosa que necesitaba, y también por invitarme de vez en cuando a tomar algo para desconectar. En concreto, Paula, me gustaría decirte lo importante que has sido para mí, aunque ya lo sabes. Más allá de las increíbles

coincidencias entre nosotros (los dos somos de Menorca, tenemos hermanos mellizos casi idénticos a nosotros, que curiosamente están los dos en Bilbao), eres la primera persona sin contar familiares con la que he compartido piso (aún recuerdo cuando se nos cerró la puerta del piso con las llaves dentro el día que viniste a instalarte, los dos esperando sentados en el suelo del rellano a que viniera el cerrajero, con todas las cajas por en medio…), eres una persona encantadora, lista, trabajadora… Ya te lo he dicho en alguna ocasión, pero me pareces una chica 10. Me alegro mucho de haberte encontrado aquí, porque me llevo a una gran amiga. Noto complicidad contigo, por todo lo que nos une, y creo que podemos contar el uno con el otro para lo que sea. Te tengo un cariño especial, que creo que durará por siempre.

Sobre todo, quiero agradecer a todos los que han pasado por mi grupo, los ADHs, porque sois las personas con las que he compartido mi día a día durante esta etapa, y he tenido la suerte de que sois todos estupendos. Nuestros estudiantes de prácticas, Bea, Maria, Jan y Anna, valéis oro, estoy seguro de que os irá genial en cualquier sitio porque podéis con todo lo que os echen. Maria, gracias por descubrirme el Croq & Roll, por ir viéndonos de vez en cuando y por compartir conversaciones tan interesantes y agradables. Me encanta tenerte ahí como amiga. Nuestros estudiantes de estancia, Vito, Viola, Till, Alessandra y Bet, sois de esa clase de personas que transmiten buen rollo y energía positiva, un poco alocadas en el buen sentido, con humor y, además, cercanos y muy trabajadores. Fuisteis un soplo de aire fresco para el grupo. Gracias por las quedadas y las risas. Alessandra, he conocido a pocas personas más currantes y perfeccionistas. Gracias por tu genial compañía en la época en la que más solo estaba en el laboratorio. Bet, a día de hoy, los calcetines de flamencos que me regalaste siguen siendo mis preferidos. Gracias por ser como eres, y por "inspirarme" a hacer cosas que nunca pensé que me atrevería a hacer y que me han dado vidilla (tú ya me entiendes). Nuestras estudiantes de máster del año pasado, Laura Costa (paisana mía) y Daniela, sois un ejemplo de constancia y trabajo bien hecho. Cualquier grupo de investigación sería afortunado de teneros como parte de su equipo, sois muy buenas las dos, y estoy contento de que hayáis podido empezar vuestro doctorado. Me alegro mucho de poder llamaros amigas y de haber encontrado la confianza en vosotras para desahogarme de mis cosas. Sé que seguiremos en contacto siempre. Nuestros estudiantes de máster de este año, Laura Torres y Tarik, sé que vuestros proyectos no están siendo fáciles, pero estoy seguro de que podéis con cualquier cosa, porque tenéis buena mano, y que lo acabaréis sacando con nota. ¡Mucho ánimo a los dos en esta recta final! Y por último, Raquel, la que ha sido mi directora, compañera, psicóloga y amiga durante los últimos casi 6 años. La única constante en el laboratorio durante toda mi etapa de doctorado. Desde que llegué, hemos sido siempre ella y yo. Recuerdo que al poco de llegar estaba hablando un día con

Núria, de SysBio, y me dijo: “tú eres el nuevo estudiante de máster que está con Raquel, ¿no? ¡Qué suerte has tenido!” Y confirmo que Núria estaba en lo cierto, he sido muy afortunado.

Raquel, creo que podría escribirte un montón de páginas sólo dándote las gracias a ti, pero intentaré resumirlo. Tengo mucho que agradecerte. Gracias por inculcarme una buena filosofía de trabajo en el laboratorio, por tener siempre los mejores consejos (tanto en lo profesional como en lo personal), por confiar en mí todas las veces que yo no lo hacía y por hacerme crecer en todos los sentidos. No soy el mismo que entró en el grupo hace ya casi 6 años. Siento que he evolucionado mucho, y te lo debo en gran parte a ti. Eres justo el tipo de persona que necesitaba encontrar: una persona muy agradable y muy cercana, siempre comprensiva, perfeccionista, trabajadora y con seguridad en lo que hace. No he podido tener una compañera mejor. Siempre hablo con orgullo de ti, y ya todos los que me conocen, te conocen. Nunca tendré malas palabras para ti. Eres el motivo por el que, después de mis viajes a Menorca por vacaciones, tenía siempre ganas de volver al laboratorio. Cuando me pasaba algo, o estaba frustrado o triste, y me sentía solo, sabía que podía contártelo, que me escucharías y que me sentiría mejor después. Gracias por saber siempre qué decirme y cómo animarme. En estos años he pasado por algunos de los cambios más importantes en mi vida a nivel personal, y te agradezco mucho que hayas estado ahí para poder confiártelos y apoyarme. Tú también has pasado por momentos muy importantes en tu vida en este tiempo, y me alegro mucho por todo lo bueno que te ha pasado, te lo mereces. Estoy muy contento de que hayas podido formar esa familia tan bonita con Víctor y Kai. En resumen, mil gracias, porque me has llenado de confianza y me has dado alas. No sé adónde me llevarán, pero ya formarás parte de mí siempre.

Otras personas externas al departamento a las que me gustaría dar las gracias son todo el personal del SCAC, en especial a Fran y a Olga, por enseñarme tan bien a trabajar con cultivos celulares y por ser siempre tan majos. Y no puedo dejar de dar las gracias tampoco a Mileidys, por acogerme con tanta amabilidad en ABD durante mi estancia en Lyon, así como al resto de la empresa: Ismail, Guillaume, Patricia, Andrada, Muhube, Narimane, María, Mathieu, Morgane, Alice, Tchikakpa y Laurent. Estuve muy a gusto con vosotros, me encantó la experiencia.

Por último, me gustaría agradecer a mi familia, en especial a mis padres y a mi hermano Dani, por haber sido sin duda un pilar fundamental para mí. Gracias por vivir desde fuera toda esta experiencia conmigo, por darme ánimos a todas horas, por escucharme siempre que lo he necesitado y, en definitiva, por apoyarme siempre incondicionalmente. Nunca lo digo, pero os quiero mucho. Dani, me ha ayudado mucho que hayamos hecho el doctorado en paralelo, aunque en cosas totalmente distintas, y hayamos podido contarnos en cualquier momento lo

que sea, compartir lo bueno y lo malo… Como siempre hemos hecho y seguiremos haciendo. También quiero dar las gracias a mi prima Lucía, por ir encontrando findes sueltos para vernos y poder desconectar. Cada vez que nos juntamos, vivimos una nueva anécdota para recordar (la noche del Drinkin' no se me olvidará nunca). Contigo siempre me lo paso genial, desde que éramos pequeños, y espero que sigamos manteniendo esta relación tan guay toda la vida. Además, quiero agradecer a mi grupo de amigos de Menorca, Júlia, Alba, Elena, Ramiro, Germán, Aida, Laura, Mare, Amanda, Dani Febrer… Aunque ya nos veamos menos por la distancia y por tener cada uno nuestras vidas independientes, me alegra que sigamos quedando de vez en cuando y que el vínculo siga estando después de tantísimos años; a mis amigas de la carrera, Sara y Alba, porque de verdad creo que es difícil encontrar a personas tan buenas como vosotras, y las quedadas con gente así siempre son un buen plan, y también a Aida Carreño, por todas las veces que nos hemos cruzado por el campus y hemos podido ponernos al día de nuestras tesis y darnos ánimos mutuamente. Y para terminar, gracias también a los amigos más recientes que he hecho aquí, en Barcelona: Albert, gracias por mostrar siempre tanto interés en lo que hago, te irá muy bien en todo lo que te propongas porque a esfuerzo y talento en lo tuyo no te gana nadie; Toni, gracias por descubrirme sitios tan guays para ir a comer y por compartir conmigo ese lado "gamer"; y Carlos (Celemé), gracias por ser mi confidente en literalmente todo durante este último año, por compartir conmigo esa pasión por la música, y, en general, por haberte convertido en tan poco tiempo en una de las personas más importantes para mí (la verdad, ya no sé qué haría sin ti).

Muchas gracias a todos. De una manera u otra, me habéis ayudado un montón en esta etapa de mi vida. No hubiera sido lo mismo sin vosotros.

Targeting aldehyde dehydrogenases in combined therapy against glioblastoma

Rafael Jiménez Aguilar

Abstract

Glioblastoma (GB) is the most common and aggressive type of primary malignant central nervous system (CNS) tumor. This disease is still incurable nowadays, with few therapeutic options and poor advances in the last decades. Difficulties in developing an effective treatment against GB reside, among others, on its high degree of infiltration in the brain parenchyma, its high heterogeneity and, remarkably, resistance to chemotherapy such as temozolomide (TMZ), the standard chemotherapeutic agent used currently. Recently, some enzymes belonging to the superfamily of aldehyde dehydrogenases (ALDHs) have been reported to be deeply involved in the mechanisms of chemoresistance and in the regulation of the so-called cancer stem cell (CSC) subpopulation of the tumor, thought to be the main responsible for tumor recurrence. In fact, some ALDH isoforms have been found overexpressed in CSCs and are considered universal markers for their identification and isolation. These enzymes play a key role in the detoxification of aldehydes, participate in the regulation of a broad spectrum of biological processes such as proliferation, differentiation and apoptosis via production of retinoic acid (RA), are known to interact with several oncogenic pathways and in the immune microenvironment of CSCs, and are reported to contribute to resistance to antineoplastic drugs and radiation. Because of this, ALDHs are arising as promising pharmacological targets for the treatment of different cancer types, including GB. Some ALDH inhibitors have been recently described in the literature as potential drugs for cancer treatment, with encouraging results in pre-clinical stages of research. In the case of GB, few examples can be found. In this thesis, some novel compounds, synthesized by the biotechnology company Advanced BioDesign (ABD) and previously shown to be ALDH inhibitors, have been studied as potential candidates for the treatment of GB. These compounds are three α,β-acetylenic amino thiolester compounds named DIMATE, ABD0099 and ABD0171, and a lipidic nanoemulsion of DIMATE named ABD-3001.

The experiments carried out in this thesis can be classified in three different blocks: characterization of ABD-3001 nanoparticles, *in vitro* studies in a panel of GB cell lines, and *in vivo* studies in a murine model of GB. In the first block, ABD-3001 nanoparticles were characterized

by cryogenic transmission electron microscopy (Cryo-TEM) to assess their shape and size, and then, analyzed by dynamic light scattering (DLS) to determine their diameter, polydispersity index (PdI) and zeta potential in solution. In addition, the release of the drug DIMATE from the nanoparticles was characterized. In the second block, firstly, the expression of ALDH1A isoforms was assessed in a panel of different human GB cell lines and a murine GB cell line. Then, inhibitors were tested for their cytotoxicity and their ability to inhibit the cellular ALDH activity. Drug combination assays with the standard of care TMZ were also performed, as well as experiments to determine the cell death mechanism and generation of reactive oxygen species (ROS) after treatment. In the final part of this block, a knockout of several ALDH genes was carried out in one of the human GB cell lines, which allowed us to study the role of these enzymes in some important features such as cell proliferation, migration capacity and resistance to different FDA-approved drugs. In the third block, tolerability and therapeutic efficacy assays were carried out in a murine immunocompetent GL261 GB model, using ABD-3001 at different doses administered via intranasal route, in order to assess toxicity and antitumor effect of the drug. Then, tissues of treated mice were analyzed in order to study the biodistribution of the drug and in order to detect changes in the expression of ALDHs compared to tissues of untreated mice.

The compounds tested in this thesis yielded promising results *in vitro*, since they displayed a high cytotoxicity in a panel of GB cell lines (three orders of magnitude more potent than TMZ), were able to inhibit the cellular ALDH activity, showed synergy when combined with TMZ, and induced apoptosis presumably via accumulation of ROS in the cell. Additionally, the idea of inhibiting ALDHs as a promising approach for the treatment of GB was reinforced by the results obtained in the knockout cell line. Specifically, knockout of ALDH genes in A172 cells reduced their growth rate *in vitro*, hampered their migration capacity, and sensitized them to some FDA-approved drugs, including the standard of care TMZ. Regarding the *in vivo* assays, ABD-3001 showed great potential as a therapeutic agent against GB, since it was able to slow down the growth rate of the tumor in GB-bearing mice and lengthen their lifespan compared to untreated mice, despite displaying certain toxicity that could be solved by lowering the dose of administered drug. In addition, the treatment with ABD-3001 induced some changes in the ALDH expression pattern of several tissues. Altogether, the results obtained suggest that the use of ALDH inhibitors could be an encouraging novel approach for the treatment of GB, either as monotherapy or in combination with the standard of care TMZ.

CONTENTS

TABLE LIST

FIGURE LIST

ABBREVIATIONS

ABC	ATP-binding cassette
ABD	Advanced BioDesign
ADH	Alcohol dehydrogenase
AIC	5-aminoimidazole-4-carboxamide
AKR	Aldo-keto reductase
Akt	Protein kinase B
ALDH	Aldehyde dehydrogenase
AML	Acute myeloid leukemia
AOX	Aldehyde oxidase
ATP	Adenosine triphosphate
ATRX	Alpha-thalassemia/mental retardation, X-linked
BAA$^-$	BODIPY-aminoacetate
BAAA	BODIPY-aminoacetaldehyde
BBB	Blood-brain barrier
BCNU	Carmustine
CAT	Catalase
CDKN2A/B	Cyclin-dependent kinase inhibitor 2A/B
CNS	Central nervous system
CP	Cisplatin
CRISPR/Cas9	Clustered regularly interspaced short palindromic repeats/associated protein 9
Cryo-TEM	Cryogenic transmission electron microscopy
CSC	Cancer stem cell
DCFDA	2',7'-dichlorofluorescin diacetate
DEAB	*N*,*N*-diethylaminobenzaldehyde
DIMATE	4-dimethylamino-4-methyl-pent-2-ynthioic acid S-methyl ester
DLS	Dynamic light scattering
DMEM	Dulbecco's modified Eagle's medium
EGFR	Epidermal growth factor receptor
EMT	Epithelial-to-mesenchymal transition

ERK	Extracellular signal-regulated kinase
ETL	Echo train length
ETP	Etoposide
FBS	Fetal bovine serum
FLAIR	Fluid-attenuated inversion recovery
FOV	Field of view
FPLC	Fast protein liquid chromatography
GB	Glioblastoma
GSC	Glioblastoma stem cell
GSH	Reduced glutathione
HNE	Hydroxynonenal
HPLC	High performance liquid chromatography
IDH	Isocitrate dehydrogenase
MAPK	Mitogen-activated protein kinase
MDA	Malondialdehyde
Mdm2	Murine double minute 2 homolog
MDR	Multidrug resistance protein
MGMT	O^6-methylguanine-DNA methyl transferase
MMR	Mismatch repair
M-PER	Mammalian protein extraction reagent
MRI	Magnetic resonance imaging
MTIC	Monomethyl triazene 5-(3-methyltriazene-1-yl)-imidazole-4-carboxamide
mTOR	Mammalian target of rapamycin
NA	Number of averages
NAD^+	Nicotinamide adenine dinucleotide (oxidized)
NADH	Nicotinamide adenine dinucleotide (reduced)
NSCLC	Non-small cell lung cancer
PBS	Phosphate-buffered saline
PdI	Polydispersity index
PI3K	Phosphatidylinositol 3-kinase
PTEN	Phosphatase and tensin homolog

RA	Retinoic acid
RAL	Retinaldehyde
RAR	Retinoic acid receptor
RARE	Retinoic acid response element
ROI	Region of interest
ROS	Reactive oxygen species
RTK	Receptor tyrosine kinase
RXR	Retinoic X receptor
SDR	Short-chain dehydrogenase/reductase
SDS-PAGE	Sodium dodecyl sulfate-polyacrylamide gel electrophoresis
SphK	Sphingosine kinase
ST	Slice thickness
TAT	Total acquisition time
TEeff	Effective echo time
TERT	Telomerase reverse transcriptase
TFA	Trifluoroacetic acid
TMZ	Temozolomide
TP53	Tumor protein 53
T-PER	Tissue protein extraction reagent
TR	Repetition time
Tregs	Regulatory T cells
TTF	Tumor-treating field
WHO	World Health Organization
XO	Xanthine oxidase

INTRODUCTION

1.1. Glioblastoma

1.1.1. What is glioblastoma?

Cancer is one of the leading causes of death worldwide. In 2020, it accounted for nearly 10 million deaths globally, and an estimated 19.3 million new cases were diagnosed. Compared to other types of cancer, central nervous system (CNS) cancers are relatively rare: they represent between 1 and 2% of all cancer types, being the 21st most common malignancy. In absolute numbers, cancers of the CNS are responsible for nearly 300,000 new cases and 250,000 deaths worldwide annually [1], [2]. Glioblastoma (GB), which is the focus of study of this thesis, belongs to this group of cancers.

Traditionally, CNS tumors have been classified according to morphological features examined in histological specimens [3], but recent knowledge about the molecular characteristics of these tumors has been integrated into a new classification criterion [4]. Based on this, as well as on other aspects with a clinical utility such as tumor location and patient age, the 2021 World Health Organization (WHO) classification categorizes the wide variety of existing CNS tumors into 12 different groups [5], as shown in **Figure 1**. The first of these groups comprises a heterogeneous collection of brain tumors called gliomas, which constitute the most common type of malignant primary CNS tumors in adults [6]. Gliomas are considered to derive from glial cells and/or their precursors [7], [8], and can be either astrocytomas or oligodendrogliomas according to the predominant cell type observed in histological analysis [9]. Within the group of gliomas, glioneuronal tumors, and neuronal tumors, the term “diffuse gliomas” can often be found. Such gliomas are characterized by diffusely infiltrative growth throughout the brain parenchyma [10], ultimately leading to neuronal dysfunction and death [11]. Specifically, adult-type diffuse gliomas account for the majority of primary brain tumors in adults, and can be classified into three different subtypes, including GB.

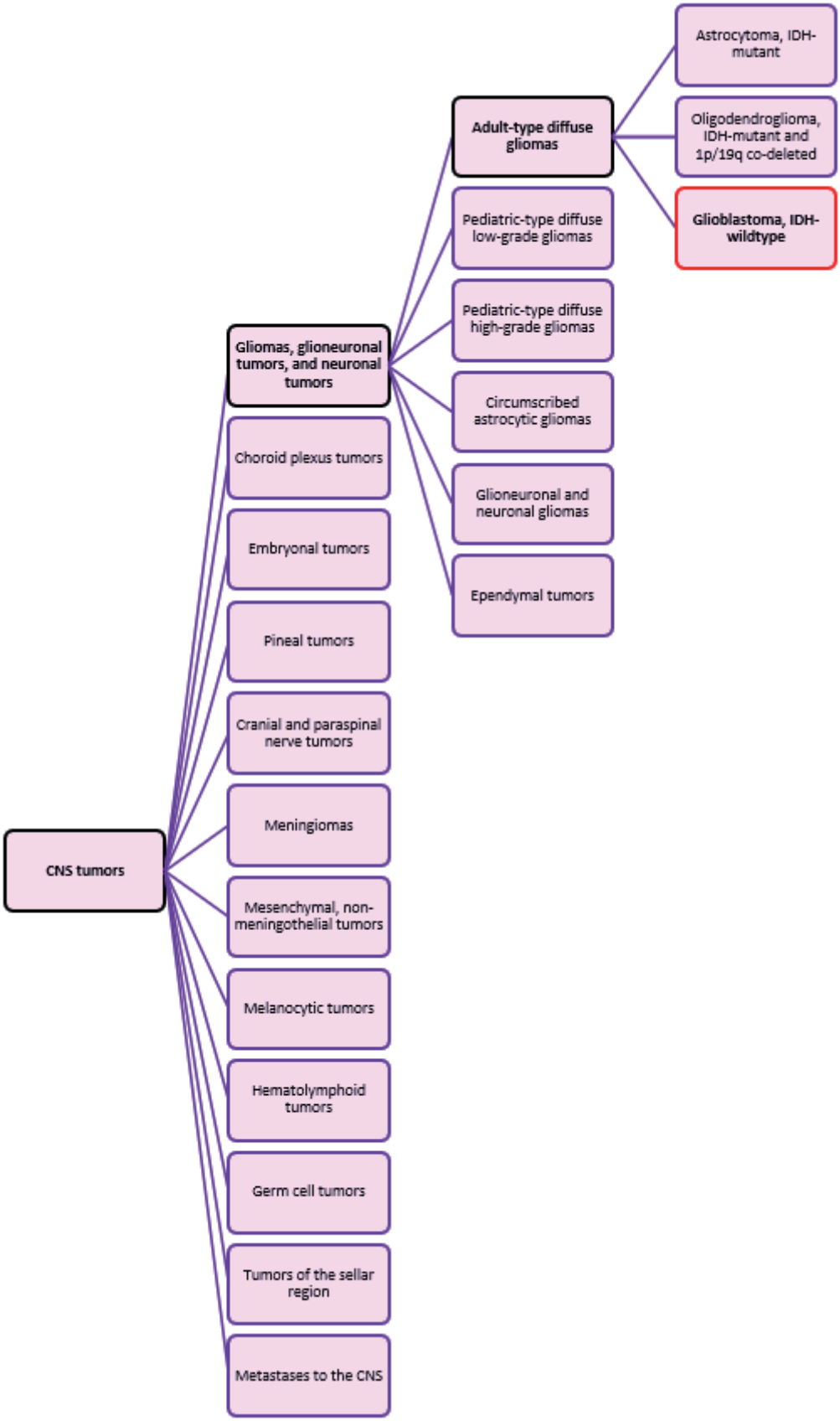

Figure 1. Simplified 2021 WHO classification of CNS tumors. Subtypes of tumor groups beyond the scope of this thesis have been omitted. GB is boxed in red. CNS: central nervous system; IDH: isocitrate dehydrogenase.

The classification criteria for adult-type diffuse gliomas are further detailed in **Figure 2**. This group of gliomas, apart from being categorized as astrocytomas or oligodendrogliomas based on histology as commented above, is distributed in two major categories depending on the presence or absence of mutations in the genes coding for isocitrate dehydrogenases 1 and 2 (IDH1 and IDH2, respectively), being the absence considered to have the worst prognosis [3], [12]. Tumors are then graded on a scale from 1 to 4 based on the degree of malignancy [13], and assigned to one of the 3 following types according to different histological and molecular features [6], [12], [14]: (1) astrocytoma, IDH-mutant; (2) oligodendroglioma, IDH-mutant and 1p/19q co-deleted (that is, concurrent complete deletion of both 1p and 19q chromosomal arms); or (3) GB, IDH-wildtype.

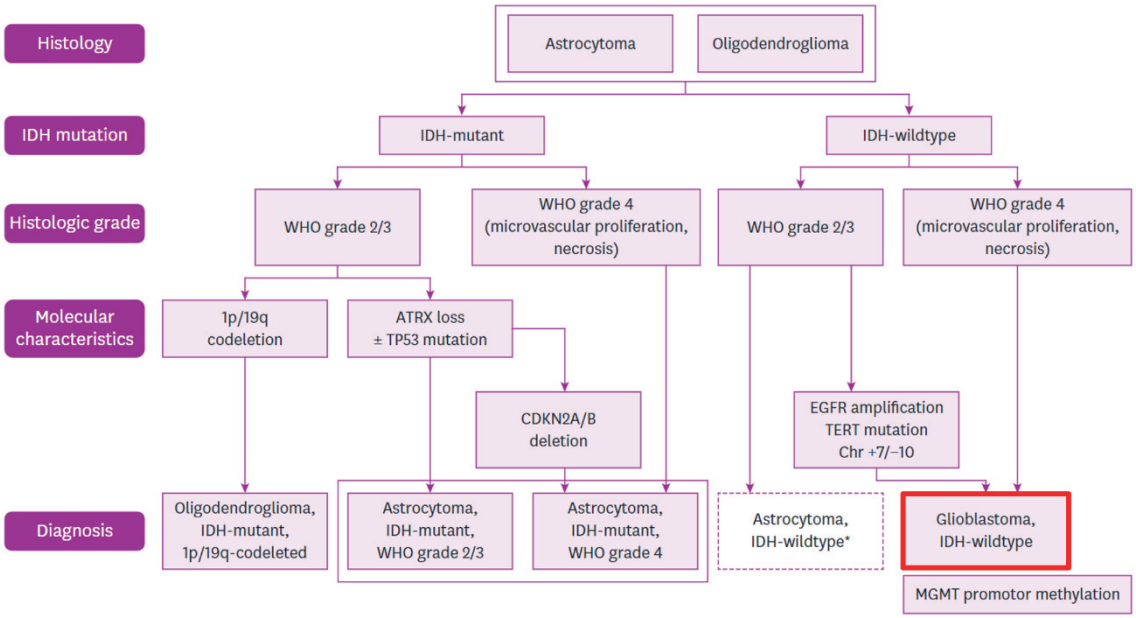

Figure 2. 2021 WHO classification of adult-type diffuse gliomas. GB is boxed in red. IDH: isocitrate dehydrogenase; WHO: World Health Organization; ATRX: alpha-thalassemia/mental retardation, X-linked; TP53: tumor protein 53; CDKN2A/B: cyclin-dependent kinase inhibitor 2A/B; EGFR: epidermal growth factor receptor; TERT: telomerase reverse transcriptase; MGMT: O^6-methylguanine-DNA methyl transferase. Adapted from [6]. *IDH-wildtype glioma without high-grade features (WHO grade 2/3) should be further investigated and classified into other categories.

In accordance with the classification criteria shown in **Figure 2**, GB is a grade 4 diffuse astrocytoma characterized by two main histologic hallmarks: (1) abundant microvascular proliferation, and (2) presence of central necrotic areas [6], [7], [15]. The typical appearances of this type of tumor are shown in **Figure 3**. At the genetic level, GB is defined by these 3 parameters: (1) epidermal growth factor receptor (*EGFR*) amplification, (2) telomerase reverse transcriptase (*TERT*) promoter mutation, and (3) the combined gain of entire chromosome 7 and loss of entire chromosome 10 [6], [16]. In addition, GB is also characterized by uncontrolled cellular proliferation, diffuse infiltration, and resistance to apoptosis-inducing stimuli, all of these enabled by extensive genomic instability [17], [18].

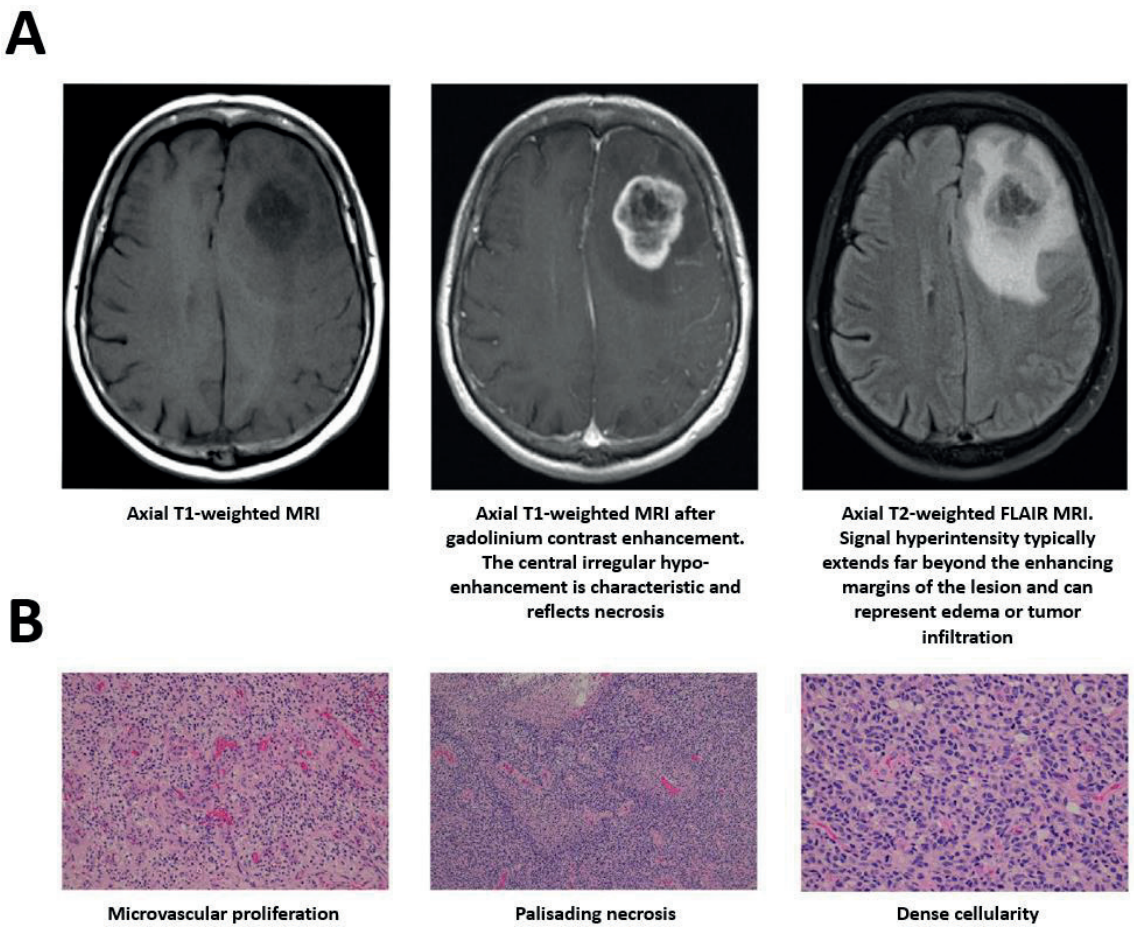

Figure 3. Typical radiographic and histologic appearances of GB. (A) Magnetic resonance imaging (MRI); **(B)** Histology. FLAIR: fluid-attenuated inversion recovery. Adapted from [19].

Another relevant hallmark feature of GB is its marked heterogeneity, not only between tumors of different individuals (intertumoral heterogeneity) but also within the same tumor (intratumoral heterogeneity). This is regarded to be one of the main factors underlying treatment failure [20], [21], a topic that will be discussed in more detail in the following sections of this thesis.

The high degree of molecular heterogeneity in this type of tumor has led to the subclassification of GB into 4 different subtypes [22]–[24]: (1) proneural, which displays features of oligodendroglial cells and appears in younger patients; (2) neural, which arises from astrocytes and oligodendrocytes and expresses neuron-related genes; (3) mesenchymal, which resembles cultured astrocytic gliomas; and (4) classical, which shows characteristics of astrocytes and expresses neuron precursor and stem cell markers.

Altogether, GBs constitute the most common type of malignant gliomas, accounting for nearly 50% of malignant CNS tumors and approximately 15% of all CNS tumors [25]. It is not easy to define precisely the incidence of GB, since it varies depending on the report, but it ranges from

0.59 to 5 cases per 100,000 people and year [26]. According to several studies, the incidence of this disease is currently on the rise, and it is the cause of the majority of the deaths related to tumors of the CNS worldwide each year [27]. Although GB can occur both in children and adults, the median age at diagnosis is 65 years. In addition, it is approximately 1.6 times more common in males than females [28], and its incidence is significantly lower in non-Caucasian populations [6].

Furthermore, GB is not only the most common type of malignant glioma, but also the most aggressive and lethal. This disease remains still incurable with a poor overall prognosis, presenting a 5-year survival rate of only 5%. The median survival averages <15 months since diagnosis [29], which has remained nearly unchanged over the last 50 years [30].

1.1.2. Current treatment for GB and pitfalls

GB treatment remains challenging due to several reasons. Firstly, the presence of the so-called blood-brain barrier (BBB), a multicellular vascular structure that separates the CNS from the peripheral blood circulation and keeps a protective environment for the brain tissue by tightly controlling the passage of molecules [31], limits directly drug bioavailability. In addition, GB tumors in particular present a wide infiltration in the brain parenchyma, are highly heterogeneous both at the genetic and cellular level, are able to evade the immune system and often develop resistance to chemotherapy and radiotherapy. Altogether, all these factors explain why GB is considered one of the most challenging tumor types to treat [9], [32], [33].

The current standard-of-care treatment for GB consists of surgical resection of the tumor, followed by radiotherapy with concomitant daily temozolomide (TMZ) chemotherapy, followed by additional TMZ therapy [34], [35]. This regimen was proven to have a survival benefit on patients in the studies performed by Stupp and colleagues [36]–[38] in 2005, and has remained the gold standard for GB treatment until now.

TMZ is an oral alkylating agent prodrug which is able to penetrate the BBB due to its low molecular weight and lipophilic character. In its passage into the cytoplasm, TMZ is spontaneously hydrolyzed to 5-(3-methyltriazene-1-yl)-imidazole-4-carboxamide (MTIC), which is then further hydrolyzed to the degradation product 5-aminoimidazole-4-carboxamide (AIC) and the active methyldiazonium cation. This highly reactive ion transfers a methyl group to the O^6 and N^7 positions of guanine residues and N^3 position of adenine residues during DNA replication. This leads to mismatched lethal base pairs that result in DNA strand breaks, inducing cell cycle arrest at G2/M and eventually leading to cell apoptosis, senescence or autophagy [39]–[42]. This mechanism of action is depicted in **Figure 4**.

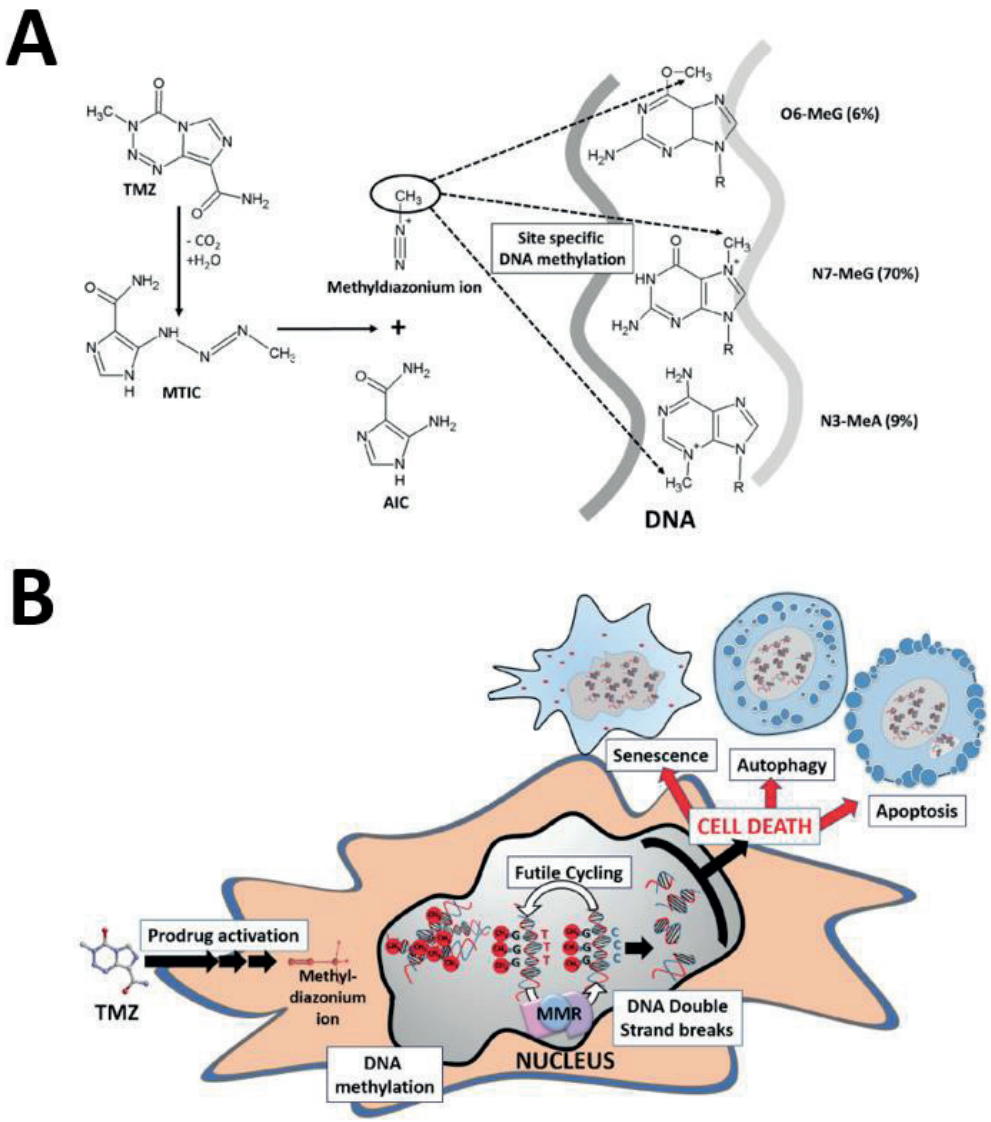

Figure 4. Mechanism of action of TMZ. (A) TMZ prodrug activation and specific sites of DNA methylation; **(B)** Schematic illustration of the action of TMZ in the cell. Guanine, methylated by the TMZ-derived active ion, pairs with thymine instead of cytosine. The DNA repair system MMR detects this mispairing and removes thymine from the newly synthesized strand, but leaves the methylated guanine in the template strand intact. In the next replication cycle, the mismatch occurs again and the repair cycle is repeated. This ends up in a futile cycle of MMR, which leads to the production and accumulation of DNA double-strand breaks. These double-strand breaks are cytotoxic to cells, and induce senescence, autophagy or apoptosis. MMR: mismatch repair. Adapted from [41].

Since GB diffusely infiltrates the brain early in its course (and is often detected late), the main pitfall of the current treatment is that it is nearly impossible to reach complete surgical resection. Then, remaining tumor cells typically develop resistance to TMZ, leading to recurrence and tumor progression [43], [44].

Understanding resistance to TMZ is not straight-forward since it can be either inherently characteristic of certain tumors or acquired after initial treatment [45]. It is widely accepted that the most important contributor to TMZ resistance is the methylation status of the promoter region of the gene encoding the enzyme O^6-methylguanine-DNA methyl transferase (MGMT),

which directly counteracts DNA alkylation damage. Specifically, unmethylated tumors present higher MGMT concentration and commonly exhibit intrinsic resistance to TMZ and a worse clinical response [46]–[48]. However, there are reported cases of patients who suffer from TMZ resistance despite their low MGMT activity, which reveals that MGMT is not the only factor contributing to the development of TMZ resistance [49], [50].

Other DNA-repair systems, such as the base excision repair (BER) pathway, are also known to be important in mediating TMZ resistance [51], [52], as well as other mechanisms such as autophagy [53]–[55], ferroptosis [56]–[58], some unregulated signaling pathways [41], [59], and remarkably, the presence of the so-called GB stem cells (GSCs) [52]. **Figure 5** provides a schematic summary of different mechanisms known to be involved in the development of TMZ resistance in GB.

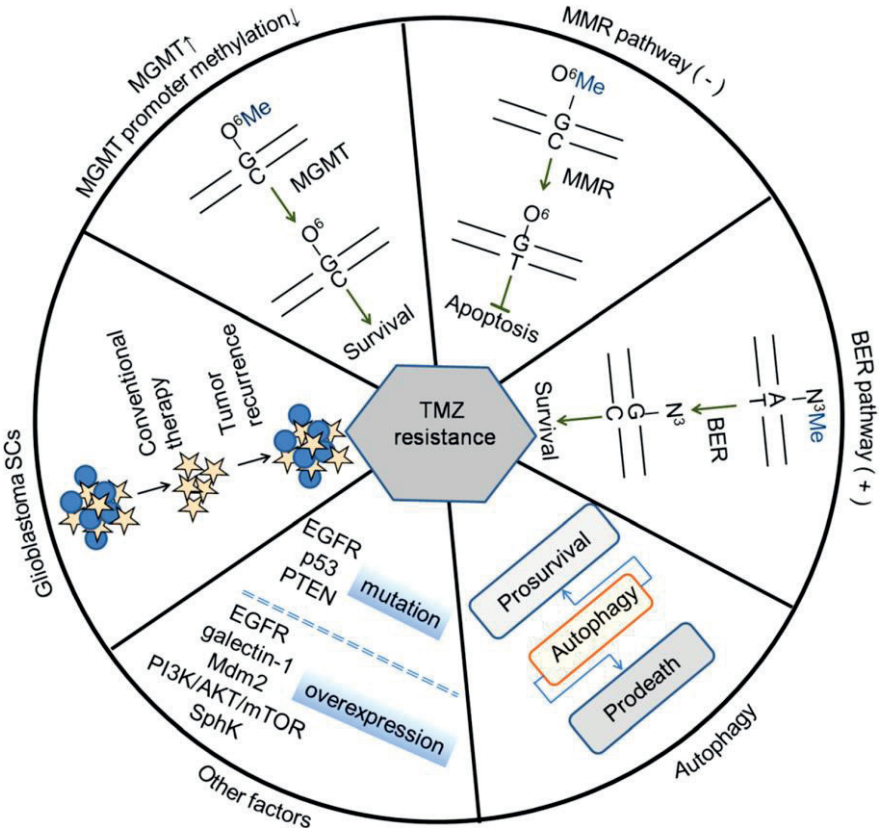

Figure 5. Known mechanisms of TMZ resistance in GB. TMZ: temozolomide; MGMT: O^6-methylguanine-DNA methyl transferase; MMR: mismatch repair; BER: base excision repair; EGFR: epidermal growth factor receptor; PTEN: phosphatase and tensin homolog; Mdm2: murine double minute 2 homolog; PI3K/AKT/mTOR: phosphatidylinositol 3-kinase/protein kinase B/mammalian target of rapamycin; SphK: sphingosine kinase; SCs: stem cells. Taken from [52].

1.1.3. GSCs and general concepts of cancer stem cells

GSCs represent a small subset of undifferentiated cells within a GB tumor, known generally as cancer stem cells (CSCs), which display higher resistance to radiation and chemotherapy than

bulk tumor cells. It is believed that this subpopulation of quiescent, pluripotent, and self-renewing cells is triggered after therapy and is responsible for the repopulation of recurrent GB tumors [50], [60], [61]. These cells are defined by a series of functional criteria, illustrated in **Figure 6**, including: (1) tumor-initiating capacity following serial transplantation, (2) ability to recapitulate the heterogeneity of the primary tumor, and (3) higher self-renewal properties compared with non-CSCs [29], [62].

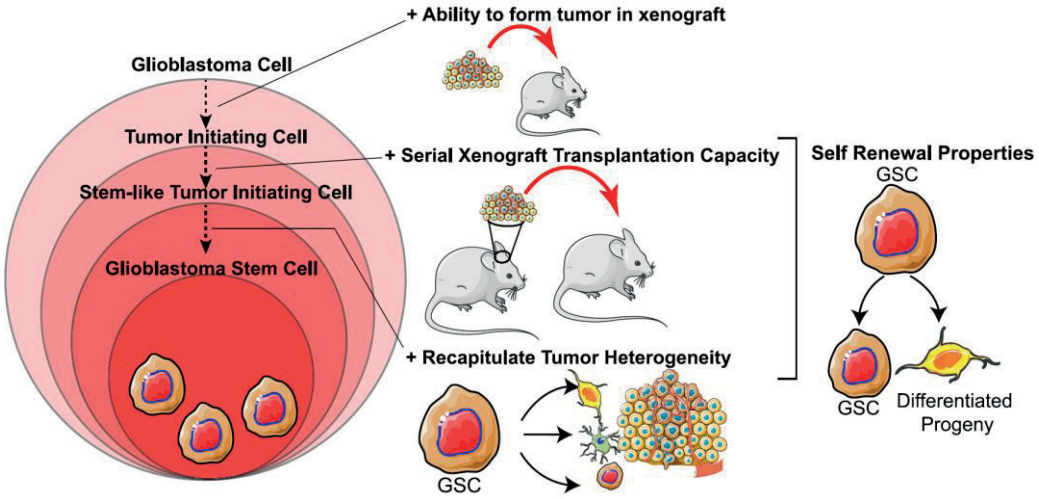

Figure 6. Key functional defining features of GSCs. These cells are able to initiate a tumor in xenografts, even after serial transplantation, recapitulate tumor heterogeneity, and self-renew. GSC: glioblastoma stem cell. Taken from [29].

According to this, the CSC hypothesis of tumor growth proposes the existence of a cellular hierarchy within the tumor, where CSC reside at the apex. These CSCs self-renew, divide and differentiate to give rise to the variety of cells that populate a tumor. Thus, CSCs are thought to be responsible for tumor initiation, propagation and maintenance. As cells differentiate, they lose self-renewal capabilities, but it has recently been demonstrated that this is not an irreversible process: some stimuli, such as hypoxia or exposure to chemotherapeutic agents such as TMZ, can induce the dedifferentiation of non-CSCs to cells with CSC phenotype [63], [64]. Therefore, CSCs have to be thought as plastic and dynamic entities [65], [66].

Conversely, the traditional model of tumor growth, the so-called stochastic model or clonal evolution model, postulates that tumor progression is driven by clonal evolution of acquired genetic mutations, and that many clones display comparable levels of tumorigenicity [63]. Although this model seems at first glance opposite to the hierarchical or CSC model, they are not mutually exclusive. Most likely, the two models co-exist and are complementary in tumorigenesis [67].

A schematic representation of both models of tumor growth is shown in **Figure 7**.

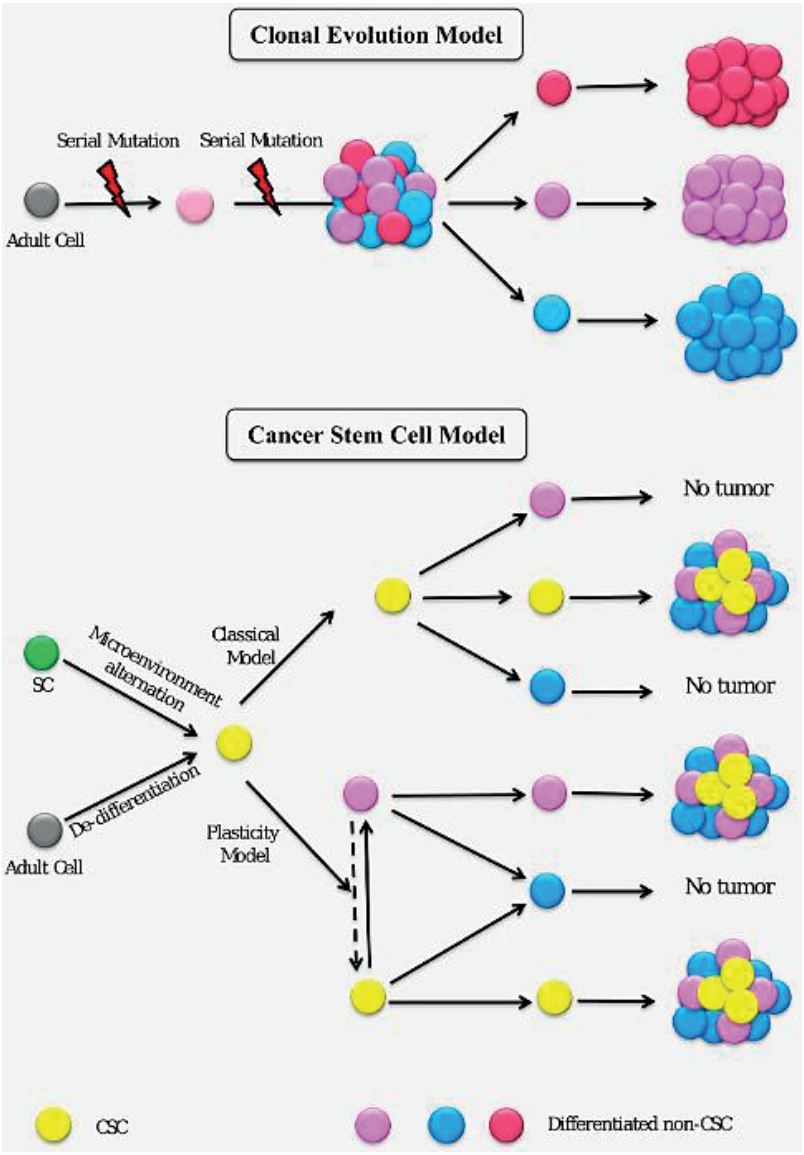

Figure 7. Schematic illustration for the different models of tumor growth. In the clonal evolution model, different clones in the tumor are generated by accumulation of mutations, and all clones have the same capacity of tumor formation. In the CSC model, also known as hierarchical model, only the so-called CSCs are thought to be able to give rise to a tumor, although some non-CSCs can eventually dedifferentiate to a CSC phenotype and thus, could also contribute to tumor formation. SC: stem cell; CSC: cancer stem cell. Taken from [66].

CSCs were described for the first time in leukemia, by Lapidot *et al*., in 1994 [68]. It was not until 2003 when CSCs were identified in solid tumors, specifically in breast cancer by Al-Hajj *et al*. [69]. Since then, CSCs have been detected in a wide variety of tumors including myeloma, colon cancer, pancreatic cancer, prostate cancer, lung cancer, ovarian cancer, melanoma, and GB (initially recognized by Singh *et al*. in 2003 [70]), among others. In most of these cases, some enzymes belonging to the superfamily of aldehyde dehydrogenases (ALDHs) have been found overexpressed in this subpopulation of cells, and their presence has been correlated with worse prognosis [71], [72]. In fact, ALDHs are known to play critical roles also in normal stem cells during development, and are regarded as universal markers for both normal stem cells and CSCs

[73], [74]. Importantly, only specific ALDH isoforms that are expressed at high levels in CSCs compared to the corresponding para-neoplastic tissues can be used as suitable markers. In GB, it is accepted that this is the case for the isoform ALDH1A3, whose high expression has been observed in high-grade gliomas, but not in low-grade gliomas or in normal brain samples [75]–[77].

ALDH activity is commonly used as a biomarker for the isolation of CSCs in the well-known Aldefluor assay, described for the first time in 1999 by Storms *et al*. [78]. Briefly, this assay uses a substrate called BODIPY-aminoacetaldehyde (BAAA), which penetrates viable cells by passive diffusion and is converted by ALDHs to the negatively charged, fluorescent product BODIPY-aminoacetate (BAA^-). BAA^- is retained inside the cells due to its charge and also because of the addition of inhibitors to block the action of ATP-binding cassette (ABC) transporters, which otherwise may pump the product out of the cells [79]. Consequently, the subset of cells with a high ALDH activity becomes highly fluorescent, and can be sorted using the green fluorescence channel of a standard flow cytometer. These ALDH-bright populations of cells can be detected specifically by adding an ALDH inhibitor, namely *N*,*N*-diethylaminobenzaldehyde (DEAB) [74], [80]. A scheme of the Aldefluor assay is shown in **Figure 8**.

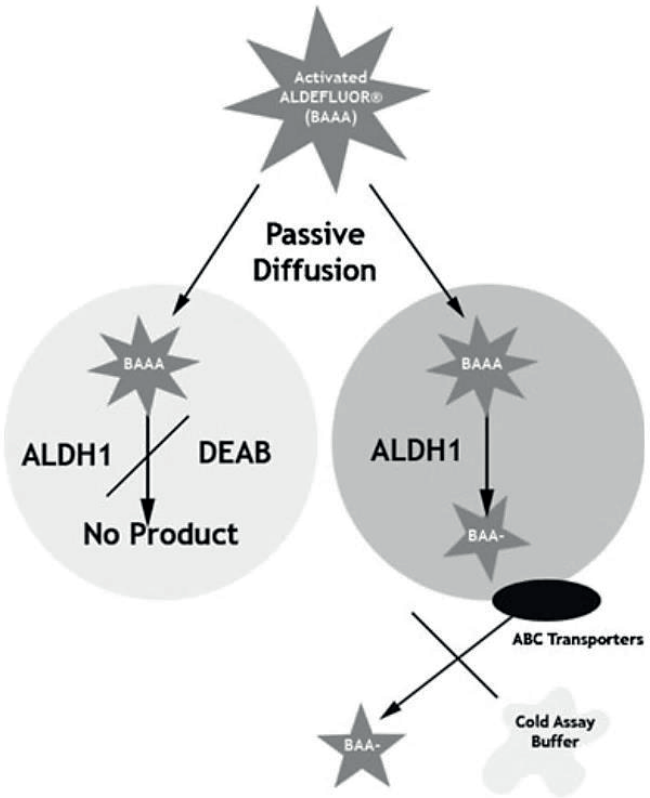

Figure 8. Scheme of the Aldefluor assay, the standard method for the identification and isolation of CSCs. BAAA: BODIPY-aminoacetaldehyde; BAA^-: BODIPY-aminoacetate; ALDH1: aldehyde dehydrogenase family 1; DEAB: *N*,*N*-diethylaminobenzaldehyde; ABC: ATP-binding cassette. Taken from [74].

Although this method has been accepted and is frequently used for the separation of CSC populations of many cancers, at the protein level, the ALDH isoforms responsible for the enzymatic activity are different and cancer-specific. One of the main drawbacks of the Aldefluor assay is that several ALDH isoforms take part in the metabolization of the BAAA substrate, so it does not allow for the identification of specific isoforms responsible for the activity [81]. In addition, the DEAB inhibitor used in this assay is reported to inhibit different ALDH isozymes. Finding the active ALDH isoforms for specific cancers would have major diagnostic and prognostic implications [82]–[87]. Furthermore, that would pave the way for the design of isoform-selective ALDH inhibitors that could serve as therapeutic agents targeting specifically CSCs, since ALDHs have been considered not only markers, but also to play relevant roles in CSC regulation and resistance to chemotherapy and radiotherapy.

As mentioned above, CSCs present higher resistance to therapy compared to the rest of the cells in the tumor. These cells can be either intrinsically resistant to therapy and thus persist after treatment and cause tumor relapse, or extrinsically instructed by the tumor microenvironment to become resistant under the selective pressure of therapy [62]. One of the main mechanisms of intrinsic resistance is the activation of DNA damage checkpoints, which makes CSCs less sensitive to most current therapies targeting DNA replication. Additionally, CSCs are known to be quiescent, maintaining a low but steady level of unlimited proliferation with low activity of DNA synthesis [88]. This explains that these therapies are not that effective in these cells compared to actively dividing cells. Another relevant example of the intrinsic mechanism of resistance is the increased expression of ABC transporters, which facilitate drug efflux [32], [89], [90]. **Figure 9** shows some mechanisms involved in CSC resistance to therapy and consequent relapse of the tumor. Among them, ALDH activity has been shown to be particularly relevant in recent studies, and its role will be discussed in further detail in the following sections of this thesis.

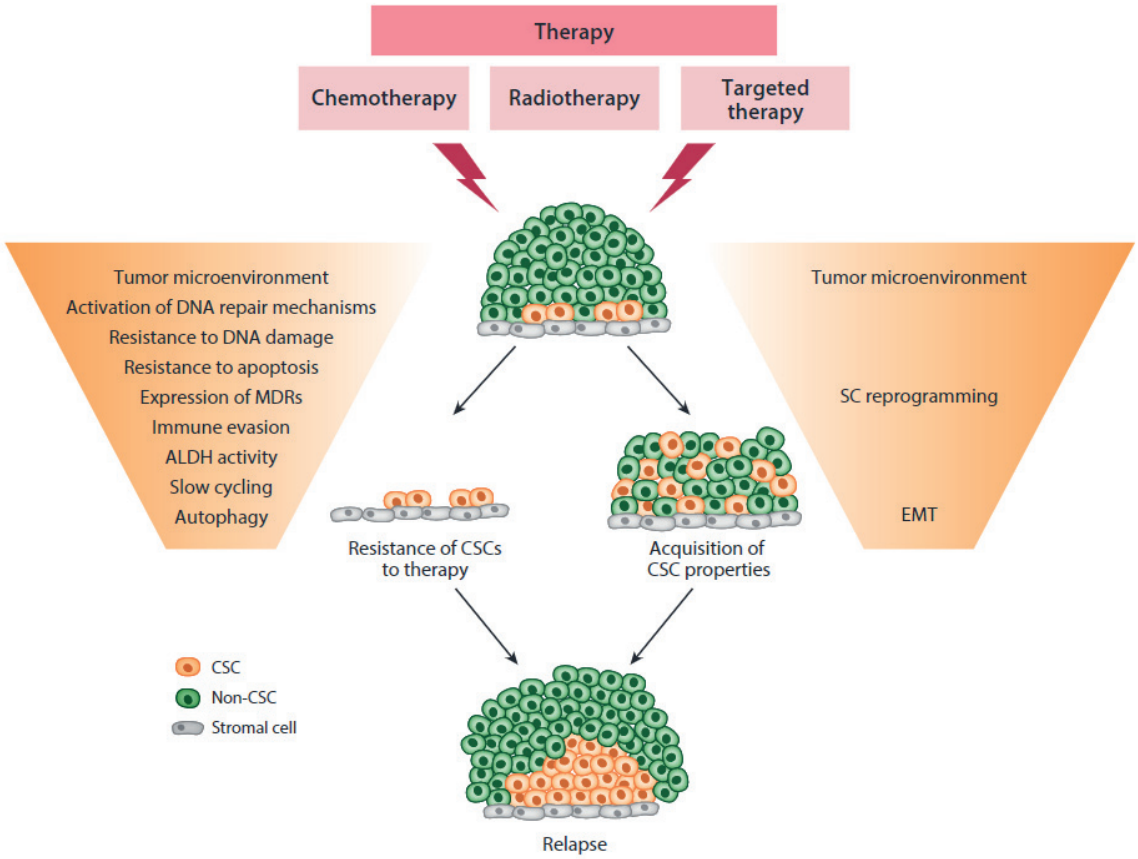

Figure 9. Mechanisms underlying therapy resistance in CSCs. CSC: cancer stem cell; SC: stem cell; MDRs: multidrug resistance proteins; ALDH: aldehyde dehydrogenase; EMT: epithelial-to-mesenchymal transition. Taken from [62].

1.2. ALDHs

1.2.1. Structure and function of ALDHs

ALDHs constitute a superfamily of enzymes (EC 1.2.1.3) that catalyze the irreversible $NAD(P)^+$-dependent oxidation of a wide variety of endogenous and exogenous aldehydes to their corresponding carboxylic acids. Endogenous aldehydes are produced in the metabolism of amino acids, carbohydrates, lipids, biogenic amines, vitamins and steroids, whereas exogenous aldehydes come from the biotransformation of xenobiotics, drugs and environmental chemicals [91]. Although some aldehydes play fundamental roles in physiological processes such as vision, embryonic development, and neurotransmission, their highly reactive electrophilic nature renders them cytotoxic and carcinogenic in many cases [92]. Aldehydes are known to be toxic due to their propensity to form adducts with various cellular targets such as glutathione (GSH), nucleic acids, and protein amino acids, leading to impaired cellular homeostasis, enzyme inactivation, DNA damage, and cell death [93], [94]. In this regard, ALDHs play a critical role in the cellular protection against these toxic species by oxidizing and detoxifying them. This notion is strongly supported by the fact that allelic variants in *ALDH* genes are the molecular basis of

numerous metabolic diseases, such as Sjögren-Larsson syndrome, type II hyperprolinemia and pyridoxine-dependent epilepsy, among others [91], [95], [96].

Although ALDHs are particularly relevant in the detoxification of aldehydes, other enzymes also contribute to their metabolism, including the reduction systems alcohol dehydrogenase (ADH), aldo-keto reductase (AKR) and short-chain dehydrogenase/reductase (SDR), and the oxidation systems xanthine oxidase (XO) and aldehyde oxidase (AOX) [97], as shown in **Figure 10**.

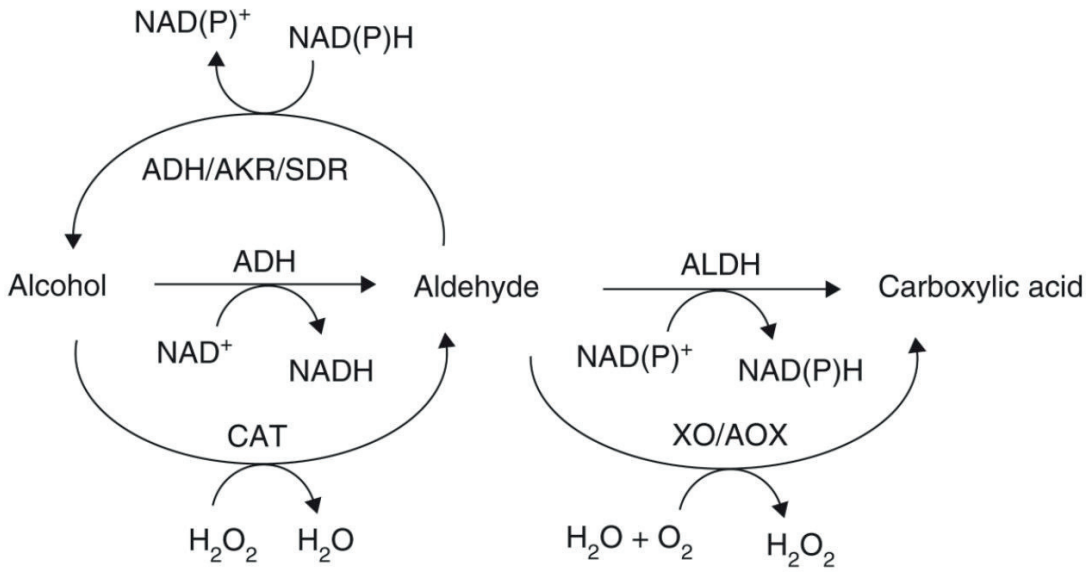

Figure 10. Enzymatic metabolism of aldehydes. ALDHs are involved in the irreversible oxidation of aldehydes into carboxylic acids. ADH: alcohol dehydrogenase; AKR: aldo-keto reductase; ALDH: aldehyde dehydrogenase; AOX: aldehyde oxidase; CAT: catalase; SDR: short-chain dehydrogenase/reductase; XO: xanthine oxidase. Taken from [97].

Furthermore, some ALDHs play a particularly relevant role in cell signaling via the oxidation of retinaldehyde (RAL) to retinoic acid (RA), a reaction which is mainly carried out by the cytosolic isoforms ALDH1A1, ALDH1A2 and ALDH1A3, also referred to as RAL dehydrogenases [98]–[100]. RA is a key signaling molecule that can function in a paracrine or intracrine manner by diffusing from the cytosol into neighboring cells or the nucleus [84]. Once inside the nucleus, RA regulates gene expression through the activation of two classes of nuclear ligand-dependent receptors, namely RA receptor (RAR) and retinoid X receptor (RXR) [100], [101]. Upon binding to RA, the receptors form dimers and become active. These dimers bind to RA response elements (RAREs), which are regulatory sequences located in the promoters of RA target genes, and this leads to their transcription and consequent modulation of a broad spectrum of biological processes including cell proliferation, differentiation, cell cycle arrest, changes in morphology and apoptosis [84], [102], [103], as depicted in **Figure 11**.

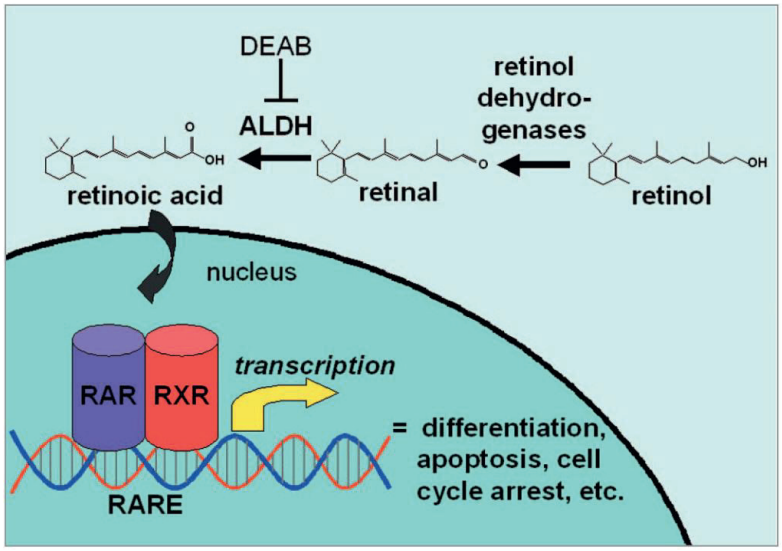

Figure 11. Role of ALDHs in RA signaling. Retinol dehydrogenases transform retinol into RAL, which is converted into RA by ALDHs. This second reaction can be inhibited by DEAB. RA then enters the nucleus and modulates transcription of genes. ALDH: aldehyde dehydrogenase; DEAB: *N*,*N*-diethylaminobenzaldehyde; RAR: retinoic acid receptor; RXR: retinoid X receptor; RARE: retinoic acid response element. Taken from [84].

The human ALDH superfamily consists of 19 putatively functional genes in different chromosomal locations, as indicated in **Figure 12**. This figure also presents some anomalies associated with mutations in each of these 19 genes. The standard nomenclature system for this superfamily of enzymes is based on divergent evolution. Accordingly, the different ALDH enzymes are classified into families and subfamilies based on amino acid sequence identity: ALDH proteins belonging to the same family are defined as presenting more than 40% amino acid identity, whereas two members of the same subfamily share more than 60% amino acid identity. The nomenclature system consists of the root symbol "ALDH" followed by a number which represents the family (e.g. ALDH1), which is in turn followed by a letter that assigns the subfamily (e.g. ALDH1A), which is finally followed by a number that defines the individual enzyme within the subfamily (e.g. ALDH1A1). The eukaryotic ALDH superfamily comprises 24 families with enzymes that are found in all subcellular regions including cytosol, mitochondria, endoplasmic reticulum and nucleus, depending on the isoform, and most of them have a wide tissue distribution [97], [104].

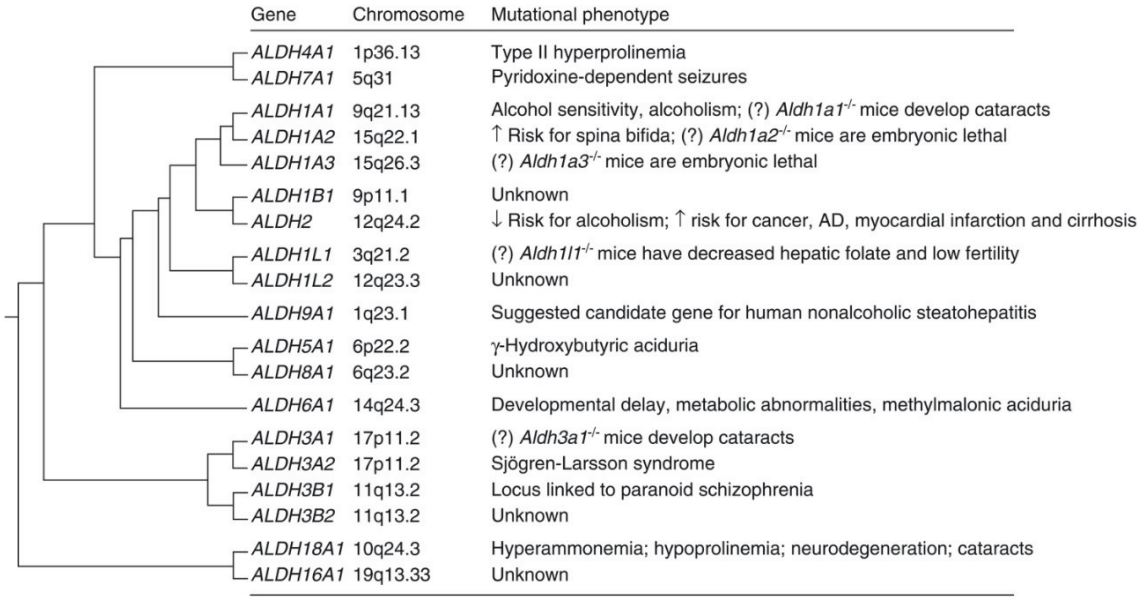

Figure 12. Evolutionary relationship and mutational phenotypes of the 19 human *ALDH* genes. Although *ALDH2* is formally a member of the ALDH1 family, it keeps its historic name. (?) indicates phenotype demonstrated in animals but not yet described in humans. Taken from [97].

ALDHs are homodimeric or homotetrameric enzymes. The subunit structures of different ALDH members are very similar, sharing a high sequence identity [105]. In fact, ALDH enzymes share a number of highly conserved residues necessary for catalysis and cofactor binding. The invariant catalytic Cys-302 (numbering based on the mature human ALDH2 protein), Glu-268, Gly-299, and Asn-169 are all essential for catalysis, whereas Gly-245 and Gly-250 are key residues for cofactor binding [97]. Generally, the molecular weight of ALDH subunits varies between 50 and 60 kDa, and 3 different, conserved domains can be observed in their structure: (1) the $NAD(P)^+$ binding domain, (2) the catalytic domain, and (3) the oligomerization domain [106]. The typical structure of ALDH enzymes is depicted in **Figure 13**.

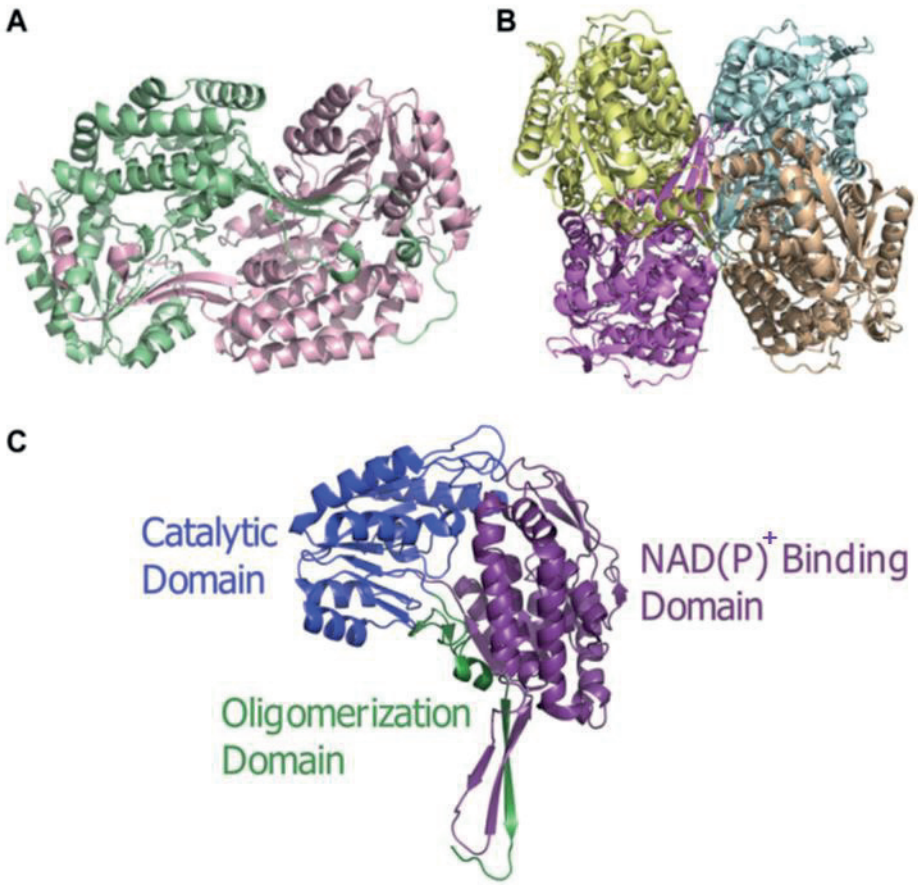

Figure 13. Typical three-dimensional structure of ALDH enzymes. (A) Dimeric structure, observed for example in ALDH3A1. **(B)** Tetrameric structure, observed for example in ALDH1A1, ALDH1A2 and ALDH1A3. **(C)** Domains of ALDH monomers. Adapted from [106].

A funnel-shaped cavity with an opening leading to the catalytic pocket, which contains the conserved catalytic Cys residue, resides at the interface of the domains just explained above [107]. Despite the high grade of homology between ALDH isozymes, differences in the size and architecture of this cavity lead to distinct substrate specificities. However, the kinetic mechanism seems to be similar in all ALDH enzymes, which is generally an ordered bi-bi sequential mechanism: briefly, the oxidized cofactor first binds to the enzyme to make possible the attachment of the substrate; then, oxidation occurs, and the product is released prior to the reduced cofactor [108], [109]. Specifically, catalysis is known to occur in 5 distinct steps, detailed in **Figure 14**: (1) activation of the catalytic thiol (Cys302) by water-mediated deprotonation carried out by Glu268; (2) nucleophilic attack on the aldehyde by the activated catalytic Cys; (3) formation of a tetrahedral thiohemiacetal intermediate, which transfers a hydride to the pyridine ring of the cofactor; (4) hydrolysis of the resulting thioester intermediate; (5) dissociation of the reduced cofactor and regeneration of the enzyme by the addition of oxidized cofactor [106], [110].

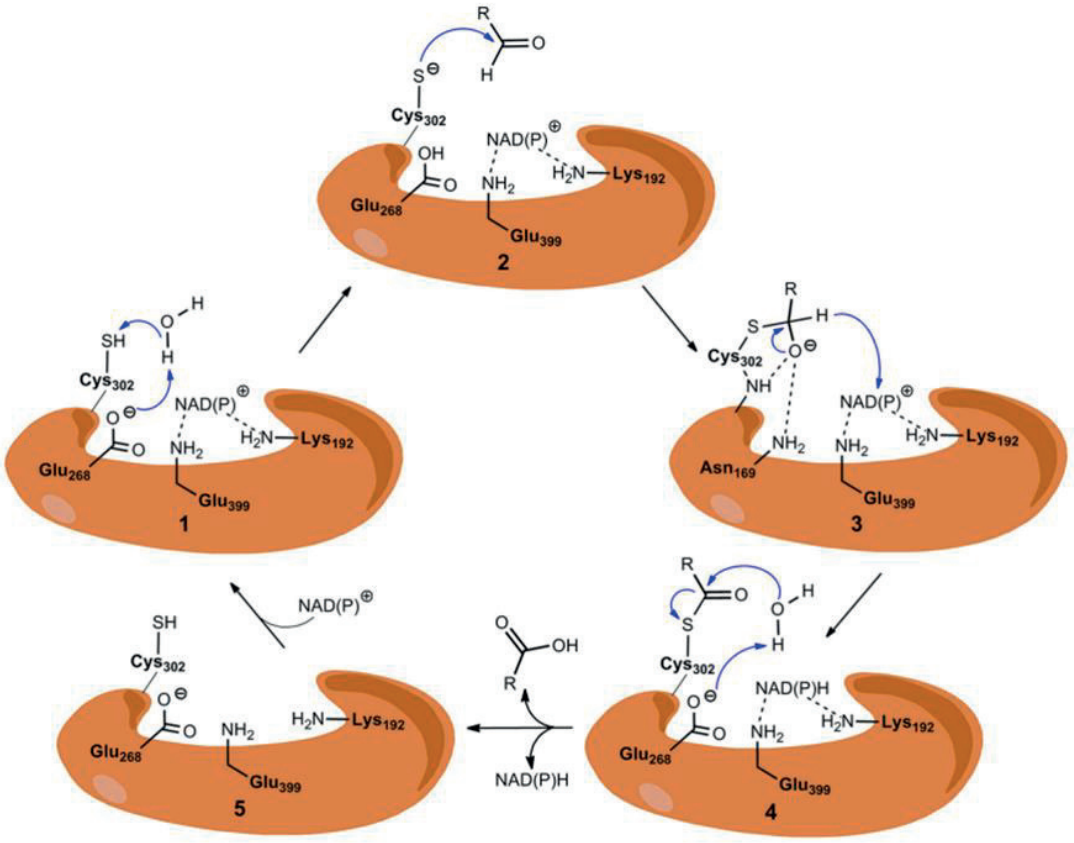

Figure 14. Catalytic mechanism of ALDH reaction. (1) Activation of the catalytic thiol (Cys302); (2) nucleophilic attack on the aldehyde by the activated Cys302; (3) formation of a tetrahedral thiohemiacetal intermediate; (4) hydrolysis of the resulting thioester intermediate; (5) dissociation of the reduced cofactor and regeneration of the enzyme. Taken from [110].

Apart from their role in aldehyde detoxification, ALDHs count with multiple additional catalytic and non-catalytic functions. On the one hand, some isoforms are known to possess additional catalytic functions, such as ester hydrolysis [111], [112] and nitrate reduction [113], [114]. On the other hand, non-catalytic roles [115] include structural function in the eye (lens and corneal crystallins) [104], [116]; antioxidant function by absorption of UV light, production of NADPH for the regeneration of GSH, and scavenging of hydroxyl radicals [117]–[121]; and role as binding proteins for various endogenous and exogenous compounds [122].

1.2.2. Role of ALDHs in CSCs and GB

The signaling pathways activated by RA have been proven to modulate the stemness characteristics of CSCs [123], [124]. On the one hand, the so-called classical pathways are known to induce loss of stem cell markers, cellular differentiation, apoptosis and cell cycle arrest, eventually reducing tumor propagation and inhibiting tumor growth [125]. In fact, the different isomers of RA, namely all-*trans*-RA, 9-*cis*-RA and 13-*cis*-RA, have been extensively investigated for their roles in cancer treatment [126], [127]. On the other hand, however, RA can also

participate in non-classical pathways, including those for anti-apoptosis, anti-differentiation and growth. These pathways, in contrast to the classical pathways, promote tumorigenesis and stemness [128], [129]. Examples of pro-survival pathways activated by RA in CSCs are the phosphatidylinositol 3-kinase (PI3K)/protein kinase B (Akt) and the mitogen-activated protein kinase (MAPK)/extracellular signal-regulated kinase (ERK) pathways [90].

Apart from their role in RA-mediated signaling pathways, ALDHs exert other important functions in CSCs. For instance, these enzymes have been directly related to resistance to drug toxicity and radiation. Both chemotherapy and radiotherapy usually induce the generation of reactive oxygen species (ROS), which cause lipid peroxidation and subsequent production of toxic aldehydes. As mentioned above, ALDHs act as antioxidant and detoxifying enzymes. Accordingly, ALDHs take part in resistance by scavenging ROS and by oxidizing toxic aldehydes. In addition, these enzymes have been shown to directly metabolize antineoplastic drugs containing aldehyde groups into non-toxic forms [128], [130], [131]. A number of common drugs used in cancer treatment have been reported to lose efficacy due to ALDH activity, such as cyclophosphamide [132], doxorubicin [133], cisplatin, arabinofuranosyl cytidine [134], and dacarbazine [135], among others.

In GB, ALDH1A1 and ALDH1A3 have recently been associated with TMZ resistance. Although TMZ is known to exert its cytotoxic effect by generating DNA damage, as explained above, it has recently been suggested that oxidative stress is also a critical component of TMZ-mediated cytotoxicity. In this regard, superoxide radicals generated after TMZ treatment lead to lipid peroxidation, and the resulting aldehydes cause damage by binding to cellular proteins and DNA. ALDH1A1 and ALDH1A3 appear to contribute to TMZ resistance by detoxifying these reactive aldehydes. Accordingly, some studies have demonstrated that ALDH1A3-knockout cells are significantly more sensitive to TMZ treatment than wild-type cells [136]–[138].

Furthermore, ALDHs are known to be involved in the immune microenvironment of CSCs, specifically taking part in the role of the regulatory T cells (Tregs) [139]. Tregs are immune cells essential for the maintenance of immunological self-tolerance, that is, the unresponsiveness of the immune system to self-antigens [140], [141]. This is evidenced by the fact that a deficiency in Tregs can lead to the appearance of autoimmune diseases, and indeed, strategies aimed at stimulating Tregs are used to treat this kind of diseases. It has been observed that a great number of Tregs infiltrate in the tumor in many types of cancer, impairing tumor immunity. Upregulation of ALDH activity increases the production of RA, which is known to promote the induction, function and stability of Tregs, leading to immune tolerance [142], [143]. Accordingly,

inhibition of RA signaling has been proven to increase the efficacy of cancer treatments by reducing the amount of tumor-infiltrating Tregs [144].

The roles of ALDHs in CSCs just discussed above are shown in **Figure 15**.

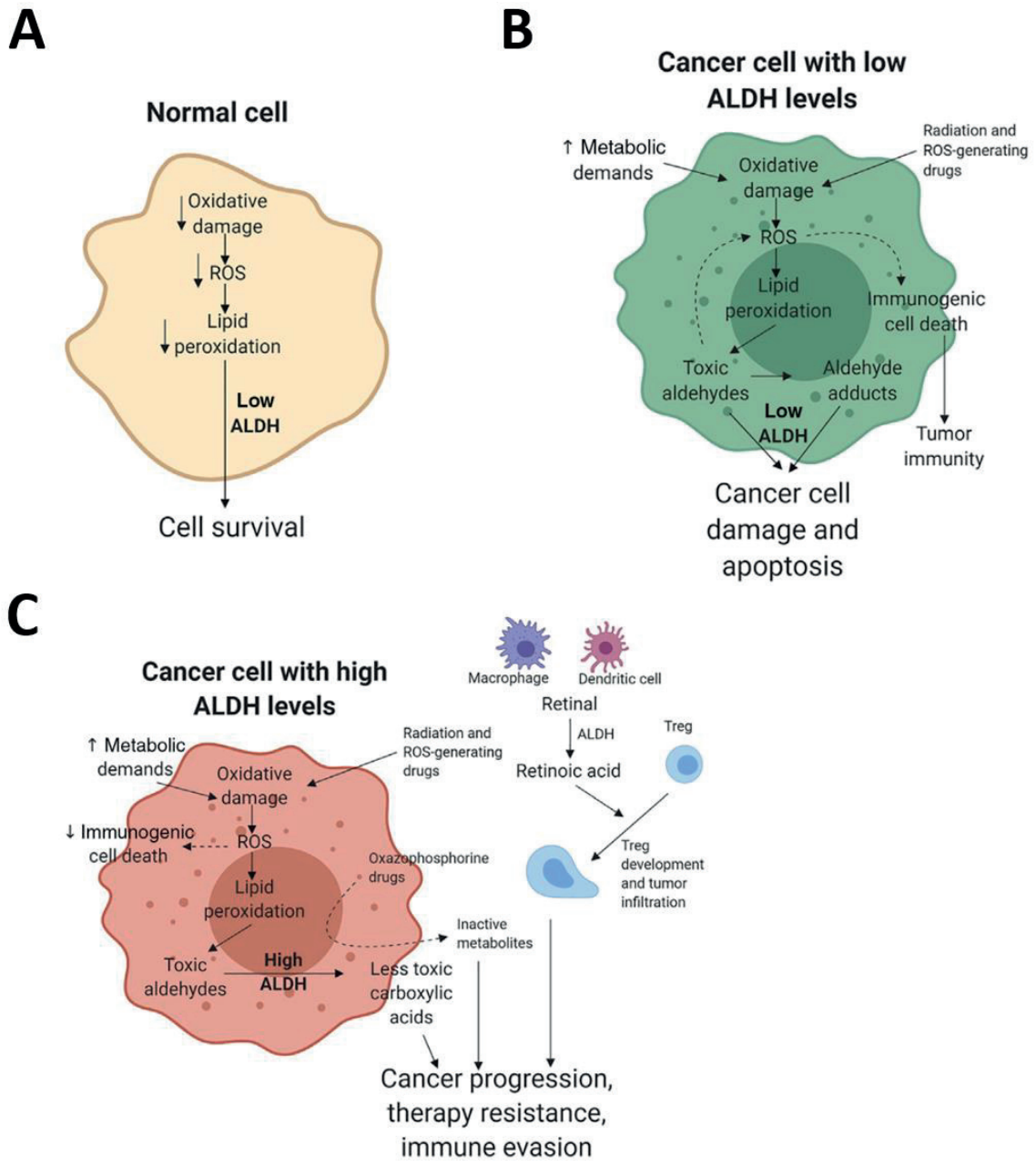

Figure 15. Roles of ALDHs in cancer progression, chemotherapy and radiotherapy resistance, and immune evasion. **(A)** Normal cell; **(B)** cancer cell with low ALDH levels; **(C)** cancer cell with high ALDH levels. Normal cells have low metabolic demands and consequently low levels of ROS, thus ALDH overexpression is not needed to combat associated damage. In contrast, the high metabolic demands of cancer cells make it necessary to overexpress ALDHs in order to counteract the effects of the consequent oxidative damage, also induced by radiation and chemotherapy. In addition, RA generated by ALDHs induces Tregs, which impair tumor immunity. ALDH: aldehyde dehydrogenase; ROS: reactive oxygen species; Treg: regulatory T cell. Adapted from [142].

ALDHs have also been shown to be important in CSC properties such as migratory ability, clonogenicity and metastatic potential [130]. For instance, a well-known study performed by

Mao *et al*. in 2013 showed that the isoform ALDH1A3 is a key driver in the radiation-induced transformation of proneural GSCs to a mesenchymal phenotype [145], which is known to be associated with a lower overall survival in GB patients [146], tumor invasiveness [147], spreading, and resistance to radiotherapy [148], [149]. Some other studies point out that ALDH1A3 is the major contributor to the overall ALDH activity in this subset of cells and is responsible for their maintenance, self-renewal, survival, proliferation and tumorigenicity [150]–[152].

In addition, ALDH1A3 has been related to the altered metabolism that cancer cells need in order to fulfill the extensive energy requirements that malignant growth demands. In this sense, ALDH1A3 seems to be linked to the so-called Warburg effect, which describes the fact that cancer cells use aerobic glycolysis instead of respiration in the mitochondria to obtain adenosine triphosphate (ATP), even in the presence of oxygen [153]. Some studies show a direct relationship between the levels of ALDH1A3 expression and glycolytic activity [145], [154], [155].

Altogether, this data suggests that ALDHs play a complex role in CSC biology and therapy resistance. Thus, these enzymes are not only consistent markers for CSCs, but they have also recently arisen as promising pharmacological targets to combat specifically CSCs.

1.3. ALDH inhibitors for the treatment of GB

No standard treatment is established yet for recurrent GB. Some recent approaches include: the application of tumor-treating fields (TTFs), which is FDA-approved and involves the delivery of low-intensity electric fields to the tumor location to disrupt cancer cell division [34], [156], [157]; immunotherapies, which are predominantly based on peptide or dendritic cell vaccines, chimeric receptor T cells, checkpoint inhibitor therapy, and oncolytic virotherapy [57], [158], [159]; and therapies based on small molecule inhibitors targeting dysregulated pathways in GB, either as monotherapies or in combination regimens [160]–[162]. Belonging to this last group of novel therapies, the development of ALDH inhibitors has become a growing focus of GB research. Since ALDHs are involved in a wide variety of processes affecting GSCs, as detailed in the previous section, ALDH inhibition could represent a promising approach to target specifically this subset of cells and could be useful in decreasing tumor recurrence and increasing the effectiveness of already existing therapies [32], [90].

ALDH inhibitors are categorized on the basis of their selectivity, being considered as broad-spectrum or isoform-selective inhibitors [163]. Whereas the $NAD(P)^+$ domain of these enzymes can be exploited for the development of broad-spectrum inhibitors, the catalytic and the oligomerization domains are used for the design of isoform-selective inhibitors [164].

Some of the best known broad-spectrum ALDH inhibitors are DEAB [83], citral [165], disulfiram [166], gossypol [167], 4-dimethylamino-4-methyl-pent-2-ynthioic acid S-methyl ester (DIMATE) [168], Aldi- 1 to 4 [169] and Aldi-6 [170]. In general, these compounds have shown antiproliferative activity *in vitro* in various types of cancer, either as monotherapies or in combination with other chemotherapeutic agents. Furthermore, some of them have been effective *in vivo*, rendering reduction of tumor growth and/or metastasis in different cancer models. However, these inhibitors often present poor pharmacokinetic properties (such as short half-time) and display off-target toxicity due to inhibition of other pathways not related to ALDHs. Also, since ALDHs have a wide tissue distribution, inhibition of other ALDH isoforms which are not involved in tumorigenesis could lead to toxic side effects [110], [142].

Attempts at reducing toxic side effects have led in the last few years to the development of isoform-selective ALDH inhibitors, usually through the optimization of the structure of already known broad-spectrum inhibitors [171]–[173]. Some relevant examples are compounds NCT-501, NCT-505 and NCT-506 [174], selective for ALDH1A1; CVT-10216 [175] and ALDH423 [176], selective for ALDH2; and CB7 [177] and CB29 [178], selective for ALDH3A1. Although some of them display promising potential *in vitro* in different cancer types, few isoform-selective inhibitors have been tested in animal models to date, mainly due to recent discovery and/or lack of bioavailability [142].

Since this is a relatively new field of research, there are few examples of ALDH inhibitors tested in GB in the literature. Specifically, ALDH1A3 has become the main target in GB due to its relevance in several processes, as explained above. As an example, Gelardi *et al*. [179] tested a novel selective ALDH1A3 inhibitor, named NR6, on GB cancer cells. This compound showed cytotoxic activity and anti-metastatic properties in wound healing and invasion assays, and furthermore, induced the downregulation of CSC markers. In an even more recent study, Gelardi *et al*. [180] presented some curcumin-based fluorescent inhibitors selective versus ALDH1A3, which were able to accumulate and produce a detectable fluorescence signal in ALDH1A3-positive GB cells both *in vitro* and *in vivo*, with a promising application as probes for early diagnosis and improvement of surgery accuracy in GB patients. Another tested compound is MCI-INI-3, which inhibited selectively ALDH1A3 activity and altered RA synthesis in mesenchymal GSCs in the study performed by Li *et al*. [181]. As a last example for ALDH1A3-selective inhibitors, Quattrini *et al*. [182] showed that a novel class of imidazo[1,2-*a*]pyridine derivatives had antiproliferative efficacy at the picomolar level against patient-derived GSCs. ALDH3A1-selective inhibitors have also been examined in GB, in the work carried out by Parajuli *et al*. [178]. Briefly, a novel small molecule inhibitor called CB29 and its analogs were tested on

the GB cell line SF767. These compounds rendered ineffective as monotherapy, but were able to increase the sensitivity of cells toward mafosfamide, an oxazaphosphorine alkylating agent. Lastly, Park *et al*. [183] combined the ALDH pan-inhibitor gossypol with phenformin, an inhibitor of mitochondrial complex I, in GB tumorspheres. The combination treatment resulted in a reduction of ATP levels, stemness, invasiveness and cell viability, and consistently, in a decrease of the expression of genes associated with these features. In a later study performed by the same group, the effects of this dual inhibition of bioenergetics by targeting ALDH and oxidative phosphorylation were even enhanced when this treatment was combined with TMZ [184].

In the work carried out during this thesis, we aimed to contribute to this emerging and expanding field by studying the effect of some ALDH inhibitors synthesized by the biotechnology company Advanced BioDesign (ABD), namely DIMATE, ABD0099 and ABD0171, on GB cells. On the one hand, DIMATE is one of the broad-spectrum inhibitors mentioned before, which has shown antiproliferative activity both *in vitro* and *in vivo* in different cancer models, but has not been tested in GB yet. Specifically, DIMATE has been shown to cause the accumulation of toxic aldehydes leading to apoptosis and tumor growth inhibition in acute myeloid leukemia (AML) [185], melanoma [186], and non-small cell lung cancer (NSCLC) [187]. On the other hand, DIMATE analogs ABD0099 and ABD0171 have not been tested in GB either. The structure of these inhibitors is shown in **Figure 16**. These α,β-acetylenic amino thiolester compounds were designed as putative ALDH inhibitors, with a proposed mechanism of inhibition based on the interaction of their electrophilic atoms with the catalytic Cys residue of ALDHs. In fact, DIMATE has been characterized as an irreversible inhibitor of ALDH1 isoforms [168], and the two analogs have been already proven to inhibit the activity of different isoforms of recombinant human ALDHs, a study that has been carried out by other members of our research group (Pequerul *et al*., unpublished results).

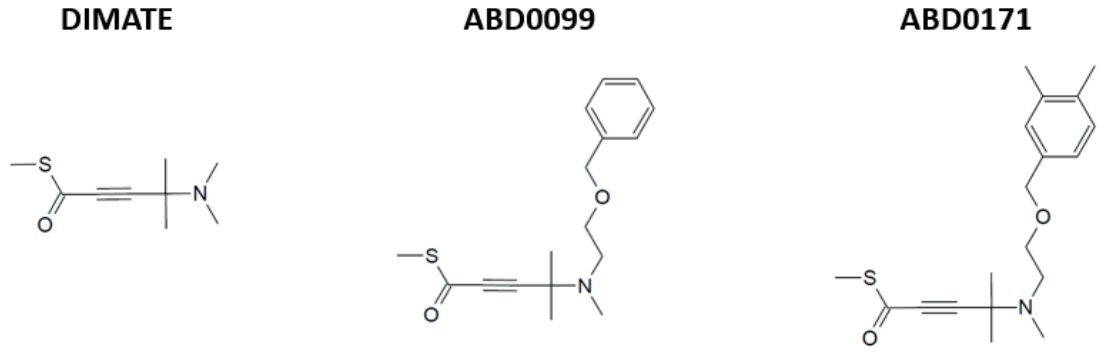

Figure 16. Chemical structure of the ALDH inhibitors DIMATE, ABD0099 and ABD0171, synthesized by ABD. DIMATE: 4-dimethylamino-4-methyl-pent-2-ynthioic acid S-methyl ester.

As stated above, some of the main pitfalls of using small-molecule inhibitors *in vivo* are their poor pharmacokinetic properties, as well as possible off-target toxicities. In the case of brain malignancies, in addition, the presence of the BBB represents an obstacle for drugs to reach the tumor site in a suitable therapeutic dose. In order to obtain a therapeutic effect, it is crucial to reach a specific target zone with sufficient concentration of the drug, duration of its action, and safety for the surrounding healthy tissue. To achieve this, the encapsulation of therapeutic molecules in nanoparticles has become a first-line strategy in the recent years [188], [189]. Some nanoencapsulation approaches with ALDH inhibitors such as citral [165], [190] and disulfiram [191] have already been tested, and in fact, the company ABD has developed lipidic nanoparticles containing DIMATE [192]. This lipidic nanoemulsion of DIMATE, which was named ABD-3001, has also been studied in this thesis on GB cancer cells and is currently in clinical phase I for the treatment of AML (https://beta.clinicaltrials.gov/study/NCT05601726).

In addition, the use of nanocarriers for the co-administration of multiple therapeutic molecules with different targets has a considerable potential for the treatment of GB, given the high grade of heterogeneity and complexity of this tumor type. In fact, these so-called combination therapies are currently arising as a standard practice for cancer treatment [193]. Also, the route of administration of these carriers is a crucial point to consider. A suitable strategy to bypass the BBB and reach the brain with a sufficient dose of a drug is the intranasal administration route. By its anatomy, the nasal cavity represents the only contact region between the CNS and the external environment, and therefore, constitutes a direct and non-invasive way of accessing the brain, consequently limiting the side effects for the patient [194]. Several therapeutic agents are currently being studied for the treatment of GB by exploiting this route of administration, mostly in preclinical phases, and are yielding promising results in terms of biodistribution and therapeutic effect [195]. In the final part of this thesis, the intranasal administration route has been used for the treatment of GB-bearing mice with ABD-3001 nanoparticles.

OBJECTIVES

The main objective of this thesis is to contribute to the recent and expanding field of research on ALDH inhibitors as potential anticancer therapeutic agents, with a specific focus on GB, which still lacks effective treatment options. In particular, this thesis aims to study the anticancer effect of the compounds DIMATE, ABD-3001 (encapsulated DIMATE), ABD0099 and ABD0171 in GB.

The experiments conducted during this thesis can be divided into three different blocks, each with its own set of partial objectives:

Block 1. Characterization of ABD-3001 nanoparticles.

1.1. To assess the size and morphology of ABD-3001 nanoparticles by cryogenic transmission electron microscopy (Cryo-TEM).
1.2. To determine the hydrodynamic diameter, polydispersity index (PdI) and zeta potential of ABD-3001 nanoparticles by dynamic light scattering (DLS).
1.3. To study the release profile of DIMATE from ABD-3001 nanoparticles by an HPLC-based method optimized for the detection of DIMATE.

Block 2. *In vitro* studies in a panel of GB cell lines.

2.1. To determine the expression levels of the isoforms of the ALDH1A subfamily in a panel of GB cell lines by an automated capillary-based immunoassay.
2.2. To evaluate the cytotoxic effect of DIMATE, ABD-3001, ABD0099, ABD0171 and TMZ in a panel of GB cell lines, by calculating the EC_{50} values.
2.3. To investigate the ability of DIMATE, ABD0099 and ABD0171 to inhibit the ALDH activity in extracts of the human GB cell line A172 and the murine GB cell line GL261, using two different substrates, namely hexanal and RAL, and by means of fluorometric and HPLC-based methods, respectively.
2.4. To explore potential synergistic effects of TMZ in combination with ALDH inhibitors (DIMATE, ABD-3001, ABD0099 or ABD0171) in the GB cell lines A172 and GL261.
2.5. To study the mechanism of cell death induced after treatment with TMZ, DIMATE, ABD-3001, ABD0099 or ABD0171 in the GB cell lines A172 and GL261 by flow cytometry.
2.6. To assess whether the treatment with TMZ, DIMATE, ABD-3001, ABD0099 or ABD0171 led to the accumulation of ROS in the GB cell lines A172 and GL261.
2.7. To generate an *ALDH* gene knockout in the human GB cell line A172 and examine its impact on growth, migration and sensitivity to some FDA-approved drugs.

Block 3. *In vivo* studies in a murine model of GB.

3.1. To perform a tolerability assay in C57BL/6J wild type mice in order to assess the toxicity of ABD-3001 nanoparticles administered via the intranasal route.

3.2. To perform therapeutic efficacy assays in GL261 tumor-bearing C57BL/6J mice at different doses of ABD-3001 nanoparticles administered via the intranasal route in order to evaluate the antitumor effects of the drug.

3.3. To study the biodistribution of DIMATE in the tissues of GL261 tumor-bearing C57BL/6J mice treated with ABD-3001 nanoparticles by an HPLC-based method optimized for the detection of DIMATE.

3.4. To determine changes in the expression of ALDH enzymes in various tissues of GL261 tumor-bearing C57BL/6J mice treated with ABD-3001 nanoparticles compared to untreated mice, by an automated capillary-based immunoassay.

MATERIALS & METHODS

3.1. Compounds tested

The ALDH inhibitors tested in this study, namely DIMATE, ABD0099, and ABD0171, as well as the lipidic nanocapsules of DIMATE [192], referred to as ABD-3001, were synthesized and provided by the biotechnology company ABD. The structure of these compounds has been already shown in **Figure 16**, and are dissolved in ethanol. ABD-3001 nanocapsules are composed of caprylic/capric triglyceride, macrogol 15 hydroxystearate and soy phosphatidylcholine, and are dispersed in saline solution (NaCl 0.9% w/v). Empty liposomes, named ABD-3000, were also provided by ABD, and are also dispersed in saline solution.

3.2. Cell culture

All human GB cell lines (LN229, T98G, U251-MG, U373, U87-MG and A172) were acquired from ATCC and cultured in DMEM (Life Technologies) with 10% FBS (Life Technologies) in the absence of antibiotics. Cells were incubated in a humidified atmosphere with 5% CO_2 at 37°C. The murine cell line GL261 was acquired from DSMZ and cultured under the same conditions as for the human GB cell lines. A pellet of the non-cancerous human astrocytic cell line Ax-0019, obtained as described by Perriot *et al*. [196], was kindly provided by Dr. Arranz's research group (Laboratory of Humanized Models of Disease, Achucarro Basque Center for Neuroscience, Science Park of the UPV/EHU) and used only for immunoblot analysis.

All cells were subcultured after two or three days per week as follows. Firstly, medium was removed from the flask and cells were washed with 5 mL phosphate-buffer saline (PBS, Life Technologies). Then, 3 mL of trypsin (Life Technologies) were added to the cells and they were incubated for 1-2 min at 37°C. After visualizing detached cells under an inverted microscope, 6 mL of medium were added, and the culture was centrifuged at 300 x g for 5 min. Then, the supernatant was discarded and the pellet was resuspended in a proper volume of medium according to the desired dilution (usually between 1:6 and 1:10, depending on the cell line). The culture was then incubated under the conditions mentioned above until next passage.

3.3. Animals

All animal experiments were approved by the local ethics committee (Comissió d'Ètica en l'Experimentació Animal i Humana de la UAB, https://www.uab.cat/etica-recerca/) and conducted under the principles of regional and state legislations (protocol CEEAH-4859). Female C57BL/6J mice were purchased from Charles River Laboratories (l'Arbresle, France) and housed at the animal facility of UAB, in cages with free access to standard food and water, under uniform

environmentally controlled conditions. Mice spent at least three weeks under these conditions prior to any experiment.

3.4. Cryogenic transmission electron microscopy

Cryogenic transmission electron microscopy (Cryo-TEM) analysis of ABD-3000 and ABD-3001 was performed by the Microscopy Service of UAB. Briefly, 10 µL of nanoparticles resuspended in saline solution were collected and deposited on Formvar/carbon electron microscopy grids. Then, the sample was frozen with ethane and kept at −182°C during visualization under a JEM-2011 transmission electron microscope. The images obtained were analyzed using ImageJ software in order to determine the diameter of the nanoparticles.

3.5. Dynamic light scattering

Dynamic light scattering (DLS) analysis of ABD-3001 nanoparticles was performed at Institut Català de Nanociència i Nanotecnologia (ICN2), in a Zetasizer Nano ZS analyzer (Malvern). Nanoparticles were analyzed during four consecutive days at two different conditions: storage conditions (at 4°C, at a concentration of 8.35 mg/mL in saline solution) and physiological conditions (at 37°C, at a concentration of 0.2 mg/mL diluted in saline solution). Briefly, 1 mL of sample was introduced in a plastic cuvette, placed inside the analyzer, and tested for hydrodynamic diameter, polydispersity index (PdI) and zeta potential.

3.6. Dialysis

An ABD-3001 solution (700 µL) was placed inside a 6000-8000 Da molecular weight cut-off dialysis membrane, which in turn was placed in 50 mL PBS both at pH 5 and pH 7, at 37°C and agitation. Samples from PBS were taken during 4 days at the following times: 0, 0.5, 1, 2, 4, 6, 8, 10, 24, 48, 72, and 96 h. Samples were stored immediately at −80°C and kept at this temperature until HPLC analysis.

3.7. HPLC for the detection of DIMATE

Samples were diluted in a solution containing a final concentration of 0.1% (v/v) trifluoroacetic acid (TFA) (Sigma) and 80 µL were loaded onto a Restek Ultra C18 (250 mm x 4.6 mm) column. A mixture of two different solvents was used as the mobile phase: solvent A was 0.1% v/v TFA in MilliQ water, and solvent B was acetonitrile (Fisher Scientific). A gradient was set up with the following conditions: flow rate of 0.75 mL/min and final time of 25 min; initially, the ratio A:B was 96:4; using the time intervals 0 to 7.5 min: gradient from 96:4 to 75:25; 7.5 to 12 min: gradient from 75:25 to 0:100; 12 to 20 min: proportion maintained at 0:100; 20 to 23 min:

gradient from 0:100 to 96:4; 23 to 25 min: proportion maintained at 96:4. DIMATE was detected by reading the absorbance using a 2487 dual wavelength absorbance detector (Waters), set up at 210 nm and 270 nm. The amount of DIMATE was determined by interpolation of HPLC peak areas at 270 nm into a calibration curve of known amounts of DIMATE (**Annex 1.1**).

3.8. Automated capillary-based immunoassay

Immunoassays were performed at the company ABD, on a WES system (ProteinSimple) using a 12-230 kDa Separation Module (ProteinSimple, SM-W004) and the Anti-rabbit HRP Detection Module (ProteinSimple, DM-001), according to the manufacturer's instructions. Samples were diluted at 1 mg/mL in Sample Buffer 0.1X (10X Buffer provided in the Separation Module), then mixed with Fluorescent Master Mix, vortexed, and heated for 5 min at 95°C, then kept on an ice bath. The samples, blocking reagent (antibody diluent), primary antibodies (in antibody diluent), HRP-conjugated secondary antibodies and chemiluminescent substrate were pipetted into the plate (provided in the Separation Module). The following instrument settings were used: stacking and separation at 375 V for 25 min; blocking reagent for 5 min; primary and secondary antibody each for 30 min (except for 1 h incubation in the case of ALDH1A2 primary antibody); luminol/peroxide chemiluminescence detection for approximately 15 min (exposures of 1-2-4-8-16-32-64-128-512 s). The resulting graphs were checked and acquired, and the automatic peak detection was manually corrected. Data was visualized as lanes.

Table 1. **Description of the antibodies used in the immunoassays**.

Primary antibody	Reference	Dilution	Specificity	Secondary antibody
ALDH1A1	Proteintech, 15910-1-AP	1/5	Human, mouse	Anti-rabbit (WES detection kit)
ALDH1A2	Proteintech, 13951-1-AP	1/10	Human, mouse	Anti-rabbit (WES detection kit)
ALDH1A3	VWR, ABGEAP7847A	1/5	Human, mouse	Anti-rabbit (WES detection kit)
ALDH1B1	Proteintech, 15560-1-AP	1/50	Human, mouse	Anti-rabbit (WES detection kit)
ALDH2	Proteintech, 15310-1-AP	1/50	Human, mouse	Anti-rabbit (WES detection kit)
ALDH3A1	Proteintech, 15578-1-AP	1/50	Human, mouse	Anti-rabbit (WES detection kit)
ALDH3A2	Proteintech, 15090-1-AP	1/10	Human, mouse	Anti-rabbit (WES detection kit)
ALDH3B1	Abcam, ab236673	1/50	Human, mouse	Anti-rabbit (WES detection kit)
ALDH3B2	Proteintech, 15746-1-AP	1/50	Human, mouse	Anti-rabbit (WES detection kit)
ALDH7A1	Proteintech, 10368-1-AP	1/10	Human, mouse	Anti-rabbit (WES detection kit)
Loading control	ProteinSimple, 042-196	1/10	Rabbit	Anti-rabbit (WES detection kit)

3.9. Cell viability assays

Cells were seeded in 96-well plates at a density of 2,000 cells per well for all human GB cell lines, and 4,000 cells per well for GL261, and incubated overnight at 37°C and 5% CO_2. The following day, cells were treated with different concentrations of the compound of interest and incubated under the conditions mentioned above for 48 h. Cell viability was measured by PrestoBlue™ assay (ThermoFisher). The reagent was added in each well at 10% v/v and fluorescence was read after 3 h incubation in a SPARK multilabel plate reader, using excitation at 531 nm and emission at 572 nm.

3.9.1. Cytotoxicity assays with single compounds

Cell viability assays using single compounds were performed with ALDH inhibitors at concentrations ranging from 0 to 1 mM; TMZ (Sigma) at concentrations from 0 to 20 mM; all-*trans*-RAL (Sigma) at concentrations from 0 to 20 µM; CP (Sigma) at concentrations from 0 to 1 mM; BCNU (Sigma) at concentrations from 0 to 750 µM; and ETP (Sigma) at concentrations from 0 to 250 µM. The proportion of ethanol or DMSO solvents never exceeded 1% v/v in the final volume of the well. In the case of all-*trans*-RAL, the compound was added to the wells under dim red light in order to prevent the photoisomerization of retinoid double bonds. EC_{50} values, defined as the concentration of drug that exerts half of the maximal response, were calculated by nonlinear fitting of the obtained data to a sigmoidal plot using GraFit 5.0 (Erithacus software), with the following 4-parameter equation: $y = \frac{range}{1+\left(\frac{x}{EC_{50}}\right)^s} + background$, where y is the percentage of viable cells, x is the concentration of the compound, *background* is the minimum y value, *range* is the fitted uninhibited value minus the *background*, and s is a slope factor.

3.9.2. Synergy assays

For synergy assays, ALDH inhibitors and TMZ were concomitantly added to the wells in the concentrations mentioned above, combining each concentration of one drug with each concentration of the other drug. Data resulting from these assays were analyzed with SynergyFinder software (https://synergyfinder.fimm.fi/) [197] in order to obtain the synergy maps and scores, calculated according to the reference model of Bliss [198].

3.10. ALDH activity assays

ALDH activity assays were performed with cells collected during the exponential phase of growth. First, cell lysates were obtained using a mammalian protein extraction reagent (M-PER,

ThermoFisher), following the manufacturer's instructions. Subsequently, total protein concentration of the lysate was determined by performing a Bradford assay.

3.10.1. Activity assays using hexanal as a substrate

Enzymatic activity was monitored using a Cary Eclipse (Varian) fluorimeter at 37°C. All reactions were performed in quartz cuvettes in a final volume of 1 mL, using 50 mM HEPES (Sigma), 50 mM $MgCl_2$, pH 7.2 as the reaction buffer, in the presence of 1% ethanol (ethanol is the solvent in which ALDH inhibitors are diluted). After adding the cell lysate and 15 µM inhibitor to the reaction buffer, the mixture was incubated for 20 min at 37°C to let the inhibitor bind to the enzyme. Then, 0.5 mM NAD^+ cofactor (Apollo Scientific), 5 µM NADH (Apollo Scientific) and, finally, 250 µM hexanal substrate (Sigma) were added to start the reaction. Fluorescence of NADH was followed at 460 nm with excitation at 340 nm and spectral bandwidth of 10 nm. Five µM NADH was added to the reaction mixture as an internal standard to obtain absolute reaction rates, which were calculated according to the equation: $v = \frac{dF}{dt} \cdot \frac{C_{st}}{F_{st}}$, where C_{st} is the standard NADH concentration, F_{st} is the standard fluorescence, and *dF/dt* is the slope of the time dependent fluorescence [199]. Specific activity was expressed in milliunits (mU) per mg of total protein of the lysate, 1 mU being defined as 1 nmol of product formed per min. Percentages of remaining activity were calculated for each reaction containing inhibitor, relative to a control without inhibitor.

3.10.2. Activity assays using all-*trans*-RAL as a substrate

In this case, enzymatic activity was determined using an HPLC-based method. All reactions were performed in glass disposable tubes in a final volume of 0.5 mL, in DMEM with 10% FBS, in the presence of 1% ethanol. First, culture medium, cell lysate (at a final total protein concentration ranging from 1 to 2 mg/mL) and inhibitor (at final concentrations of 5, 50 and 250 µM) were incubated for 1 h at 37°C to let the inhibitor bind to the enzyme. Then, 0.5 mM NAD^+ cofactor and 10 µM all-*trans*-RAL substrate were added to start the reaction. From the moment the substrate was added to the reaction mixture, the experiment was carried out under dim red light in order to prevent photoisomerization of retinoid double bonds. After 1 h at 37°C, the reaction was stopped by adding 1 mL of cold methanol. Then, 0.1 mL of 2.5 M ammonium acetate, pH 4.5, was added in order to acidify the aqueous phase and facilitate the retinoic acid recovery [200]. Subsequently, retinoid extraction was performed by two rounds of addition of 2 mL of hexane, vortex mixing for 30 sec and centrifugation at 16,110 x g for 1 min. The aqueous phase was removed, and the organic phase was evaporated under a N_2 stream. Then, retinoids were resuspended in 200 µL of hexane and 75 µL were loaded into a Novapak® Silica column (4

µm, 3.9 mm x 150 mm) in hexane/methyl-*tert*-butyl ether (96:4 v/v) mobile phase, at a flow rate of 2 mL/min, using a Waters Alliance 2695 HPLC. Elution was monitored at 370 nm for all-*trans*-RAL and 350 nm for all-*trans*-RA, using a Waters 2996 photodiode array detector. Quantification of retinoids was performed by interpolating HPLC areas into a calibration curve of known retinoid concentrations, and the specific activity was calculated from the amount of RA produced [201], [202]. Specific activity was expressed in milliunits (mU) per mg of total protein of the lysate, 1 mU being defined as 1 nmol of product formed per min. Percentages of remaining activity were calculated for each reaction containing inhibitor, relative to a control without inhibitor.

3.11. Cell death analysis

Cells were seeded in 12-well plates at a density of 16,000 cells per well for A172 and at a density of 32,000 cells per well for GL261, and incubated overnight at 37°C and 5% CO_2. The following day, cells were treated with the required concentration of ALDH inhibitors (5 µM in all cases except for 20 µM ABD0099 in GL261) or TMZ (5 mM) and incubated under the conditions mentioned above for 24 h. After that, cells were collected and treated with the eBioscience™ Annexin V-FITC Apoptosis Detection Kit (ThermoFisher), following the manufacturer's recommendations. Cell samples were analyzed in a Cytoflex LX flow cytometer (Beckman Coulter), and cell death mechanism was assessed by calculating the percentage of cells marked with annexin V (indicator of apoptosis) or propidium iodide (indicator of necrosis), and comparing to the corresponding untreated control.

3.12. ROS assays

Cells were seeded in 96-well plates at a density of 20,000 cells per well and incubated overnight at 37°C and 5% CO_2. The following day, cells were treated with 25 µM 2',7'-dichlorofluorescin diacetate (DCFDA, Sigma) and incubated protected from light under the conditions mentioned above for at least 30 min. Then, DCFDA was removed from the wells and cells were treated with ALDH inhibitors or TMZ at the concentration equal to the EC_{50} value. Treatment with 500 µM H_2O_2 was used as a positive control. Cells were incubated for 6 h and fluorescence was read in a SPARK multimode microplate reader (Tecan), using excitation wavelength at 485 nm and emission wavelength at 535 nm.

3.13. CRISPR/Cas9 knockout

A172 cells were transfected with a CRISPR/Cas9 plasmid (Santa Cruz Biotechnology, SC-401630: ALDH1A3 CRISPR/Cas9 KO plasmid (h)) following manufacturer's instructions. The targeting

sequence of the guide RNA was 5'-CGTCCCGGAGCAATCTGAAG-3', which is highly specific for the *ALDH1A3* gene. After 48 h, single transfected cells were sorted in a 96-well plate by using a BD FACSJazz Cell Sorter. Clones were let to grow at 37°C and 5% CO_2 for several weeks and then scaled up to T75 flasks for further use.

3.14. RT-PCR

RT-PCR was performed at the company ABD. RNA from A172 WT and A172 KO cells was firstly obtained using the E.Z.N.A. Total RNA Kit 1 (Omega Bio-tek, GA, USA), following the manufacturer's instructions. Extracted RNA was stored at −80°C until use. Secondly, cDNA was obtained from RNA using the qScript XLT cDNA SuperMix (Quantabio, Qiagen Beverly, MA, USA), following the manufacturer's recommendations. Finally, the PCR amplification was performed with 1 µg template cDNA using the PerfeCTa SYBR Green FastMix, ROX (Quantabio, Qiagen Beverly, MA, USA), following the manufacturer's instructions. The primers used for each ALDH isoform are indicated in **Table 2**.

Table 2. Description of the primers used for RT-PCR.

Target gene	Forward primer (5' to 3')	Reverse primer (5' to 3')
ALDH1A1	TTGGAAATCCTCTGACCCCA	CCTTCTTTCTTCCCACTCTC
ALDH1A2	CATTGGAGTGTGTGGACAGA	GGAGCTATTTTCCAGGCA
ALDH1A3	TTTTCATCGACCTGGAGG	GACGTTGTCATCTGTGGG
ALDH1B1	ACTTGGCCTCACTCGAGA	CCAGCAAAGTACCGATAC
ALDH2	GTCAGATGCCGATATGGAT	GCCCTGGTTGAAGAACAG
ALDH3A1	CACATCACCTTGCACTCTCT	AGCTCTTCTTGCCATGGT
ALDH3A2	TAGCTTTTGGTGGGGAGA	CTTGCATCACCTTGGTTT
ALDH3B1	TATCTAATCACGGGCCAC	AGCTGCTTGTTTTCTTGC
ALDH3B2	TTCTCCAACAGCAGCCAG	CGGACAGCAGAGATATGTAG
ALDH7A1	GACCTATTGCCCTGCTAA	CCATGCTTCTCTTGCTTTC

3.15. Growth curve

A172 WT and A172 KO cells were seeded in a total of 36 10 cm-diameter culture dishes at a density of 300,000 cells per dish. During the following 12 days, cells from 3 different dishes for each cell line were counted every 24 h using Trypan Blue staining. The doubling time (*DT*) for each cell line was calculated according to the following equation (as detailed in the ATCC Animal Cell Culture Guide, https://www.atcc.org/resources/culture-guides/animal-cell-culture-guide): $DT = T \cdot \frac{\ln 2}{\ln\left(\frac{X_e}{X_b}\right)}$, where T is the incubation time, X_b is the cell number at the beginning of the incubation time, and X_e is the cell number at the end of the incubation time. *DT* of each cell line

was calculated taking two points of the exponential phase of the growth curve, specifically day 5 (at the start of the exponential phase, where the number of cells of each cell line is still very similar) and day 8 (a day within the exponential phase).

3.16. Migration assays

Migration assays were performed at the company ABD, using the Oris™ Cell Migration Assembly Kit – FLEX. First, the bottom of the wells of a 96-well black plate with clear bottom was coated with 20 µg/mL bovine fibronectin (PromoCell) to avoid cell detachment in following steps of the protocol. The plate was incubated for 1 h at room temperature, protected from light. Then, the excess fibronectin was removed, Oris™ Cell Seeding Stoppers were inserted in the desired wells, and 50,000 cells/well were seeded in a final volume of 100 µL per well. The seeded plate was incubated overnight at 37°C to let cells adhere. The following day, Oris™ Cell Seeding Stoppers were removed, the wells washed with PBS, and calcein fluorescent dye (ThermoFisher), diluted in culture medium without FBS, in a final concentration of 0.25 µM, was added to the wells. The plate with calcein was incubated for 20 min at 37°C. After that, calcein was removed, the wells washed with PBS, and complete culture medium added to the wells. Fluorescence images at times 0 and 30 h were obtained in a SpectraMax plate reader, using excitation wavelength at 456 nm and emission wavelength at 541 nm. Migration areas were analyzed by ImageJ software, and migration was determined as percent closure calculated as follows: $Percent\ closure = \frac{premigration\ area - migration\ area}{premigration\ area} \cdot 100$, where premigration area is the area at time 0 h.

3.17. *In vivo* tolerability assay

The tolerability assay was performed in 10 C57BL/6J female wild type mice with 16 weeks old at the start point. Two groups were established: the treated group (N = 5 mice) and the control group (N = 5 mice). The treatment consisted of 5 mg ABD-3001/kg, while the same dose of ABD-3000 (empty liposomes) was administered to the control group, both resuspended in 0.9% NaCl and administered intranasally using a micropipette. Mice were weighted before each drug administration in order to calculate the necessary volume of drug solution, and weight values were recorded in order to monitor weight loss during the treatment. The treatment schedule consisted of three administrations per week (Monday, Wednesday and Friday) during four weeks. One h after the last drug administration, mice were euthanized by cervical dislocation: the whole bodies of N = 2 mice of each group were fixed in 4% paraformaldehyde solution in PBS, with an incision along the frontal part of the body to better preserve the organs, for necropsy studies; and the organs of N = 3 mice of each group were resected, weighted, frozen

in liquid nitrogen and kept at −80°C, for drug biodistribution studies. Even when the four weeks of treatment were not over, mice could be euthanized at any point if they presented signs of pain as specified in the protocol CEEAH 3665, (project 4859UAB). Independently of any signal, mice could be also euthanized if they lost more than 20% of their body weight relative to their weight at the beginning of the treatment.

3.18. *In vivo* therapeutic efficacy assays

3.18.1. Generation of GB tumor-bearing mice

Firstly, the orthotopic GB tumor-bearing mice were generated through stereotactic injection of 10^5 GL261 cells into the striatum of WT C57BL/6J mice between 10 and 18 weeks old. Specifically, analgesia (Metacam, Boehringer Ingelheim, Germany) at 1 mg/kg was injected subcutaneously into each mouse 15 min before anesthesia and also 24 and 48 h after implantation. Mice were anesthetized with a mixture of ketamine (Parke-Davis SL, Madrid, Spain) at 80 mg/kg and xylazine (Carlier, Barcelona, Spain) at 10 mg/kg via intraperitoneal administration, and next, mice were immobilized on the stereotaxic holder (Kopf Instruments, Tujunga, CA, USA). Then, the head area was shaved, the incision site was sterilized with iodophor disinfectant solution, a 1-cm incision was made exposing the skull, and a 1-mm hole was drilled 0.1 mm posterior to the bregma and 2.32 mm to the right of the midline using a microdrill (Fine Science Tools, Heidelberg, Germany). Four µL of DMEM cell culture medium containing 10^5 GL261 cells were then injected at a depth of 3.35 mm from the surface of the skull at a rate of 2 µL/min, using a 26G Hamilton syringe (Reno, NV, USA) positioned on a digital push-pull microinjector (Harvard Apparatus, Holliston, MA, USA). Once the injection was completed, the Hamilton syringe was left untouched for 2 min before its removal, in order to prevent cellular liquid leakage out of the skull. Lastly, the syringe was gently withdrawn, and the scission site was closed with silk suture 6.0 (Braun, Barcelona, Spain). Mice were then left in a warm environment to recover from anesthesia.

3.18.2. Treatment of GB tumor-bearing mice

Treatment of mice began at day 6 post-implantation. Three different rounds of treatment were performed, with three different doses of ABD-3001: 5, 2.5 and 1.5 mg/kg. Each round of treatment had its own treated group (N = 3 mice) with the corresponding dose of ABD-3001, but only one control group (N = 3 mice) treated with ABD-3000 (empty liposomes) was established, at a dose of 5 mg/kg. For both ABD-3001 and ABD-3000, nanoparticles were resuspended in 0.9% NaCl and administered intranasally using a micropipette. Mice were weighted before each drug administration in order to calculate the necessary volume of drug solution, and weight

values were recorded in order to monitor weight loss along the treatment. The treatment schedule consisted of three administrations per week (Monday, Wednesday and Friday) until the animal's death or euthanasia by cervical dislocation (euthanasia was carried out on the same basis as explained in **section 3.17**). One h after the last drug administration, whole bodies and organs of some of the treated mice were kept as described in **section 3.17** for necropsy and biodistribution studies, respectively.

3.18.3. Magnetic resonance imaging

Apart from the body weight of mice, tumor volume evolution was also monitored during the treatment. Tumor volumes were assessed by magnetic resonance imaging (MRI) at a 7T BioSpec 70/30 USR spectrometer (Bruker BioSpin GmbH, Ettlingen, Germany) at the Servei de Ressonància Magnètica of UAB, twice a week (Monday and Friday) and following drug administration. Mice were positioned in a dedicated bed which allowed the delivery of anesthesia (isofluorane, 1.5-2% in O_2 at 1 L/min), with an integrated heating circuit to regulate body temperature. Frequency of respiration was monitored with a pressure probe and kept between 60-80 breaths/min. T2-weighted MRI was acquired using a rapid acquisition with relaxation enhancement sequence. The acquisition parameters were as following: repetition time (TR) / effective echo time (TEeff) = 4200/36 ms; echo train length (ETL) = 8; field of view (FOV) = 19.2 mm x 19.2 mm; matrix size (MTX) = 256 x 256 (75 µm/pixel x 75 µm/pixel); number of slices (n) = 10; slice thickness (ST) = 0.5 mm; inter-ST = 0.1 mm; number of averages (NA) = 4; total acquisition time (TAT) = 6 min and 43 s. Tumor volumes were calculated from MRI acquisitions using ParaVision 5.1 software (Bruker BioSpin GmbH, Ettlingen, Germany), by generating regions of interest (ROIs) to measure the tumor area in each slice. Tumor volumes were determined with the following equation: $TV\ (mm^3) = [(AS1\ x\ ST) + [(\sum_2^{10} ASn)\ x\ (ST + IT)]]\ x\ 0.075^2$ where TV is the tumor volume; AS is the number of pixels contained in the ROI delimited by the tumor boundaries in each slice of the MRI sequence; n is the slice number; ST is the slice thickness (0.5 mm), while IT is the inter-slice thickness (0.1 mm), and 0.075^2 is the individual pixel surface area in mm^2.

3.19. Necropsy

Necropsy studies were carried out by a service belonging to Unitat de Patologia Murina i Comparada of the Faculty of Veterinary Medicine of UAB.

3.20. Analysis of DIMATE biodistribution

Tissue samples from mice treated with ABD-3001, obtained in the tolerability and therapeutic efficacy assays, as described in **sections 3.17** and **3.18**, respectively, were firstly thawed and dissolved in tissue protein extraction reagent (T-PER, ThermoFisher), by adding 10 µL of reagent per mg of tissue. Tissue samples in T-PER were then completely homogenized by sonication (three cycles of 10 s on with 20% amplitude, separated by 15 s off). Next, homogenized samples were centrifuged at 4°C for 5 min at 9,300 x g, and supernatants were transferred to new Eppendorf tubes and kept in an ice bath. Supernatants (500 µL) were filtered with an Amicon 10K (Merck) by centrifugation at 4°C for 15 min at 14,000 x g. Finally, 10 µL of 1% TFA solution were added to 90 µL of filtered extract, in order to have the samples at 0.1% TFA, and 80 µL of these samples were injected into HPLC under the conditions described in **section 3.7** for the detection of DIMATE.

Prior to this analysis, the same method was applied to detect DIMATE in a GL261 cell culture treated with ABD-3001. Specifically, GL261 cells at the exponential phase of growth, contained in a T75 flask, were treated with 100 µM ABD-3001 and incubated at 37°C for 2 h. Next, the pellet was collected and the cell lysate was obtained using M-PER, following the manufacturer's instructions. The cell lysate was then filtered with an Amicon 10K centrifugal filter and prepared as described above before injection into HPLC.

Another preliminary study consisted in the detection of DIMATE in liver samples from control mice, only treated with ABD-3000 (empty liposomes), in which ABD-3001 was added directly. The preparation of these samples was the same as described in the first paragraph of this section, but different amounts of ABD-3001 were directly added to the tissue before the addition of T-PER. Specifically, the liver was sliced into 4 pieces of the same weight, and 0.5, 1, 2, and 4 µg of ABD-3001 were added to the different samples.

Finally, another experiment performed related to DIMATE biodistribution studies was the analysis of DIMATE incubated with reduced glutathione (GSH). Briefly, 100 µM DIMATE was incubated with 1, 10, or 100 µM GSH, at 37°C for 1 h, and then samples were prepared in a 0.1% TFA solution prior to injection into HPLC.

RESULTS

4.1. Characterization of ABD-3001 nanoparticles

ABD-3001 consists of liposomes containing DIMATE. Some properties of these nanoparticles were studied prior to their use in the *in vitro* experiments with cell cultures and in the *in vivo* experiments with mice. Specifically, the characterization of their physicochemical properties was carried out by cryo-TEM and DLS. In addition, the release of DIMATE was assessed by dialysis followed by HPLC detection.

4.1.1. Cryo-TEM

Firstly, both ABD-3000 (empty liposomes) and ABD-3001 were analyzed by cryo-TEM, in order to observe the morphology of nanoparticles and assess their diameter. **Figures 17** and **18** show ABD-3000 and ABD-3001 nanoparticles, respectively, visualized under cryo-TEM at different magnifications. Then, in order to determine the diameter of nanoparticles, 105 nanoparticles of a single cryo-TEM image were counted and analyzed using ImageJ software. The resulting size distributions for ABD-3000 and ABD-3001 are represented in **Figure 19**.

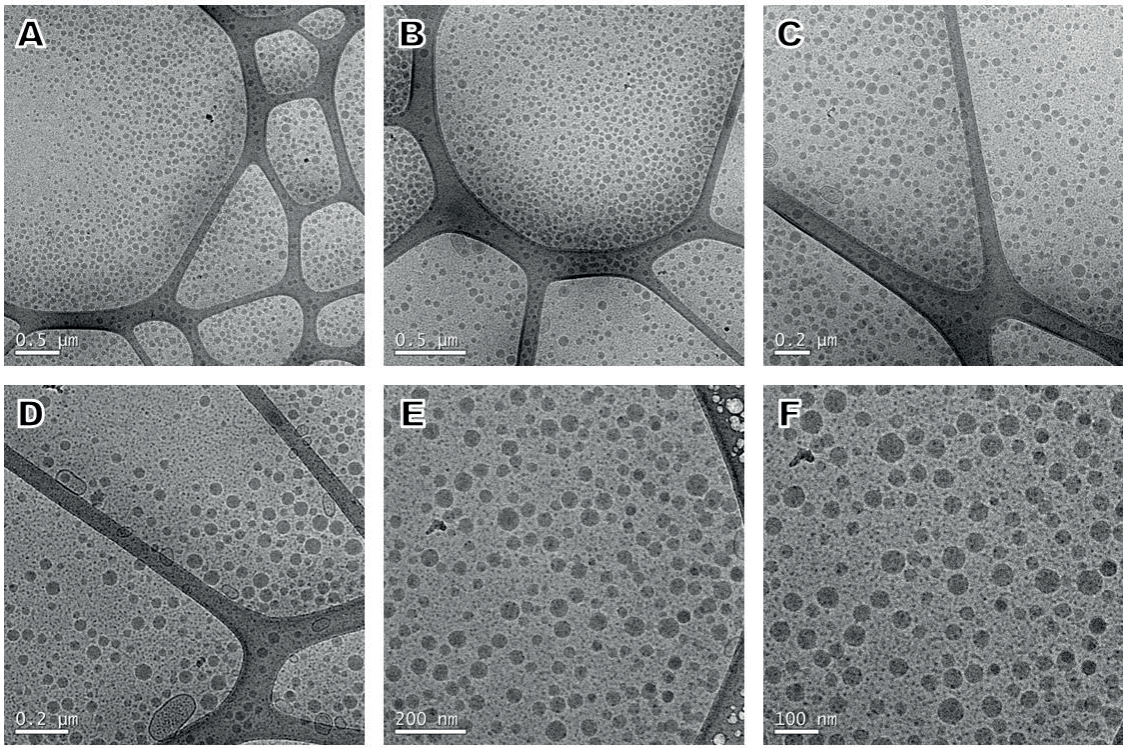

Figure 17. ABD-3000 nanoparticles visualized under cryo-TEM. (A) 5,000x; **(B)** 8,000x; **(C)** 10,000x; **(D)** 15,000x; **(E)** 20,000x; **(F)** 25,000x.

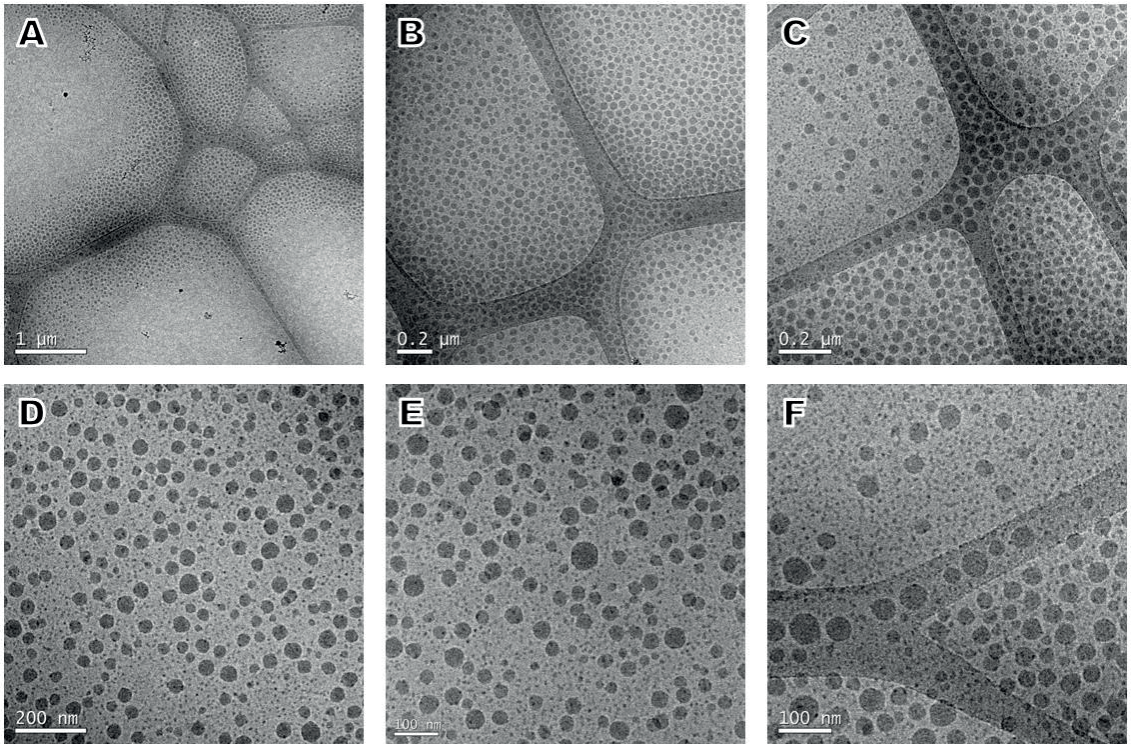

Figure 18. ABD-3001 nanoparticles visualized under cryo-TEM. (A) 4,000x; **(B)** 10,000x; **(C)** 15,000x; **(D)** 20,000x; **(E)** 25,000x; **(F)** 40,000x.

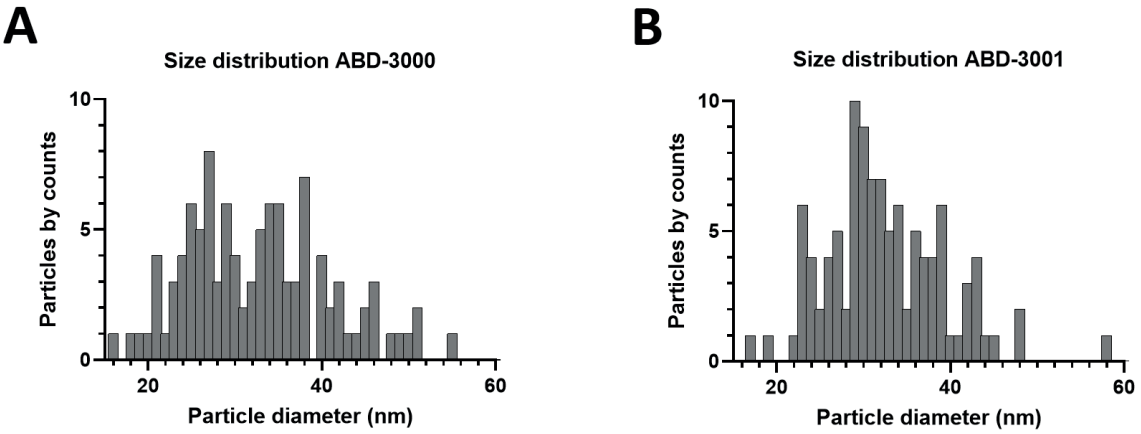

Figure 19. Size distribution of nanoparticles observed under cryo-TEM. (A) ABD-3000: the diameter of 105 nanoparticles from Figure 17F was measured using ImageJ software; the mean diameter (± SD) was 32.66 ± 8.21 nm. **(B)** ABD-3001: the diameter of 105 nanoparticles from Figure 18E was measured using ImageJ software; the mean diameter (± SD) was 32.50 ± 6.80 nm.

To sum up, cryo-TEM analysis revealed that both ABD-3000 and ABD-3001 nanoparticles have a spherical shape and a diameter around 30 nm. Furthermore, the low dispersion of diameters suggests that both solutions are highly monodisperse. These properties could make these nanoparticles suitable for drug delivery purposes. Specifically, it has been reported that nanoparticles with an average size up to 200 nm can be efficiently transported transcellularly via the intranasal route [203], which will be used for the *in vivo* experiments discussed later in

this thesis. Finally, comparison of empty and loaded nanoparticles indicates that the presence of DIMATE does not affect neither their morphology nor their size.

4.1.2. DLS

Following the observation of ABD-3001 under cryo-TEM, the nanoparticles were analyzed by DLS in order to determine their hydrodynamic diameter, PdI, and zeta potential. ABD-3001 nanoparticles were analyzed during four consecutive days to study their stability both under storage and physiological conditions.

Measurements taken along the four days of the experiment indicated that the properties of ABD-3001 nanoparticles did not change during this period of time. However, these properties were different under the two conditions tested. Comparison between the features of ABD-3001 nanoparticles under storage and physiological conditions is presented in **Table 3**.

Table 3. Hydrodynamic diameter, PdI and zeta potential of ABD-3001 nanoparticles under storage and physiological conditions, obtained by DLS analysis. Data are the mean ± SD of all measurements performed during the four days for each property tested (total of 12 measurements per property).

	Storage conditions[1]	**Physiological conditions**[2]
Diameter (nm)	60.52 ± 13.72	139.50 ± 20.60
PdI	0.35 ± 0.02	0.21 ± 0.02
Zeta potential (mV)	−0.40 ± 0.55	−0.80 ± 0.27

[1] 4°C, 8.35 mg/mL
[2] 37°C, 0.2 mg/mL

Firstly, the diameter of ABD-3001 nanoparticles obtained by DLS was higher than that obtained by cryo-TEM, which was around 30 nm (**section 4.1.1**). This was expected, since DLS measures the hydrodynamic diameter (i.e. the diameter of the nanoparticles in solution, which contain layers of solvent), whereas cryo-TEM measures the diameter of dry nanoparticles. However, the possibility that the size is higher due to some aggregation between nanoparticles cannot be discarded. In fact, the clearly higher diameter of ABD-3001 nanoparticles under physiological conditions compared to storage conditions could indicate that, in the former case, liposomes are not so stable and tend to form greater aggregates. This would agree with the fact that the zeta potential is nearly 0, since neutral surface charge is considered as a factor that can promote aggregation. In general, nanoparticles with zeta potential below −30 mV or above +30 mV are known to be more stable and less prone to aggregate. Finally, the low PdI values obtained for both conditions indicate that the nanoparticle solutions are monodisperse, as already suggested by the observations using cryo-TEM.

4.1.3. Release of DIMATE

In order to evaluate the release profile of DIMATE from ABD-3001 nanoparticles, a dialysis experiment was performed, followed by HPLC analysis. Since the mechanism of entrance of ABD-3001 nanoparticles into the cell is still unknown, release was analyzed at two different pH values: 5.0 (which could be suitable in the case that nanoparticles end up in the lysosomes) and 7.0 (physiological pH).

HPLC analysis revealed that three peaks were associated with the presence of DIMATE in the release samples collected during the 96 h of the experiment. A peak appearing at 12.4 min corresponds to the molecule of DIMATE itself, since it was the only peak appearing in the DIMATE calibration experiment (**Annex 1.1**). Additionally, two other peaks, with retention times 11.3 min and 12.9 min, appear in the chromatogram and increase with time as the peak at 12.4 min decreases. **Figure 20** shows the presence of these three peaks in the chromatogram and their evolution in time. This finding suggests that the molecule of DIMATE is degraded with time in PBS and leads to the formation of two different molecules. Interestingly, this degradation was more accentuated at pH 7.0, compared to pH 5.0. This seems to indicate that the DIMATE molecule is slightly more stable under acidic conditions.

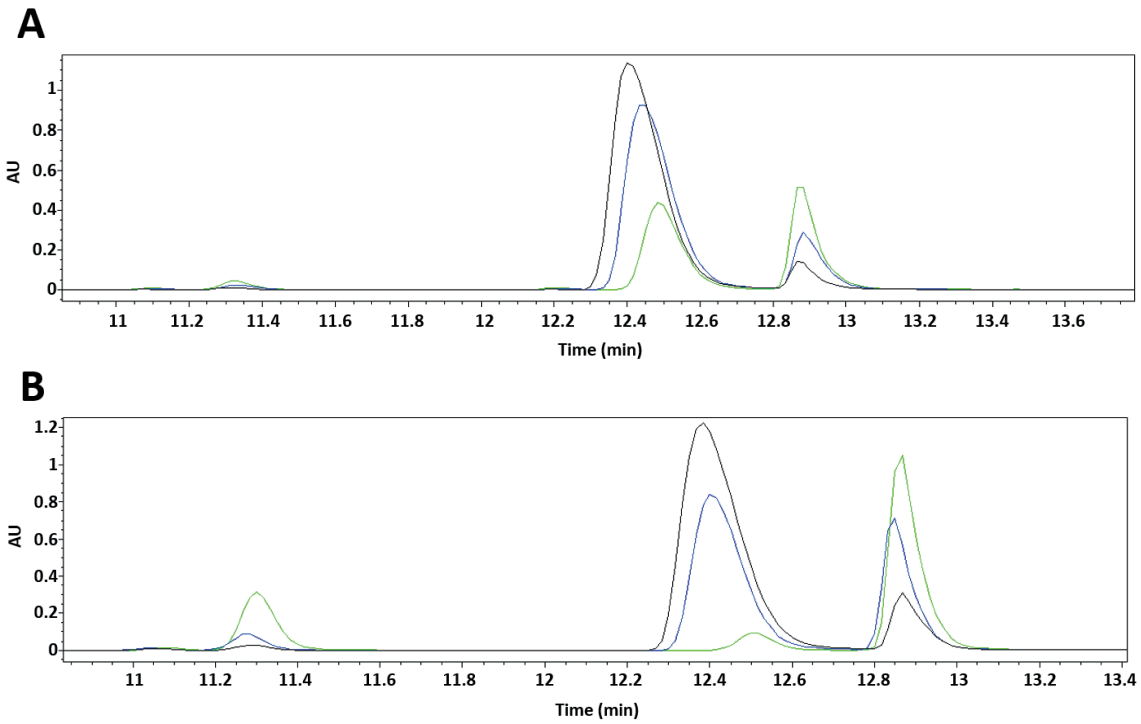

Figure 20. HPLC detection of DIMATE released from ABD-3001 nanoparticles. HPLC chromatograms show the three peaks associated with the presence of DIMATE in samples collected during the release experiment at **(A)** pH 5.0 and **(B)** pH 7.0. **Black**: chromatogram after 10 h of release; **blue**: chromatogram after 24 h of release; **green**: chromatogram after 96 h of release. AU: absorbance units.

Since the only calibration curve that could be obtained was that of the original DIMATE molecule (**Annex 1.1**), from the peak with retention time 12.4 min, absolute values for amount of DIMATE in ng could only be calculated from this peak, and not from the other two peaks presumably corresponding to degradation products. Thus, **Figure 21** only shows the percentage of the original molecule of DIMATE released from ABD-3001 nanoparticles, without considering the presence of other byproducts. For this reason, a decrease of release is observed after 4 h: DIMATE keeps releasing but, after this time, degradation is more and more evident and the original molecule of DIMATE disappears. Nevertheless, a rapid burst of DIMATE release can still be observed during the first 4 h both at pH 5.0 and pH 7.0. During this time, approximately 70% of total DIMATE is released. No major differences in the release rate are seen between the two pH values.

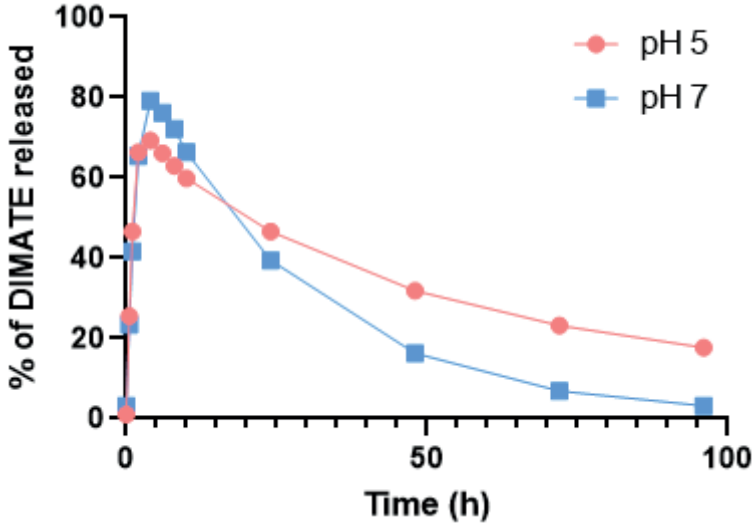

Figure 21. Follow-up of DIMATE release from ABD-3001 nanoparticles. Release of DIMATE was monitored at pH 5.0 (**red**) and pH 7.0 (**blue**) along 96 h. Percentage of DIMATE released, obtained from the 12.4-min peak areas, is plotted against time.

The observation that the molecule of DIMATE is unstable and probably degrades with time in aqueous buffer strengthens the idea that the encapsulation of this drug is necessary for drug delivery purposes when used in *in vivo* experiments.

4.2. *In vitro* studies in a panel of GB cell lines

The main part of this thesis is focused on the study of the effect of the ALDH inhibitors (structures are shown in **Figure 16**) on different GB cell lines.

4.2.1. Automated capillary-based immunoassay

The expression of ALDH isoenzymes ALDH1A1, ALDH1A2 and ALDH1A3, which are the main responsible for the generation of RA in the cell, was assessed at the protein level by an automated capillary-based immunoassay in a panel of seven GB cell lines: six human cell lines (LN229, T98G, U251-MG, U373, U87-MG and A172) and one murine cell line (GL261). In addition, a non-cancerous human astrocytic cell line derived from the stem cell line Ax-0019 [196] was also included in the study.

Figure 22 shows the expression levels of ALDH1A1, ALDH1A2 and ALDH1A3 for all the cell lines tested. Clearly, ALDH1A3 is highly expressed in all the cell lines tested except for T98G. The low expression in T98G has also been observed in other studies, such as that performed by Wu *et al*. [204]. ALDH1A1 and ALDH1A2 display the highest expression in LN229 and A172.

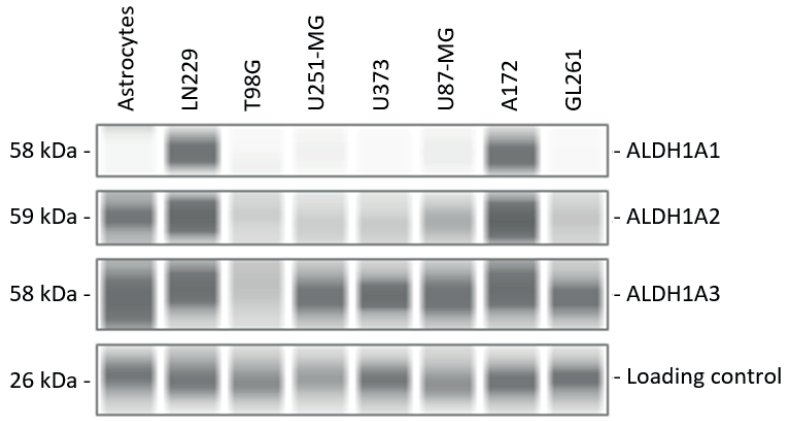

Figure 22. Immunoblot analysis of ALDH1A expression in a panel of GB cell lines and astrocytes. Comparisons here can be made across all cell lines for a single isoform, but not in the same cell line for different isoforms, since the different isoforms were tested in different runs of capillary electrophoresis, using different primary antibody dilutions and incubation times. The blot was cropped to show the ALDH bands only.

4.2.2. Cytotoxicity assays with TMZ and ALDH inhibitors as monotherapies

The cytotoxicity of the gold standard for GB treatment, TMZ, and the ALDH inhibitors presented above (namely DIMATE, ABD-3001, ABD0099 and ABD0171) was tested in the panel of GB cell lines. Briefly, cells were treated for 48 h with each compound and EC_{50} values, indicated in **Table 4**, were calculated from dose-response curves, which are shown in **Figure 23**.

Table 4. EC_{50} values (μM) ± SE of TMZ and ALDH inhibitors in the panel of GB cell lines after 48-h treatment. Shown here are the results of the fitting of the data from a single representative experiment with triplicates, performed at least twice independently, to a 4-parameter equation using GraFit 5.0 (Erithacus software). EC_{50} is defined as the concentration of drug that exerts half of the maximal response.

	Cell lines						
Drug	**LN229**	**T98G**	**U251-MG**	**U373**	**U87-MG**	**A172**	**GL261**
TMZ	3,598 ± 248	4,778 ± 490	> 5,000*	855 ± 65	> 5,000*	3,390 ± 118	3,281 ± 176
DIMATE	2.15 ± 0.27	6.72 ± 0.24	3.30 ± 0.08	6.62 ± 0.23	4.01 ± 0.15	3.77 ± 0.27	3.03 ± 0.08
ABD-3001	3.16 ± 0.16	7.97 ± 0.54	3.91 ± 0.27	22.67 ± 0.86	5.04 ± 0.44	4.48 ± 0.12	2.14 ± 0.11
ABD0099	3.41 ± 0.17	42.63 ± 1.11	14.92 ± 0.48	10.99 ± 0.40	5.39 ± 0.32	2.15 ± 0.13	8.95 ± 0.19
ABD0171	2.47 ± 0.08	8.83 ± 0.42	2.59 ± 0.11	11.78 ± 0.32	5.97 ± 0.20	5.34 ± 0.26	6.01 ± 0.09

* EC_{50} value is greater than 5,000 μM and could not be exactly determined experimentally due to the fact that 0% cell viability could not be reached at the concentrations of TMZ tested in the assay (higher concentrations of TMZ were not possible to achieve due to solubility issues).

From the EC_{50} values, it is clear that the ALDH inhibitors are far more cytotoxic than TMZ in all cell lines tested. Remarkably, there is a difference of approximately three orders of magnitude between the potency of ALDH inhibitors and TMZ, except for the cell line U373, which seems to be more sensitive to TMZ than the others. U373 is one of the cell lines expressing less ALDH1A1 (**Figure 22**), and it is already reported in the literature that ALDH1A1 is a mediator of TMZ resistance [136]. Although it could be a cause for the higher sensitivity to the drug, other factors that are beyond the scope of this work are most likely involved (such as the *MGMT* status), since the cell lines expressing the higher amount of ALDH1A1 (namely LN229 and A172) are not the most resistant to TMZ. In a similar manner, it does not seem to exist a direct relationship between ALDH1A3 expression, also involved in TMZ resistance according to literature [137], [138], and the effect of TMZ observed here, since the sensitivity of T98G (the cell line expressing less ALDH1A3) does not differ a lot from that of the rest of cell lines.

The EC_{50} value of the ALDH inhibitors in all cell lines falls within the low micromolar range. The exception is the EC_{50} value of ABD0099 in the cell line T98G, which is quite higher than in the rest of cases. A suitable explanation could be that this cell line expresses relatively low amounts of all the three ALDH1A isoforms (**Figure 22**), although further experiments would be needed to confirm this hypothesis.

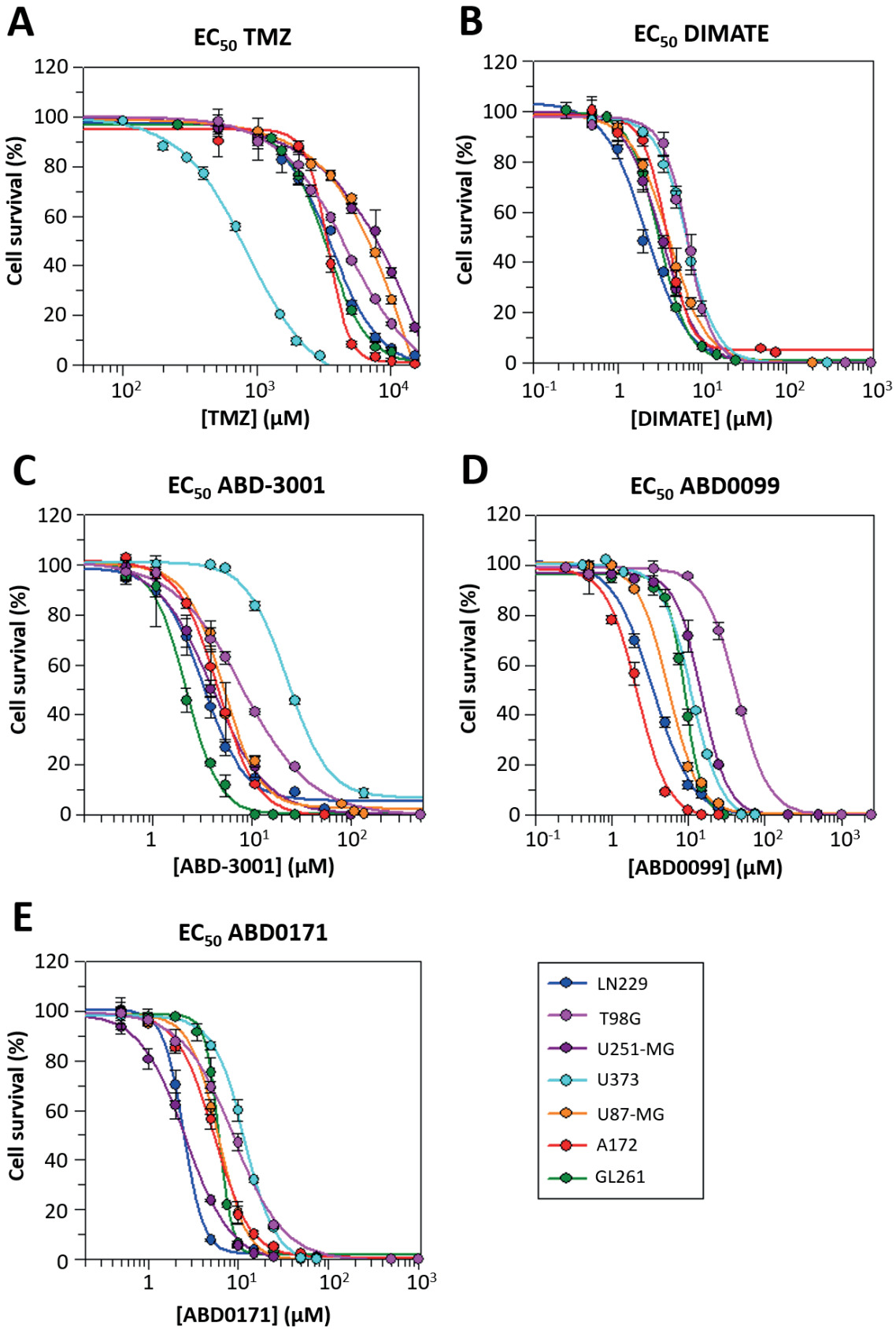

Figure 23. Dose-response curves for TMZ and ALDH inhibitors in the panel of GB cell lines after 48 h treatment. (A) TMZ; **(B)** DIMATE; **(C)** ABD-3001; **(D)** ABD0099; **(E)** ABD0171. Data points are the mean ± SE of triplicates from a single representative experiment, performed at least twice independently. Curves were obtained using GraFit 5.0 (Erithacus software).

4.2.3. ALDH activity assays

The experiments shown from now on were only performed in one of the human GB cell lines, specifically A172, and in the murine GB cell line GL261. A172 was chosen out of all the human cell lines because it was one of the cell lines expressing the highest levels of all three ALDH1A isoforms (**Figure 22**). GL261 was chosen because it is the only murine cell line out of all the cell lines tested, and it is used for the generation of the animal GB model (*in vivo* experiments in this model are detailed in **section 4.3**).

Enzymatic activity assays were performed in order to evaluate the inhibitory capacity of DIMATE, ABD0099 and ABD0171 against cellular ALDH activity. ABD-3001 was not included in these assays, since the inhibitory molecule *per se* is DIMATE. Activity was tested using two different substrates: hexanal and all-*trans*-RAL. The former is the standard substrate used routinely for the kinetic characterization of ALDH inhibitors [205]; the latter is the physiological substrate of ALDH1A1, ALDH1A2 and ALDH1A3, which is oxidized to RA, which in turn regulates numerous signaling pathways related with cell proliferation and differentiation, as mentioned above. The inhibition of this particular reaction in GB cells could be of great interest for pharmacological purposes.

Absolute values of ALDH activity in the absence of inhibitor, both with hexanal and all-*trans*-RAL as substrates, are shown in **Table 5**. Comparison of the values between cell lines indicates that ALDH activity is higher in A172 cells compared to GL261 cells with both substrates. In fact, RAL dehydrogenase activity could only be detected in A172 cells. It is conceivable that ALDH1A content in GL261 extract was not high enough in order to produce detectable levels of RA. These results are consistent with immunoblot analysis (**Figure 22**). Additionally, the activity is higher using hexanal substrate than using RAL in both cell lines, probably because more ALDH enzymes are active with hexanal.

Table 5. Absolute values of ALDH specific activity (mU/mg) in A172 and GL261 cell extracts using hexanal or all-*trans*-RAL as a substrate. Specific activity is expressed in mU per mg of total protein present in the cell extract; here, 1 mU is defined as 1 nmol of product generated per min. Values are the mean ± SD of triplicates.

	Substrate	
Cell line	**Hexanal**	**all-*trans*-RAL**
A172	1.79 ± 0.02	0.05 ± 0.01
GL261	0.47 ± 0.06	ND

ND: not detected

Remaining enzymatic activities of A172 and GL261 cell extracts were determined in the presence of each ALDH inhibitor. As shown in **Table 6**, ALDH activity with hexanal decreased in the

presence of 15 µM inhibitor. ABD0171 seemed to be the most potent inhibitor of cellular ALDH activity both in A172 and GL261, since it displayed the lowest value of remaining activity.

Table 6. Remaining ALDH activity in A172 and GL261 cell extracts using hexanal as a substrate, in the presence of 15 µM inhibitor. Values are the mean ± SD of triplicates.

	Inhibitor (at 15 µM)		
Cell line	**DIMATE**	**ABD0099**	**ABD0171**
A172	68.51 ± 4.85 %	93.32 ± 1.10 %	39.75 ± 3.07 %
GL261	71.22 ± 13.57 %	68.15 ± 8.84 %	50.61 ± 6.90 %

Remaining activities with all-*trans*-RAL are shown in **Table 7**. In this case, ALDH activity in A172 also decreased in the presence of inhibitor. Furthermore, the remaining activity decreased with increasing concentrations of compound. Specifically, DIMATE seemed to be here the most potent inhibitor.

Table 7. Remaining ALDH activity in A172 cell extract using all-*trans*-RAL as a substrate, in the presence of increasing concentrations of inhibitor. Values are the mean ± SD of duplicates.

Inhibitor								
DIMATE			**ABD0099**			**ABD0171**		
5 µM	**50 µM**	**250 µM**	**5 µM**	**50 µM**	**250 µM**	**5 µM**	**50 µM**	**250 µM**
42.09 ± 4.64 %	11.34 ± 1.36 %	6.04 ± 1.03 %	96.64 ± 2.29 %	73.89 ± 1.50 %	34.09 ± 0.09 %	66.73 ± 1.45 %	26.17 ± 1.40 %	23.91 ± 2.29 %

A graphical illustration of the inhibition assay with DIMATE using all-*trans*-RAL as a substrate is represented in **Figure 24**, where the chromatograms resulting from HPLC analysis of retinoids are shown. As indicated, the peak corresponding to RA product decreased when a higher amount of DIMATE was present in the reaction mixture.

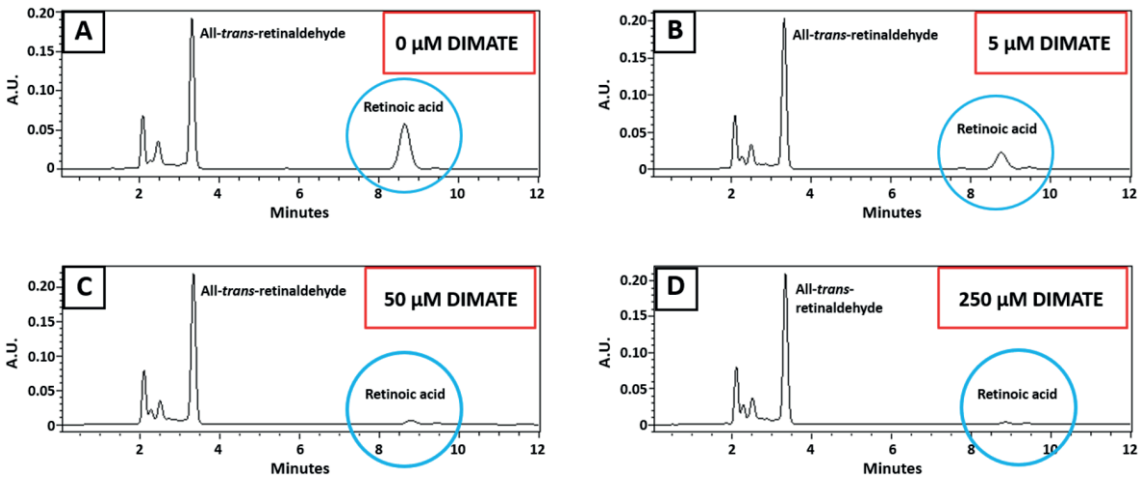

Figure 24. Representative HPLC analysis of ALDH activity in A172 cell extract using all-*trans*-RAL as a substrate in the presence of increasing concentrations of DIMATE. (A) 0 µM DIMATE; **(B)** 5 µM DIMATE; **(C)** 50 µM DIMATE; **(D)** 250 µM DIMATE. Absorbance units (A.U.) are represented in the *y* axis, while retention time (minutes) is represented in the *x* axis. The peaks corresponding to all-*trans*-RAL substrate and RA product (the latter circled in blue) appear at 3.5 and 8.5 min, respectively.

4.2.4. Synergy assays combining TMZ and ALDH inhibitors

In order to assess whether TMZ and ALDH inhibitors could act synergistically in the treatment of GB, drug combination assays were performed in A172 and GL261 cell lines.

Synergy maps and scores obtained for each drug combination are shown in **Figure 25**. Data analysis revealed that only the combination of TMZ with DIMATE was synergistic in the treatment of A172 cells (synergy score of 17.21), while the combination with the other inhibitors resulted in an additive effect (**Figure 25A**). This could be related to the fact that DIMATE was the best compound at inhibiting the production of RA (**Table 7**). Hence, this might suggest that some RA-regulated signaling pathways could be, in part, responsible for TMZ resistance in GB.

Conversely, combinations of TMZ with ABD-3001, ABD0099 and ABD0171 were synergistic in GL261 (**Figure 25B**), suggesting that ALDHs may also be somehow implicated in the mechanism of resistance to TMZ in this cell line. Specifically, the most synergistic combination was that of TMZ with ABD0171 (synergy score of 17.62). Interestingly, previous results obtained by the research group indicated that ABD0171 was the most potent inhibitor towards ALDH1A3 (Pequerul *et al*., unpublished results), which seems to be one of the predominant isoforms in GL261 (**Figure 22**). In fact, ABD0171 was the compound yielding the lowest value of remaining activity with hexanal in this cell line (**Table 6**).

Differences between the combination therapies TMZ+DIMATE and TMZ+ABD-3001 are difficult to explain. Probably, the active amount of DIMATE in ABD-3001 is lower due to DIMATE molecules getting trapped within the lipidic nanoparticles, and could be one of the reasons underlying the differences observed. In addition, in the assays performed with DIMATE, a small amount of ethanol solvent is present, conversely to the assays performed with ABD-3001. This might also be a cause of the differences observed.

Finally, since the regions of synergy appear at mid to low concentrations of TMZ, combination therapies using ALDH inhibitors could help reducing the amount of TMZ used compared to the TMZ monotherapy.

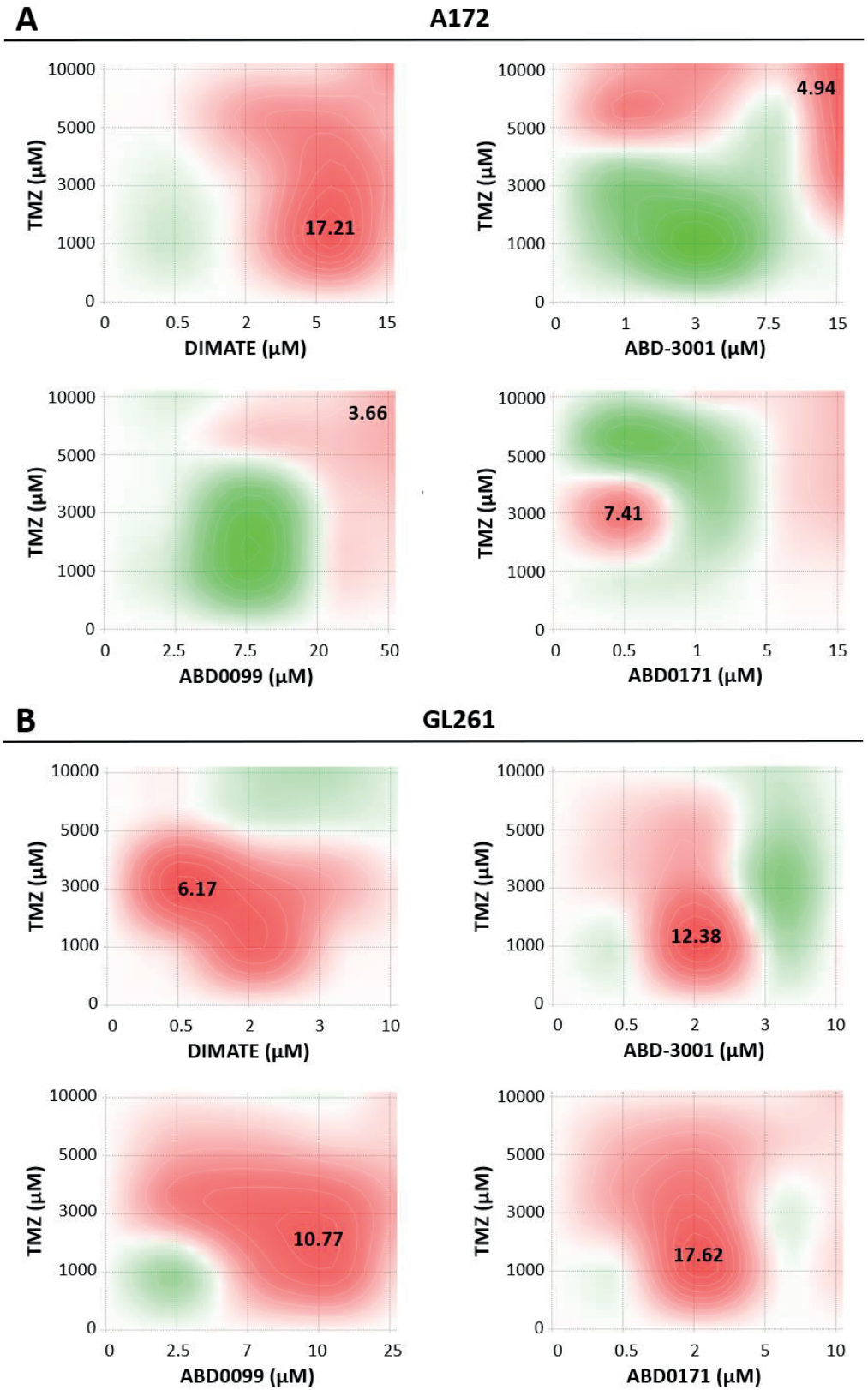

Figure 25. Synergy maps for 48-h treatments using TMZ combined with each ALDH inhibitor in (A) A172 and (B) GL261, obtained after analysis with SynergyFinder software, according to the reference model of Bliss [198]. The concentration of TMZ is represented in the *y* axis, whereas the concentration of each ALDH inhibitor is represented in the *x* axis. Synergy scores of the most synergistic areas are indicated in the map. Scores below −10 indicate antagonism (**green**); scores between −10 and 10 indicate an additive effect (**light green** to **light red**); scores above 10 indicate synergism (**red**). Shown here is the result of a single representative experiment consisting of duplicates for each drug concentration. The experiment was performed at least twice independently.

4.2.5. Assays to assess the mechanism of death induced by TMZ and ALDH inhibitors

In order to further investigate how the ALDH inhibitors tested in this study elicit their toxicity on GB, experiments to assess the mechanism of cell death and generation of ROS were performed in A172 and GL261 cell lines, respectively. TMZ was also included in these tests.

Cell death analysis by flow cytometry, after 24-h treatment with the compounds, indicated that there is a tendency towards apoptosis, rather than necrosis, since the number of cells labelled by annexin V increased more than those labelled by propidium iodide, compared to untreated cells, in both A172 and GL261 cell lines, as shown in **Figure 26**. In fact, statistical analysis revealed that only changes in apoptotic cells, and not in necrotic cells, was significant compared to the respective untreated controls.

The process by which cell death is triggered in A172 cells seems to be independent of ROS-induced damage, as none of the compounds was able to generate ROS at significant levels compared to untreated cells (**Figure 27**), except for ABD-3001. In contrast, cell death might be induced, in part, by ROS in GL261, since treated cells showed slightly but significantly higher ROS levels than the control. GL261 cells treated with compounds ABD0099 and ABD0171 displayed higher ROS levels than cells treated with DIMATE. Interestingly, TMZ combinations with ABD0099 and ABD0171 where more synergistic than that with DIMATE in this cell line (**Figure 25**), suggesting that ROS could be somehow involved in the mechanism of synergy.

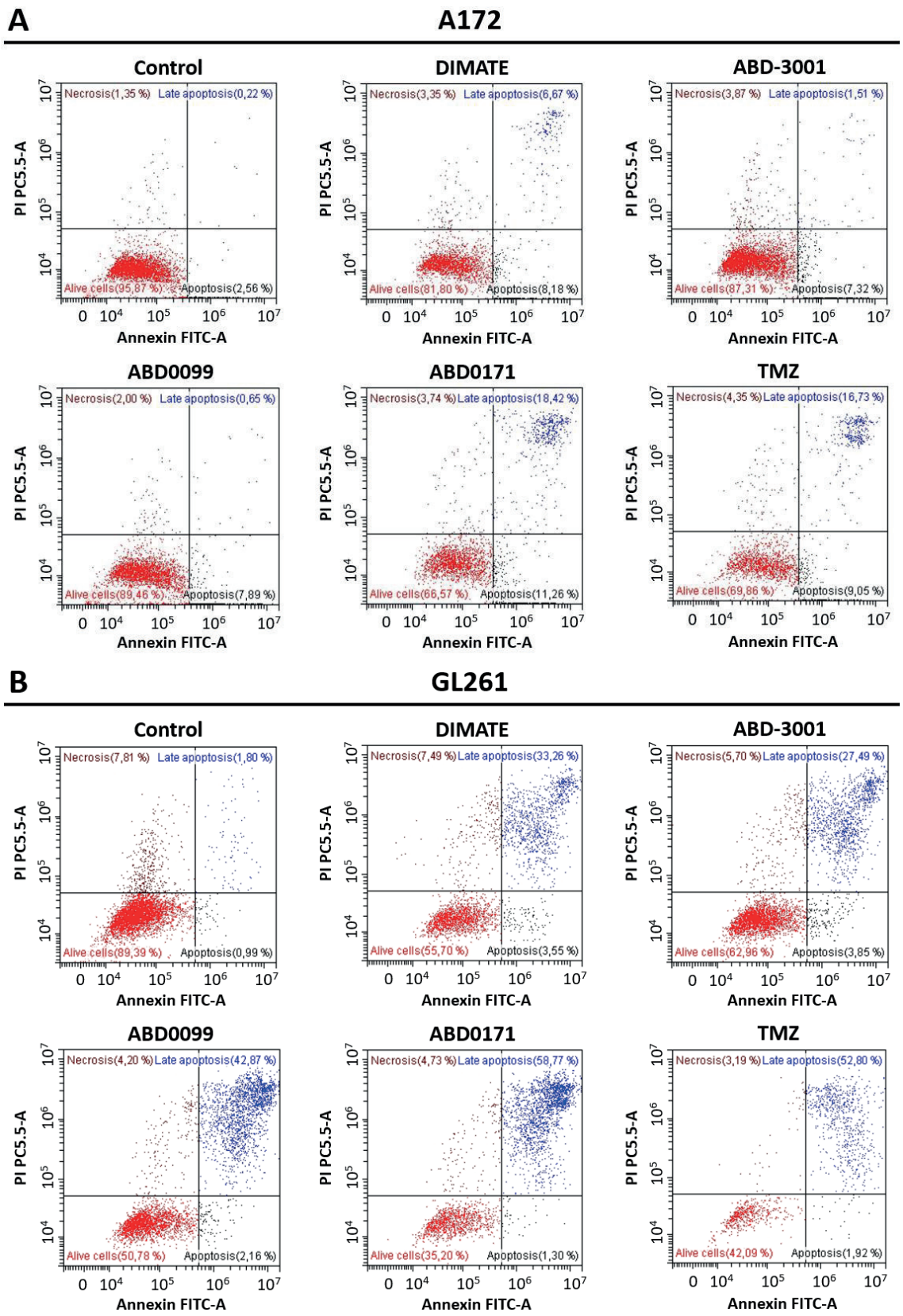

Figure 26. Cell death analysis by flow cytometry after 24-h incubation with TMZ or ALDH inhibitors in (A) A172 and (B) GL261 cells. Iodide propidium labeling (necrosis) is represented in the *y* axis, whereas annexin V labeling (apoptosis) is represented in the *x* axis. Cells in the "late apoptosis" region of the cytogram could come from either necrotic or apoptotic cells. The result of a single representative experiment is shown here, consisting of duplicates for each drug treatment (to simplify, only one of the duplicates is shown). The experiment was performed at least twice independently.

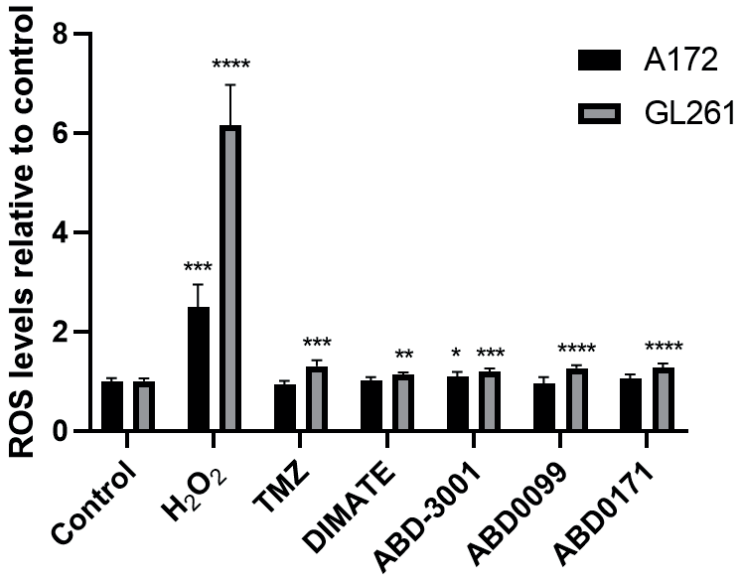

Figure 27. Relative intracellular levels of ROS in A172 and GL261 cells after 6-h treatment with 500 µM H_2O_2 (used as a positive control), TMZ or ALDH inhibitor at the concentration equal to the EC_{50} value. Data are the mean ± SD of six replicates from a single representative experiment. The experiment was performed at least twice independently. Asterisks indicate statistical significance compared to the respective control, as analyzed by unpaired t test with Welch's correction. * 0.01 < P < 0.05; ** 0.001 < P < 0.01; *** 0.0001 < P < 0.001; **** P < 0.0001.

A feasible explanation to the fact that cells treated with ALDH inhibitors show higher levels of ROS compared to untreated controls is that ROS generated by cellular processes such as lipid peroxidation cannot be detoxified anymore by ALDHs, so their levels increase in the cell. The reason why the ALDH inhibitors tested do not generate a significant increase in ROS levels in A172 but they do in GL261 might be the amount of enzyme present in each cell line. As shown in **Figure 22**, A172 cells express quite higher levels of ALDH enzymes than GL261 cells. Maybe, the amount of inhibitor used in this test was too low to inhibit all ALDH activity in A172, but it was high enough to inhibit the activity in GL261, so there were ALDH enzymes available in A172 to keep detoxifying ROS. Accordingly, A172 naturally exhibit a higher ALDH activity compared to GL261 (**Table 5**). This could explain that GL261 cells are more prone to oxidative stress than A172, as clearly suggested by the higher levels of ROS observed when cells are treated with H_2O_2.

In a similar study, Rebollido-Rios *et al*. [187] found that DIMATE induced apoptotic cell death in lung adenocarcinoma cell lines by causing the intracellular accumulation of apoptogenic aldehydes hydroxynonenal (HNE) and malondialdehyde (MDA), which led to high levels of ROS and a drop in the levels of GSH. GSH, a key molecule for the detoxification of ROS in cells [206], was shown to play a crucial role in cell survival against DIMATE-induced apoptosis.

4.2.6. Assays in an *ALDH*-knockout cell line

Finally, in order to study more deeply the role of ALDH enzymes in GB, an *ALDH* gene knockout was performed in the human cell line A172 by transfection with a CRISPR/Cas9 plasmid. From now on, the parental cell line A172 will be referred to as A172 WT, while the knockout cell line will be called A172 KO.

Firstly, immunoblot analysis and RT-PCR were performed in order to validate the *ALDH* knockout. As shown in **Figure 28**, the expression of several ALDHs was sharply reduced in A172 KO compared to A172 WT cells. At the protein level (**Figure 28A**), the most affected isoforms were the enzymes belonging to the ALDH1 family (namely, ALDH1A1, ALDH1A2, ALDH1A3 and ALDH2). The expression of other isoforms, such as ALDH1B1 and ALDH3A1, was also decreased. At mRNA level (**Figure 28B**), all screened isoforms were decreased, especially ALDH1A1 and ALDH1A3. At this time, we do not understand the mechanism by which the ALDH1A3 CRISPR/Cas9 KO plasmid also affects the expression of other *ALDH* genes. This effect has never been described before in other *ALDH1A3* gene knockout experiments [137], [181], [207], [208].

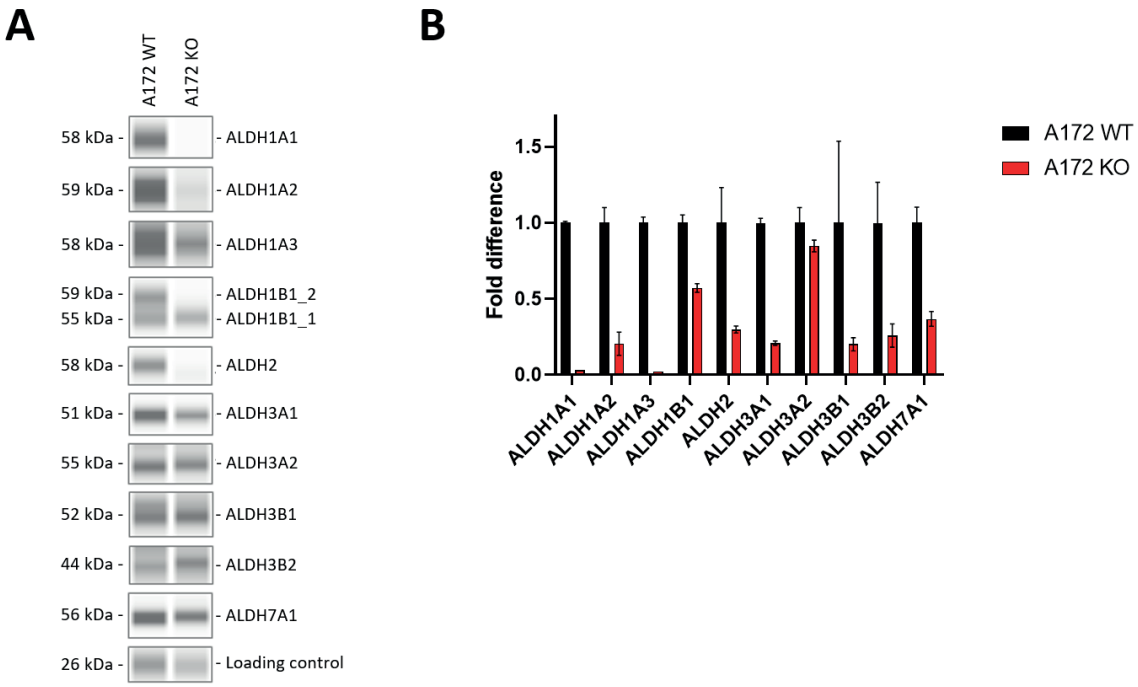

Figure 28. Validation of the *ALDH* gene knockout in the human GB cell line A172. (A) Western blot analysis of ALDH expression at the protein level in A172 WT and A172 KO cells; **(B)** RT-PCR analysis of *ALDH* expression at mRNA level in A172 WT and A172 KO cells. Data are the mean ± SD of triplicates; values were normalized by the expression of the housekeeping gene β-actin and represented relative to the WT cell line.

The ALDH activity in cell extracts from A172 WT and A172 KO cells was then determined using hexanal and all-*trans*-RAL as substrates (**Figure 29**). As expected, the enzymatic activity was much lower in A172 KO compared to A172 WT cells. In the case of hexanal substrate, a residual

activity remained in A172 KO cells (**Figure 29A**), since some of the ALDHs or other aldehyde-metabolizing enzymes that were not affected by the knockout might be able to oxidize hexanal. Conversely, when all-*trans*-RAL was used as the substrate, activity was completely abolished in A172 KO cells (**Figure 29B**). This result was not surprising, since it is well known that the main ALDH isoforms responsible for RAL oxidation are those belonging to the ALDH1A subfamily, highly affected by the knockout. Thus, the production of RA from RAL is impaired in this knockout cell line.

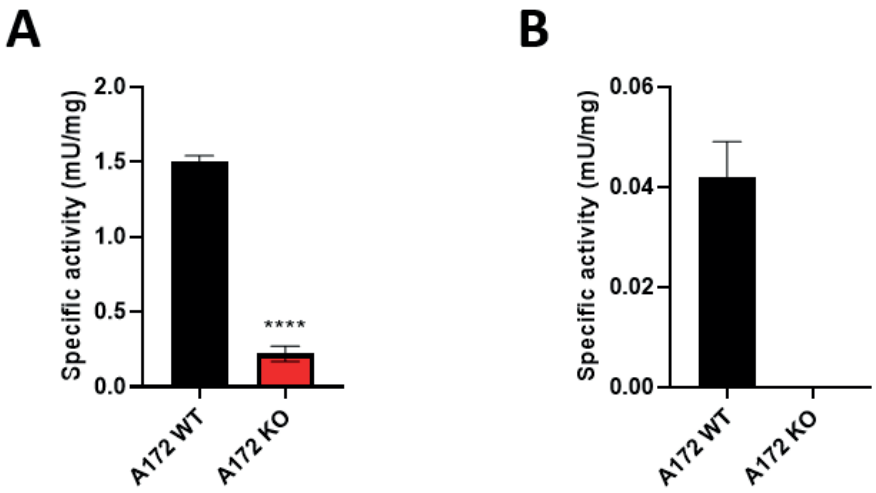

Figure 29. Comparison of ALDH activity in cell extracts from A172 WT and A172 KO cells. (A) Activity using hexanal as a substrate; **(B)** Activity using all-*trans*-retinaldehyde as a substrate. Data are the mean ± SD of triplicates. Specific activity is expressed in mU per mg of total protein present in the cell extract; here, 1 mU is defined as 1 nmol of product generated per min. Asterisks indicate statistically significant difference, as analyzed by unpaired t test with Welch's correction. **** $P < 0.0001$.

Once ALDH expression and activity had been checked in A172 WT and A172 KO cells, some experiments were performed in order to assess the impact of the lack of ALDHs on features such as cell proliferation and migration.

On the one hand, a growth curve was established for both A172 WT and A172 KO (**Figure 30**), which allowed to detect a slight decrease in the growth rate at the exponential phase in the knockout cell line compared to the wild type. The doubling time calculated for A172 WT cells was 1.68 days, whereas the doubling time for A172 KO cells was 2.27 days. The slower growth could be related with the impairment of RA production due to lack of ALDH1A enzymes, since this molecule is well known as a key regulator in the activation of a wide range of genes involved in cell proliferation. Similar results have been obtained before in other studies where ALDH knockout was carried out on GB cell lines, such the one performed by Li *et al*. [181]. It is also conceivable that toxic aldehydes generated by cellular processes such as lipid peroxidation cannot be properly eliminated because of lower ALDH activity [138], [185]–[187].

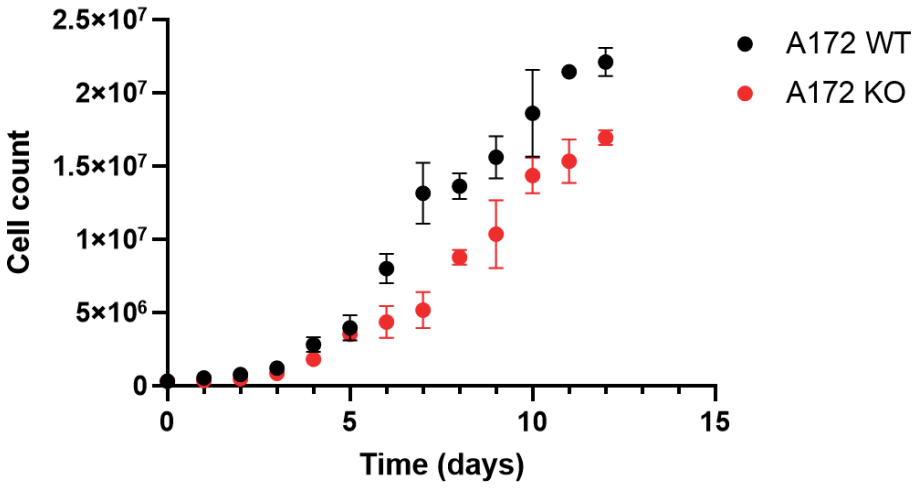

Figure 30. Growth curves for A172 WT and A172 KO cells. Data are the mean ± SD of triplicates.

On the other hand, cell migration capacity was analyzed. Results indicated that migration was also impaired in A172 KO compared to A172 WT cells (**Figure 31**), as the percent closure of the migration area in the former was approximately 16% lower compared to the latter after letting the cells migrate for 30 h.

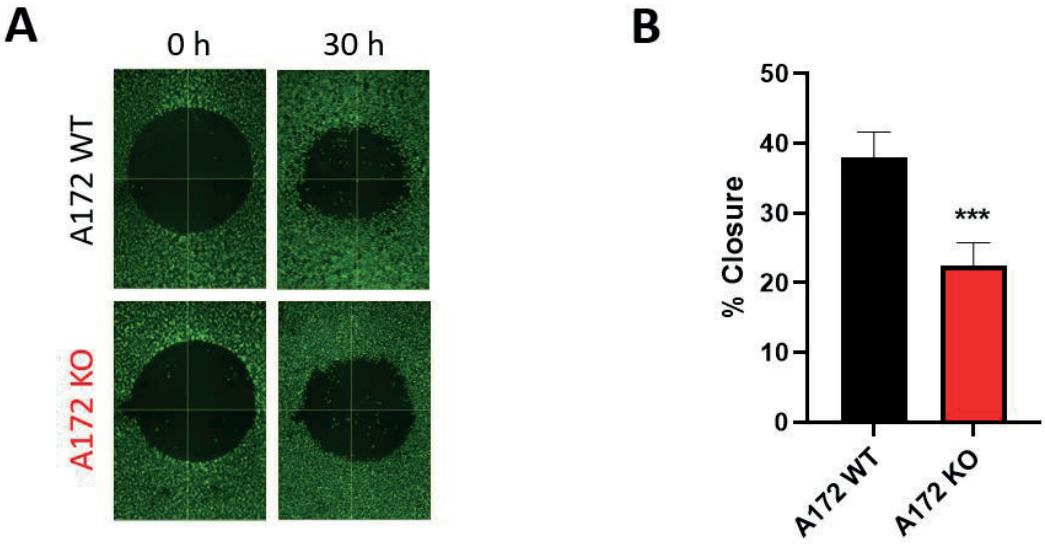

Figure 31. Comparison of the migration capacity in A172 WT and A172 KO cells. (A) Fluorescence images of migration areas of A172 WT and A172 KO cells after incubation with calcein dye, obtained in a SpectraMax plate reader at times 0 and 30 h; **(B)** percent closure of migration areas after 30 h in A172 WT and A172 KO cells. Data are the mean ± SD of four replicates. Asterisks indicate statistically significant difference, as analyzed by unpaired t test with Welch's correction. *** 0.0001 < P < 0.001.

These results strongly suggest that ALDHs are important in cancer cell processes such as proliferation and migration, directly related to features such as invasiveness and aggressiveness in GB tumors.

In the last part of the *in vitro* studies carried out on GB cell lines, the toxicity of all-*trans*-RAL, TMZ, and other FDA-approved drugs, namely cisplatin (CP), carmustine (BCNU) and etoposide (ETP), was compared between A172 WT and A172 KO cells (**Table 8** and **Figure 32**), after 48-h incubation. Sensitivity of A172 KO cells to all-*trans*-RAL increased by 25% with respect to that of A172 WT cells. This increase in sensitivity was expected, since ALDH1A enzymes are the main responsible for metabolizing this molecule, which is highly toxic in the amounts tested [202], [209], [210]. Interestingly, the EC_{50} value of TMZ decreased in approximately that same proportion in A172 KO cells, which is in good agreement with the results obtained by Wu *et al*. [138] and suggests again that ALDHs are somehow involved in the resistance mechanism to TMZ in GB. This result is also consistent with the synergistic effects observed during the combined treatment of ALDH inhibitors and TMZ (**Figure 25**), which reinforces the role of ALDHs as potential drug targets. Among the other drugs tested, the percent reduction of EC_{50} value in the knockout cell line compared to the wild type was the highest with CP.

In addition, the cytotoxicity of ALDH inhibitors DIMATE, ABD-3001, ABD0099, and ABD0171 was also compared between A172 WT and A172 KO cells. The EC_{50} values are shown in **Table 9** and the dose-response curves are illustrated in **Figure 33**. Although EC_{50} values remain in the same order of magnitude, the knockout cell line is more sensitive to DIMATE and ABD0171 than the wild type cell line. Nevertheless, the fact that differences between the two cell lines are not very accentuated suggests that ALDH enzymes might not be the only target of the compounds tested. If ALDHs were the only target, one would expect the knockout cell line to be more resistant than the wild type cell line, since these compounds would not be exerting their function as inhibitors to the same extent. However, the compounds are still cytotoxic in A172 KO cells. This could be due to the inhibition of some ALDH isoforms still present in the knockout cell line and/or due to the effect on other unknown molecular targets. More studies beyond the scope of this thesis would be needed to elucidate this aspect.

Table 8. EC_{50} values (µM) ± SE of all-*trans*-RAL (*at*RAL) and FDA-approved anticancer drugs in A172 WT and A172 KO cell lines after 48-h incubation. Shown here are the results of fitting the data from a single representative experiment run in triplicates, performed at least twice independently, to a 4-parameter equation using GraFit 5.0 (Erithacus software).

	Compound				
Cell line	***at*RAL**	**TMZ**	**CP**	**BCNU**	**ETP**
A172 WT	4.25 ± 0.31	3,390 ± 118	26.66 ± 2.89	93.08 ± 6.93	2.01 ± 0.39
A172 KO	3.20 ± 0.19	2,573 ± 223	14.62 ± 1.65	96.54 ± 8.33	3.04 ± 0.55

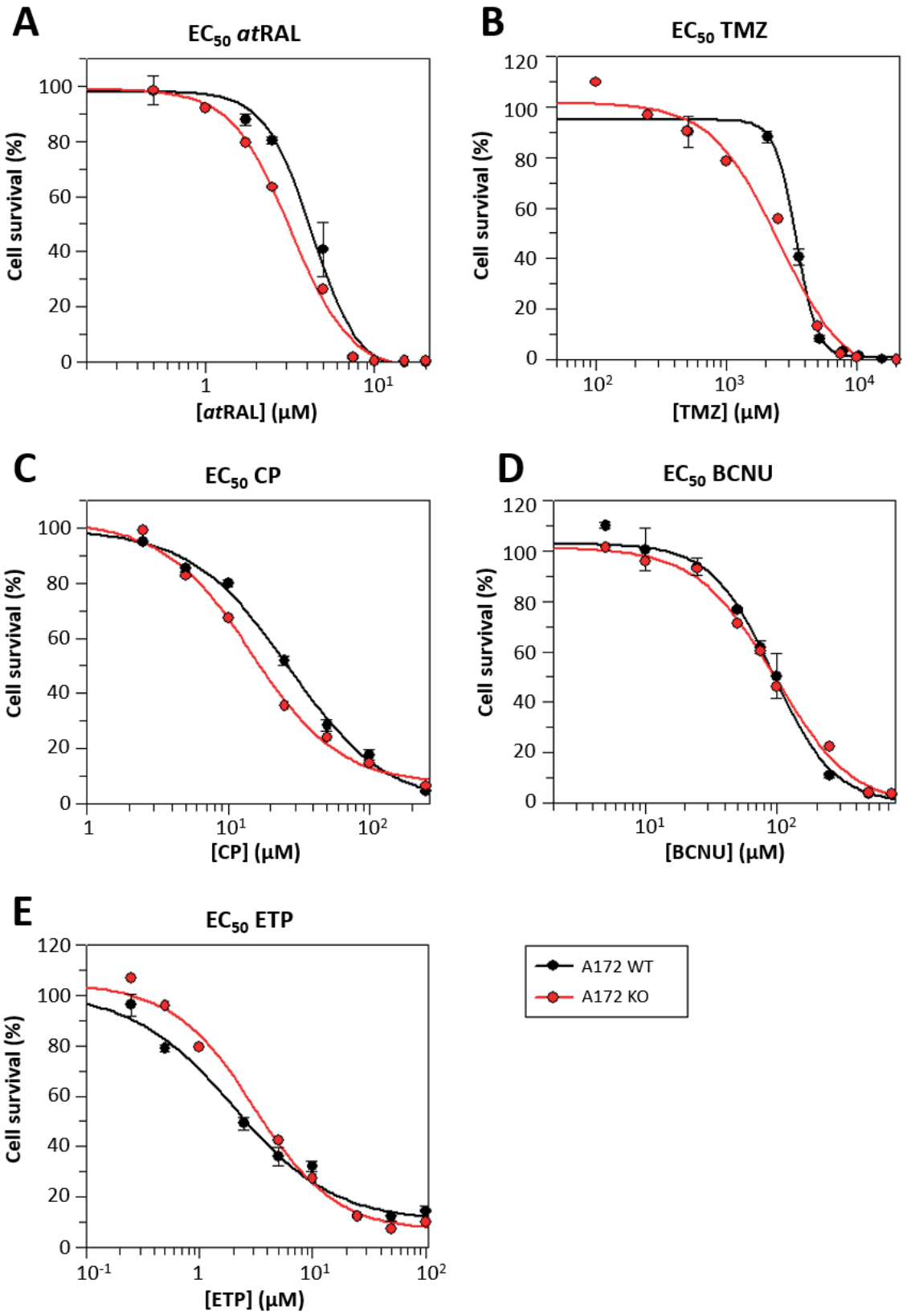

Figure 32. Dose-response curves for all-*trans*-RAL (*at*RAL) and FDA-approved drugs in A172 WT and A172 KO cells after 48-h treatment. (A) *at*RAL; **(B)** TMZ; **(C)** CP; **(D)** BCNU; **(E)** ETP. Data values are the mean ± SE of triplicates from a single representative experiment, performed at least twice independently. Curves were obtained using GraFit 5.0 (Erithacus software).

Table 9. EC_{50} values (µM) ± SE of ALDH inhibitors in A172 WT and A172 KO cell lines. Shown here are the results of the fitting of the data from a single representative experiment run in triplicates, performed at least twice independently, to a 4-parameter equation using GraFit 5.0 (Erithacus software).

	Inhibitor			
Cell line	**DIMATE**	**ABD-3001**	**ABD0099**	**ABD0171**
A172 WT	3.77 ± 0.27	4.48 ± 0.12	2.15 ± 0.13	5.34 ± 0.26
A172 KO	1.73 ± 0.13	3.52 ± 0.32	3.11 ± 0.19	2.28 ± 0.24

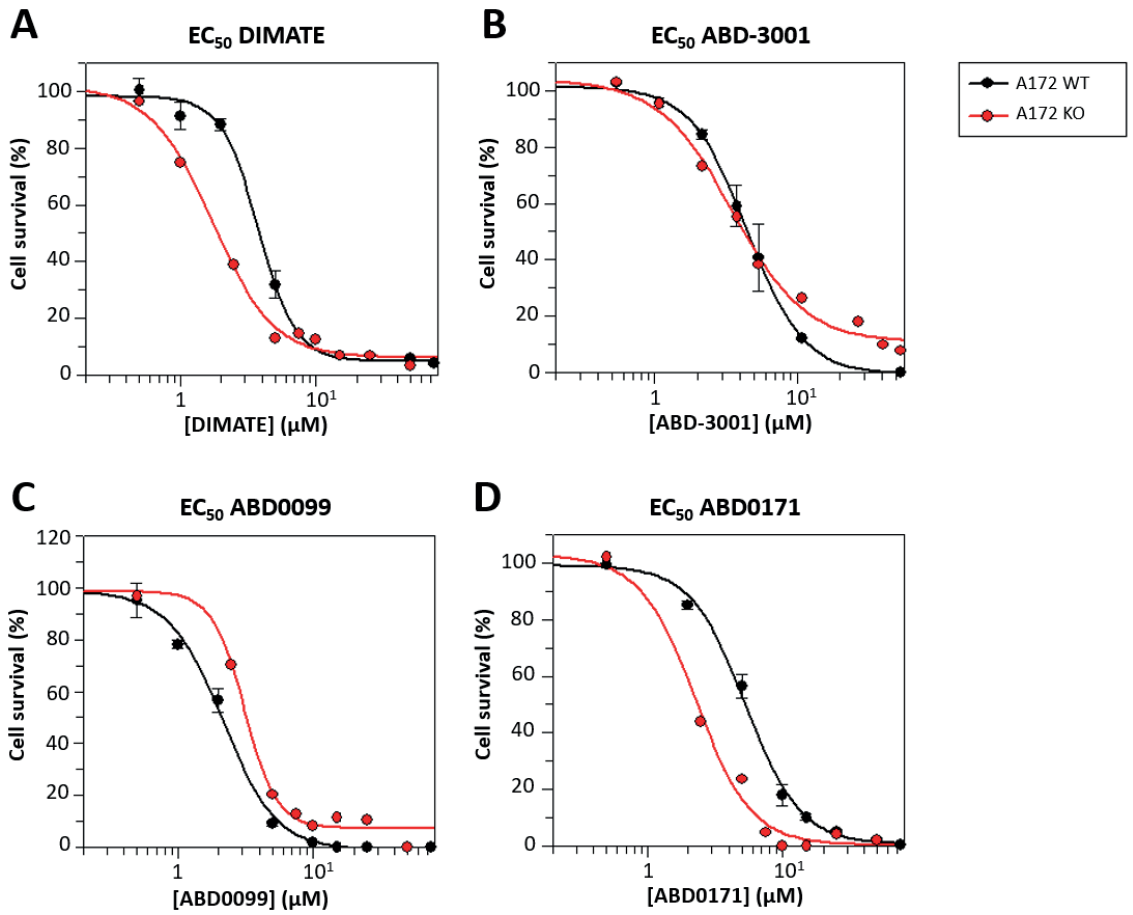

Figure 33. Dose-response curves for ALDH inhibitors in A172 WT and A172 KO cells after 48-h treatment. (A) DIMATE; **(B)** ABD-3001; **(C)** ABD0099; **(D)** ABD0171. Data points are the mean ± SE of triplicates in a single representative experiment, performed at least twice independently. Curves were obtained using GraFit 5.0 (Erithacus software).

4.3. *In vivo* studies in a murine model of GB

In the final part of this thesis, after the characterization of ABD-3001 nanoparticles and the study of their effect on GB cell culture, some experiments were performed in a murine immunocompetent GL261 GB model in order to evaluate the suitability of ABD-3001 as a novel drug for GB treatment, administered via the intranasal route. On the one hand, the size of the nanoparticles obtained in the characterization experiments discussed in **section 4.1** seems optimal for intranasal administration, since it has been reported that nanoparticles with an average size up to 200 nm can be efficiently transported transcellularly via the intranasal route [203]. In addition, the monodispersity of the nanoparticle solution is also a property that could make it suitable for *in vivo* applicability. On the other hand, *in vitro* results discussed in **section 4.2** prove that DIMATE, the active molecule in ABD-3001 formulation, is able to inhibit ALDH activity in GL261 cells. Also, ABD-3001 has been shown to display high cytotoxicity in this cell line and a synergistic effect when combined with TMZ. Nevertheless, ABD-3001 is tested here *in vivo* as a monotherapy; combinations with TMZ *in vivo* are planned to be carried out in the near future by other members of the research group.

Firstly, the *in vivo* assays performed during this thesis consist of a tolerability assay, and secondly, three therapeutic efficacy assays with various doses of ABD-3001. Additionally, tissue samples taken from the mice used in these assays were later analyzed by HPLC in order to study the drug biodistribution, and by an immunoassay to assess the expression of ALDHs before and after treatment.

4.3.1. Tolerability assay with 5 mg/kg ABD-3001

The tolerability assay was carried out in healthy mice (that is, tumor-free mice), in order to assess the potential toxicity of ABD-3001. Two experimental groups were established: a control group, treated with 5 mg/kg ABD-3000 (empty liposomes) administered intranasally; and a treated group, treated with 5 mg/kg ABD-3001, also administered intranasally. Drug toxicity was assessed, on the one hand, by monitoring the weight of mice during the time of treatment, and on the other hand, by necropsy analysis of their tissues.

Although all mice were apparently healthy by the end of the treatment, a slight loss of body weight could be observed in both the control and treated groups, as shown in **Figure 34**. **Figure 34A** represents the evolution of body weights in each group during the four weeks of treatment, while **Figure 34B** indicates the mean percentage of weight loss in each group by the end of the treatment. The final weight loss in the control group was approximately 2% with respect to the

initial body weight, whereas the treated group lost around 9%. This difference suggests that ABD-3001 may be toxic for mice to some extent.

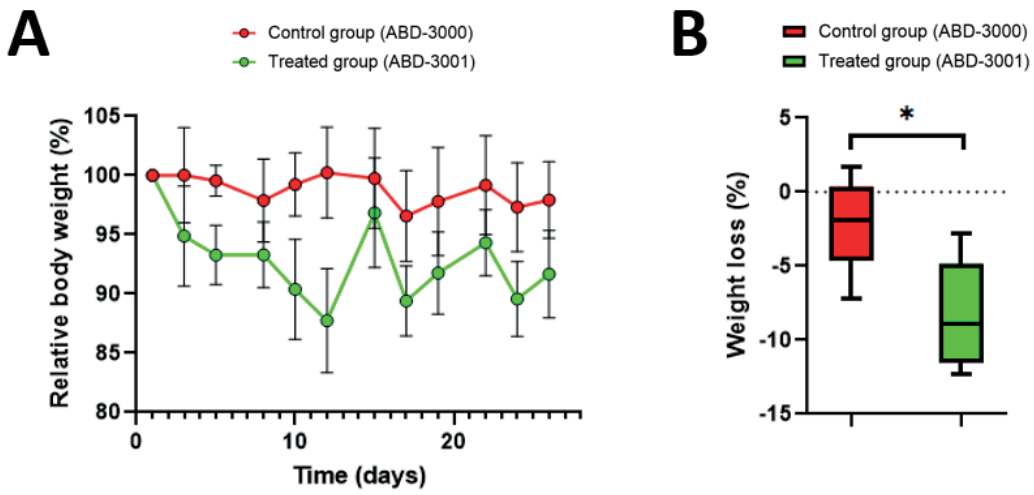

Figure 34. Analysis of the body weight of mice during the tolerability assay with ABD-3001. (A) Relative body weight (%) during the time of treatment. The mean percentage of the weight of the 5 mice in the control group (**red**) and the treated group (**green**) with respect to the initial mean weight is represented against day of treatment. Body weight was only recorded on the days of drug administration, that is, 3 days per week. **(B)** Mean body weight loss (%) of the control group (**red**) and treated group (**green**) by the end of treatment. Asterisk indicates statistical, significant difference between control and treated groups, as analyzed by unpaired t test with Welch's correction: *0.01 < P < 0.05.

Apart from monitoring body weight, necropsy studies were performed in two of the mice treated with ABD-3001 to assess potential damage in the tissues by the drug. At a macroscopic level, alterations in the nervous system and generalized pallor in liver and kidneys were observed, probably due to the method of euthanasia (cervical dislocation) and fast exsanguination of the animals during the process. At a microscopic level, black punctate material was observed inside the lung macrophages. Additionally, focal, perivascular and alveolar hemorrhages were observed in one of the two mice; the other mouse presented focally peribronchial lymphoid tissue more evidently. These damages may be probably associated with the dose of the drug used and the route of administration, and could explain, at least in part, the weight loss observed during the experiment. However, since this weight loss did not exceed 10%, and furthermore, no microscopic lesions indicating acute or chronic disease were detected, 5 mg/kg ABD-3001 was the dose considered for the first therapeutic efficacy assay, which will be discussed in **section 4.3.2.1**. In addition, the rest of evaluated organs (namely, heart, thymus, digestive tract, pancreas, bladder, ovary, uterus, skeletal muscle and skin) did not present lesions and maintained the usual architecture.

4.3.2. Therapeutic efficacy assays

As just mentioned above, in view of the results obtained in the tolerability assay, 5 mg/kg ABD-3001 was chosen as the dose for the first therapeutic efficacy assay. Contrary to the tolerability assay, the mice used here were implanted with GL261 cells and developed a tumor, thus the drug effect on tumor growth could be studied. The first drug administration was at day 6 post-implantation, and weight loss and tumor volume were monitored during the treatment. In addition, necropsy studies were also carried out in the tissues of some treated mice, in order to assess potential signs of damage.

4.3.2.1. Therapeutic efficacy assay with 5 mg/kg ABD-3001

For this first therapeutic efficacy assay, two experimental groups were established: a control group treated with 5 mg/kg ABD-3000 (empty liposomes) administered intranasally; and a treated group, treated with 5 mg/kg ABD-3001, also administered intranasally.

In **Figure 35**, the evolution of body weights in each group is represented during the time of treatment. As shown, mice treated with ABD-3001 lose more weight than those treated with the vehicle. This can be noticed from the first day of drug administration until the end of the treatment. Again, as in the tolerability assay, this result suggests that ABD-3001 has some toxic effect in mice at the dose used.

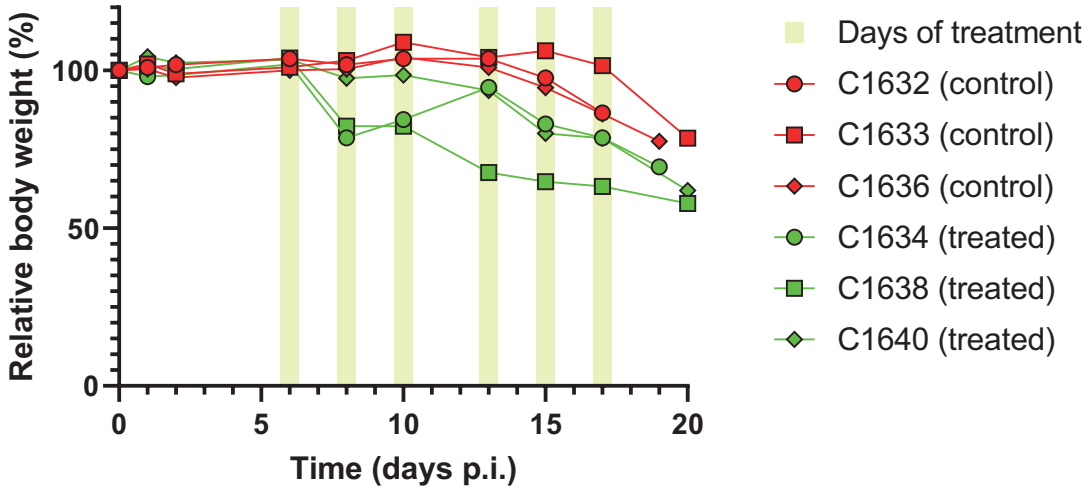

Figure 35. Relative body weight of GB-bearing mice during the therapeutic efficacy assay with 5 mg/kg ABD-3001. Mice C1632, C1633, and C1636, belonging to the control group (**red**), were treated with 5 mg/kg ABD-3000, whereas mice C1634, C1638, and C1640, belonging to the treated group (**green**), were treated with 5 mg/kg ABD-3001. The weight of the 3 mice in each group with respect to their initial weight (%) is represented against the time of treatment (days p.i.: days post-implantation). Yellow bars indicate the days of drug administration.

Tumor volumes were also monitored during the time of treatment, by MRI, and their evolution in each experimental group is shown in **Figure 36**. At the beginning of the treatment (day 6 post-implantation), the tumor volumes of all mice were similar. As observed, treated mice showed a decreased tumor growth rate with respect to the controls. Although the growth of the tumor was not completely stopped in none of the cases, these results strongly suggest that ABD-3001 has some antitumor effect. In addition, doubling time of the tumor was calculated taking the mean values of tumor volume of control mice and treated mice separately (http://radclass.mudr.org/content/doubling-time-calculation-growth-rate-lesion-or-mass). The doubling time increased from 2 days in the case of control mice to 3 days in the case of mice treated with ABD-3001.

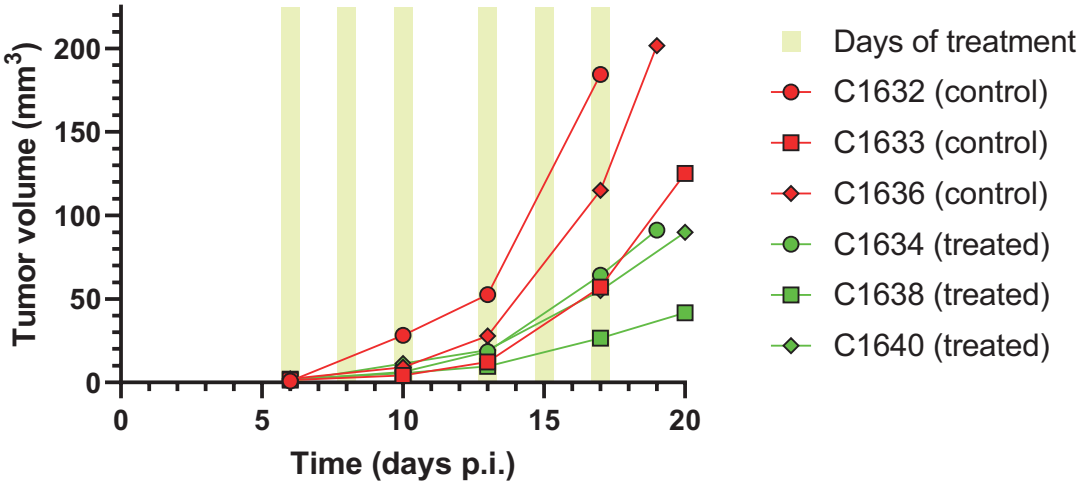

Figure 36. Evolution of tumor volumes during the therapeutic efficacy assay with 5 mg/kg ABD-3001. Mice C1632, C1633, and C1636, belonging to the control group (**red**), were treated with 5 mg/kg ABD-3000, whereas mice C1634, C1638, and C1640, belonging to the treated group (**green**), were treated with 5 mg/kg ABD-3001. Tumor volume (mm^3) is represented against the time of treatment (days p.i.: days post-implantation). Yellow bars indicate the days of drug administration.

Images of the tumors were obtained by MRI along the therapeutic efficacy assay. As examples, the tumor of a control case and a treated case are shown in **Figure 37**, specifically at day 17 post-implantation (thus, after six therapeutic doses). After this time of treatment with ABD-3001, the difference in volume between the two tumors can be clearly noticed. The rest of images of the tumors are shown in **Annex 1.2**.

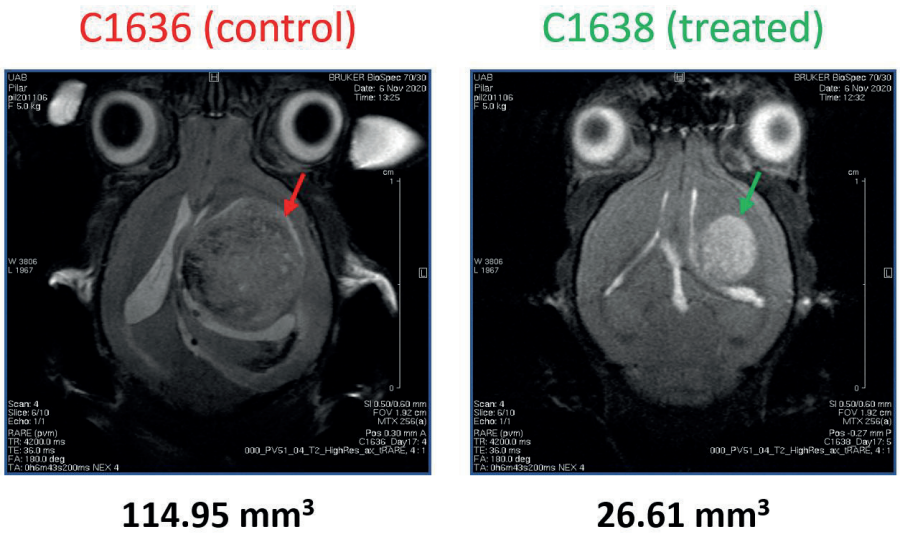

Figure 37. MRI of the tumors of mice C1636 (control) and C1638 (treated with 5 mg/kg ABD-3001) at day 17 post-implantation, after six therapeutic doses. Arrows point at the tumor. Tumor volumes (in mm^3) are indicated under the images.

Additionally, necropsy studies were performed in two of the mice treated with ABD-3001 in order to detect potential damage in the tissues by the drug. At a macroscopic level, apart from typical lesions derived from GB, lesions could be observed in lungs and intestine. In the lungs, all lobes were collapsed; in the intestine, dilation of the lumen of the distal jejunum, cecum, and proximal colon was observed due to the presence of abundant gas. At a microscopic level, in the CNS, specifically in the tumor mass, two different populations of neoplastic cells could be observed: one of these populations is composed of aberrant giant cells, whose presence is probably related to side reactions with ABD-3001. Interestingly, in previous studies performed by the research group, these cells could also be detected in mice treated with TMZ. In the lungs, congestion and hemorrhage were observed in alveoli. Finally, the rest of evaluated organs did not present lesions or, in the case of lesions, they were probably associated to the age of mice.

Taken together, these results suggest that the dose of 5 mg/kg may be too high for the treatment of these GB-bearing mice. Although this dose of ABD-3001 showed promising results in reducing the rate of tumor growth, treated mice end up losing too much weight compared to control mice, and furthermore, they displayed lesions in some organs, as revealed by the necropsy studies. This forced us to euthanize the treated mice before the chance to observe long-term effects of the drug, such as tumor regression. Thus, a second therapeutic efficacy assay with a lower dose of drug was performed, as detailed in the following section, with the aim of attenuating the adverse effects of ABD-3001 while preserving its positive effects in reducing tumor growth rate.

4.3.2.2. Therapeutic efficacy assay with 2.5 mg/kg ABD-3001

A second therapeutic efficacy assay was performed using a dose of 2.5 mg/kg ABD-3001. In this assay, a new group of mice was treated with the new dose of ABD-3001, but no new control group was added since, in principle, the response of mice treated only with the vehicle should not be expected to change. Thus, the control group from the previous therapeutic efficacy assay (treated with 5 mg/kg ABD-3000) was used in this experiment to make comparisons with the new group of treated mice. Body weight and tumor volume were monitored along the course of the assay to assess the effects of the drug on the GB-bearing mice. In this occasion, however, necropsy studies were not performed.

The evolution of the body weight of the new treated mice, along with the control mice of the previous assay, is shown in **Figure 38**. In this case, the weight loss of the treated group is more similar to that of the control group, compared to when mice were treated with a higher dose of the drug (**Figure 35**). Thus, by lowering the dose of ABD-3001 from 5 mg/kg to 2.5 mg/kg, toxicity was slightly decreased and weight loss was mitigated.

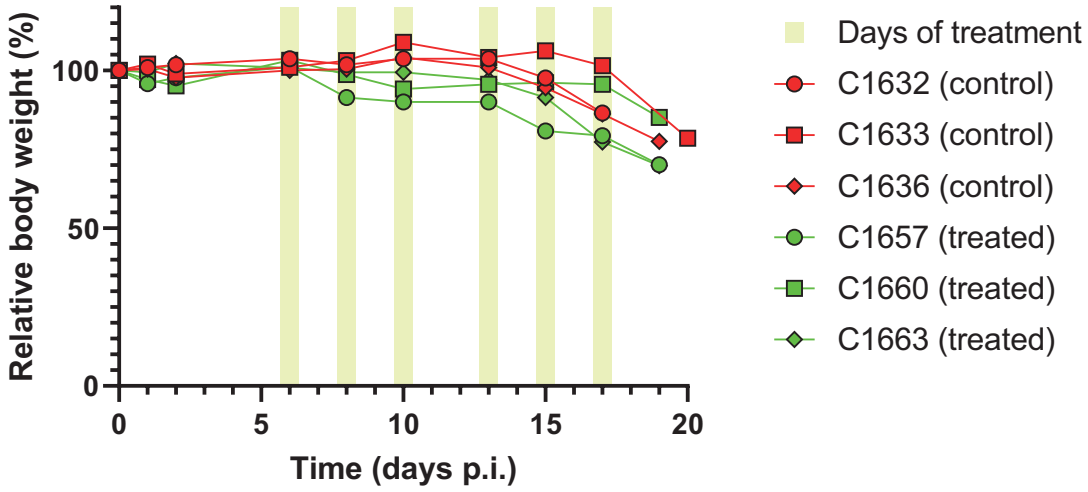

Figure 38. Relative body weight of GB-bearing mice along the therapeutic efficacy assay with 2.5 mg/kg ABD-3001. Mice C1632, C1633, and C1636, belonging to the control group (**red**), were treated with 5 mg/kg ABD-3000, whereas mice C1657, C1660, and C1663, belonging to the treated group (**green**), were treated with 2.5 mg/kg ABD-3001. The weight of the 3 mice in each group respect to their initial weight (%) is represented against the time of treatment (days p.i.: days post-implantation). Yellow bars indicate the days of drug administration.

The evolution of tumor volume during the time of treatment was followed by MRI and is represented in **Figure 39**. As in the previous therapeutic efficacy assay with 5 mg/kg ABD-3001 (**Figure 36**), tumor growth rate was reduced in the treated group compared to the control group. A comparison between the tumor of a control case and that of a treated case at day 17 post-implantation (thus, after six therapeutic doses) is shown in **Figure 40**. The rest of images of the tumors in this therapeutic efficacy assay are shown in **Annex 1.3**.

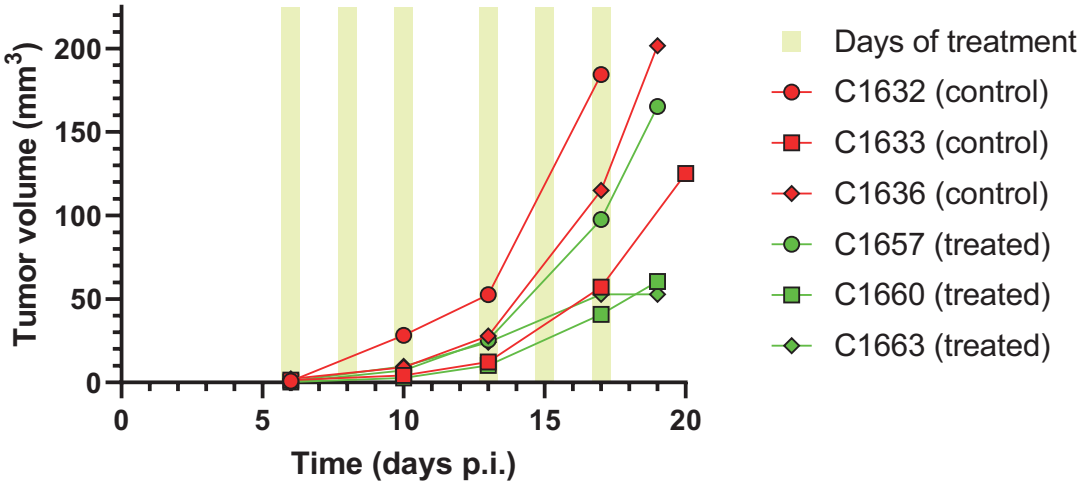

Figure 39. Evolution of tumor volumes during the therapeutic efficacy assay with 2.5 mg/kg ABD-3001. Mice C1632, C1633, and C1636, belonging to the control group (**red**), were treated with 5 mg/kg ABD-3000, whereas mice C1657, C1660, and C1663, belonging to the treated group (**green**), were treated with 2.5 mg/kg ABD-3001. Tumor volume (mm^3) is represented against the time of treatment (days p.i.: days post-implantation). Yellow bars indicate the days of drug administration.

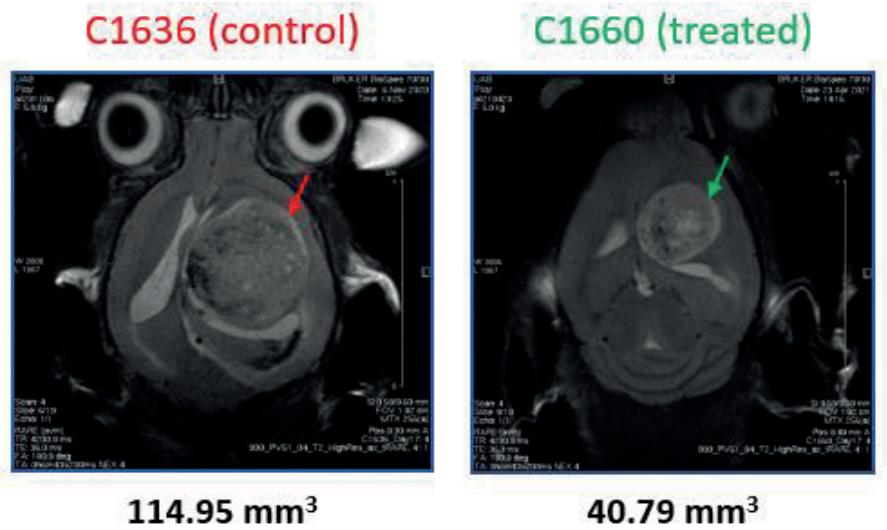

Figure 40. MRI of the tumors of mice C1636 (control) and C1660 (treated with 2.5 mg/kg ABD-3001) at day 17 post-implantation, after six therapeutic doses. Arrows point at the tumor. Tumor volumes (in mm^3) are indicated under the images.

In general, the results of the second therapeutic efficacy assay are quite similar to those obtained in the first one. Although the weight loss was slightly reduced by decreasing the dose of ABD-3001 to the half, it would be desirable to further reduce this weight loss in order to evaluate long term effects of the drug. Since the dose of 2.5 mg/kg, ABD-3001 was still able to slow down the rate of tumor development, we decided to perform a third therapeutic efficacy assay with an even lower dose of drug in order to reduce toxicity and lengthen the lifespan of GB-bearing mice.

4.3.2.3. Therapeutic efficacy assay with 1.5 mg/kg ABD-3001

A third therapeutic efficacy assay was performed using a dose of 1.5 mg/kg ABD-3001. In this assay, a new group of mice was treated with the new dose of ABD-3001, and again, no new control group was added. The control group from the first therapeutic efficacy assay (treated with 5 mg/kg ABD-3000) was used in this experiment to make comparisons with the new group of treated mice. As in the previous assay, body weight and tumor volume were monitored during the course of the assay to assess the effects of the drug on the GB-bearing mice.

The evolution of body weight of the mice treated with 1.5 mg/kg ABD-3001 is represented in **Figure 41,** together with that of the control mice from the first therapeutic efficacy assay. As observed, the decrease of weight in the new treated mice was not as fast as in the previous experiments. This allowed the lifespan of the mice to be prolonged, as well as the time of treatment with the drug.

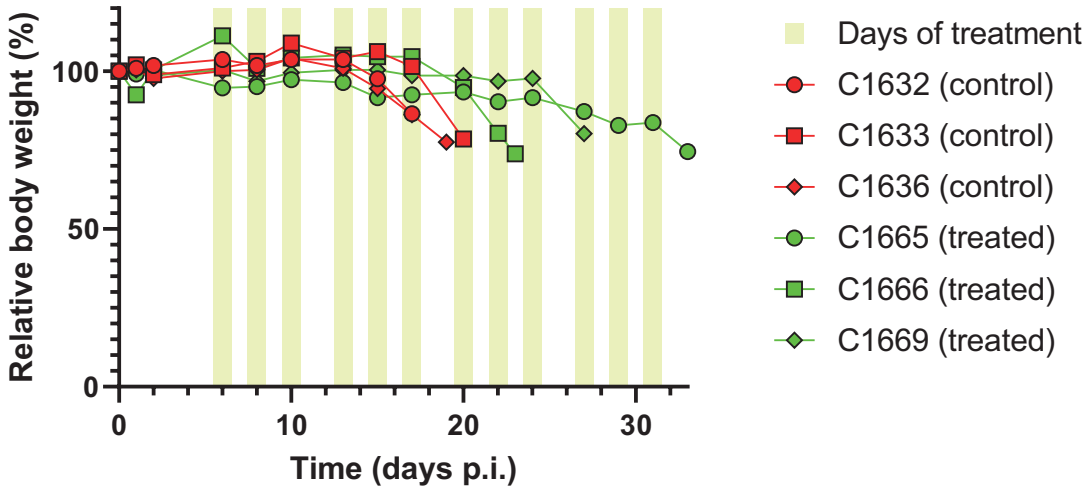

Figure 41. Relative body weight of GB-bearing mice along the therapeutic efficacy assay with 1.5 mg/kg ABD-3001. Mice C1632, C1633, and C1636, belonging to the control group (**red**), were treated with 5 mg/kg ABD-3000, whereas mice C1665, C1666, and C1669, belonging to the treated group (**green**), were treated with 1.5 mg/kg ABD-3001. The weight of the 3 mice in each group respect to their initial weight (%) is represented against the time of treatment (days p.i.: days post-implantation). Yellow bars indicate the days of drug administration.

The evolution of tumor volume during the time of treatment was followed by MRI and is represented in **Figure 42**. This time, since there was slightly more variability than expected in the tumor volumes of mice at the initiation of the treatment (day 6 post-implantation), data are shown as normalized values (tumor volumes normalized respect to the tumor volume at the beginning of the treatment). As observed, the tumor growth rate of mice treated with 1.5 mg/kg ABD-3001 is retarded compared to that of control mice, and also compared to that of the mice treated with higher doses of the drug (**Figures 36** and **39**). A comparison between the tumor of

a control case and that of a treated case at day 17 post-implantation (thus, after six therapeutic doses) is shown in **Figure 43**. Although the time of treatment could be prolonged in this assay and the tumor growth was slowed down, no tumor regression was observed.

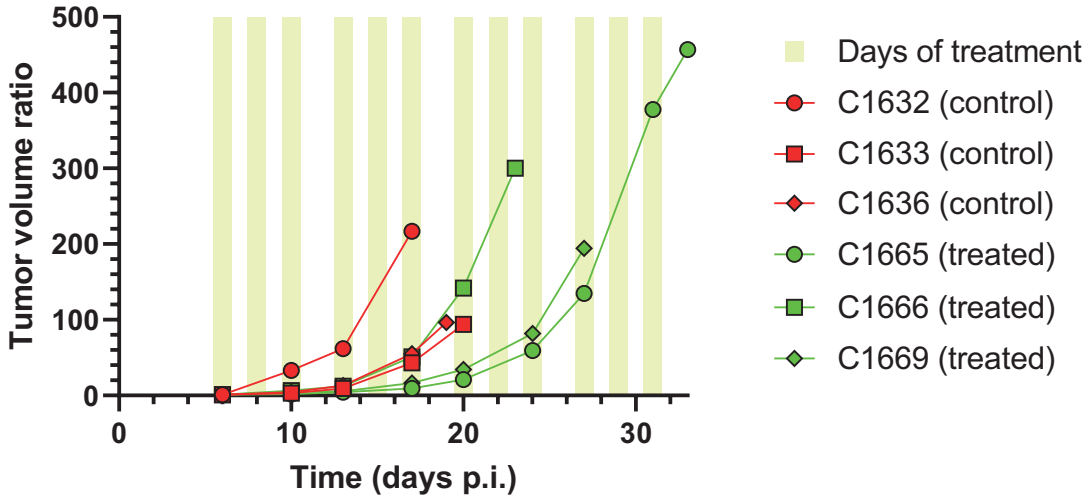

Figure 42. Evolution of tumor volumes during the therapeutic efficacy assay with 1.5 mg/kg ABD-3001. Mice C1632, C1633, and C1636, belonging to the control group (**red**), were treated with 5 mg/kg ABD-3000, whereas mice C1665, C1666, and C1669, belonging to the treated group (**green**), were treated with 1.5 mg/kg ABD-3001. Tumor volume ratio (that is, the tumor volume normalized by the tumor volume at the initial point of therapy) is represented against the time of treatment (days p.i.: days post-implantation). Yellow bars indicate the days of drug administration.

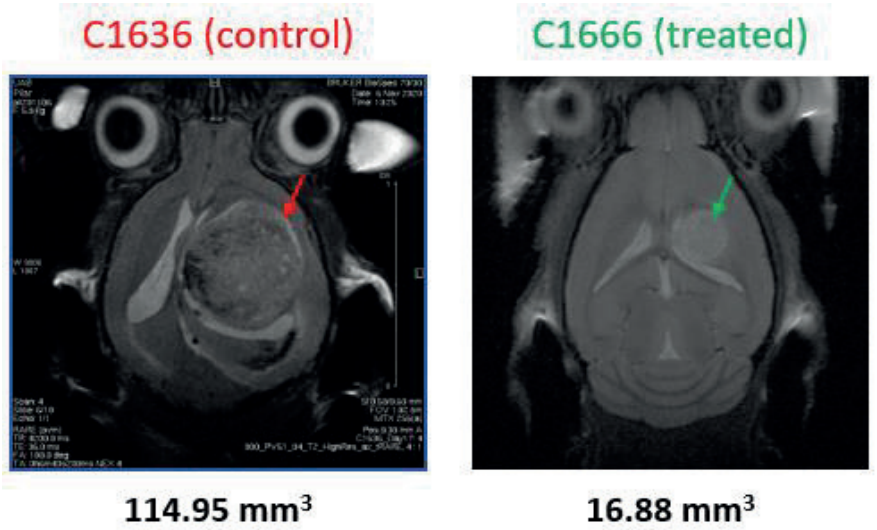

Figure 43. MRI of the tumors of mice C1636 (control) and C1660 (treated with 1.5 mg/kg ABD-3001) at day 17 post-implantation, after six therapeutic doses. Arrows point at the tumor. Tumor volumes (in mm^3) are indicated under the images.

Since the lifespan of the treated mice could be prolonged in this assay due to the reduction of the dose used, a survival analysis could be performed. A Kaplan-Meier survival plot is represented in **Figure 44**, where it can be observed that all three new treated mice lived longer than all three control mice.

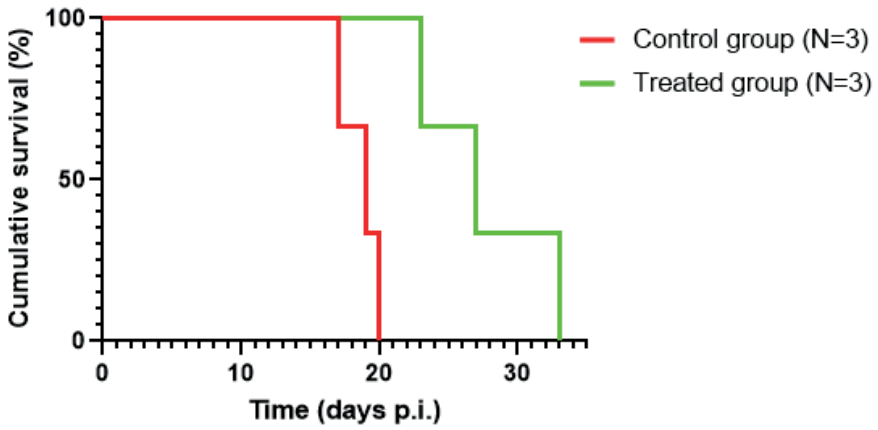

Figure 44. Kaplan-Meier survival plot for GB-bearing mice in the therapeutic efficacy assay with 1.5 mg/kg ABD-3001. Mice belonging to the control group (**red**) were treated with 5 mg/kg ABD-3000, whereas mice belonging to the treated group (**green**) were treated with 1.5 mg/kg ABD-3001. The cumulative survival (%) is represented against the time of treatment (days p.i.: days post-implantation).

Taken together, the results obtained in all these *in vivo* assays suggest that ABD-3001 may present some toxicity for mice, having as consequences the loss of body weight and damage in some organs. This issue could be solved by lowering the dose of drug. Nevertheless, ABD-3001 was proved to have antitumor effect in all three therapeutic efficacy assays performed, even at the lowest dose 1.5 mg/kg, slowing down the rate of tumor growth. Optimizations in these experiments are still required though, with using proper controls in each assay and higher number of mice in the control and treated groups. All in all, these preliminary studies suggest that ABD-3001, which is already in clinical phase I for the treatment of AML, could also be a promising drug for the treatment of GB. Once proven its efficacy in GB-bearing mice, the next step was the detection of the drug in the tissues of treated mice, as detailed in the following section.

4.3.3. Detection of DIMATE in tissues from mice treated with ABD-3001

Tissue samples from mice treated with ABD-3001 in the previous therapeutic efficacy assays were collected and analyzed by HPLC in order to assess the drug distribution in the body. Prior to this analysis, some other preparative experiments were performed, as discussed below.

In first place, ABD-3001 was injected alone into HPLC as a control, and a peak corresponding to the molecule of DIMATE was detected at an approximate retention time of 12.3 min, as observed also in the release experiments (**Figure 20**). In **Figure 45**, two independent injections of different amounts of ABD-3001 are plotted, and it could be seen that the intensity of the peak was proportional to the amount of drug loaded.

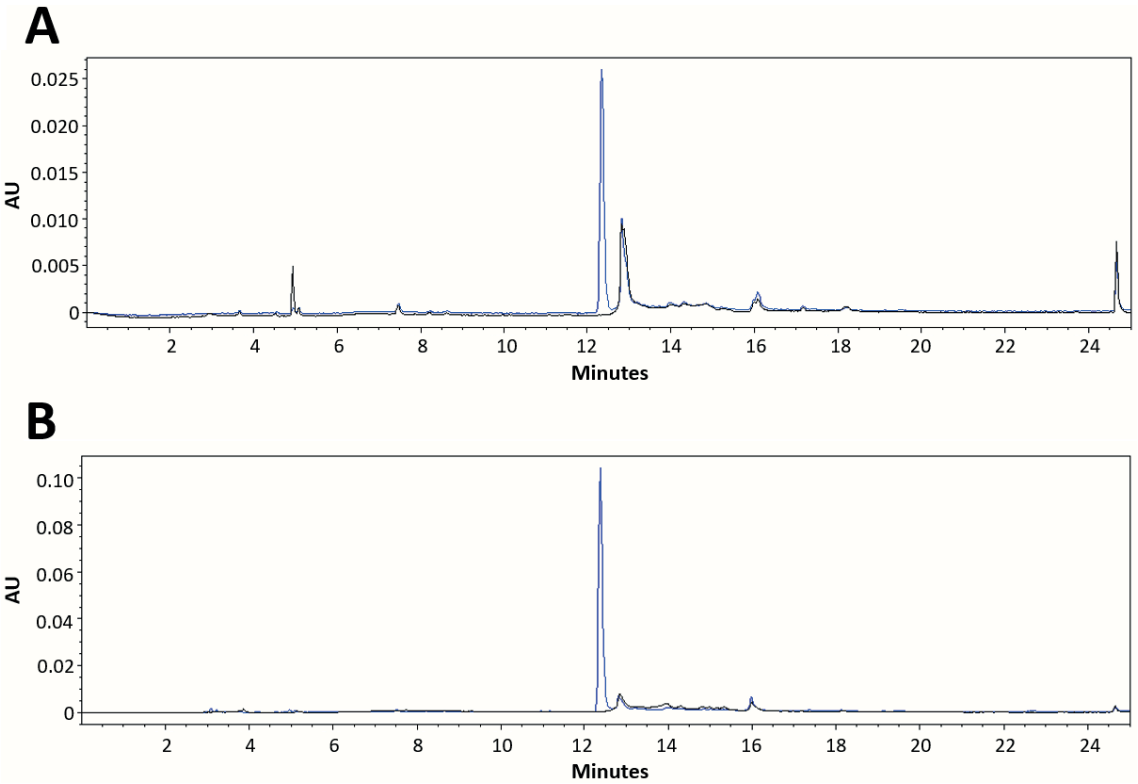

Figure 45. HPLC analysis of ABD-3001 alone. (A) Injection of 92.6 ng ABD-3001; **(B)** injection of 360 ng ABD-3001. **Black**: mobile phase; **blue**: ABD-3001. AU: absorbance units.

The next step prior to the analysis of tissue samples was to check if DIMATE was internalized in cells when an *in vitro* culture was treated with ABD-3001. The HPLC analysis of the cell extract of a GL261 culture incubated with ABD-3001 revealed that, indeed, the drug was internalized in the cells. However, as shown in **Figure 46**, several peaks corresponding to the drug appear (specifically, at retention times near 8 and 10 min) and are different from the one observed in the direct injection of ABD-3001 (**Figure 45**). This suggests that DIMATE is somehow modified in the cell, either degraded or bound to some cellular component.

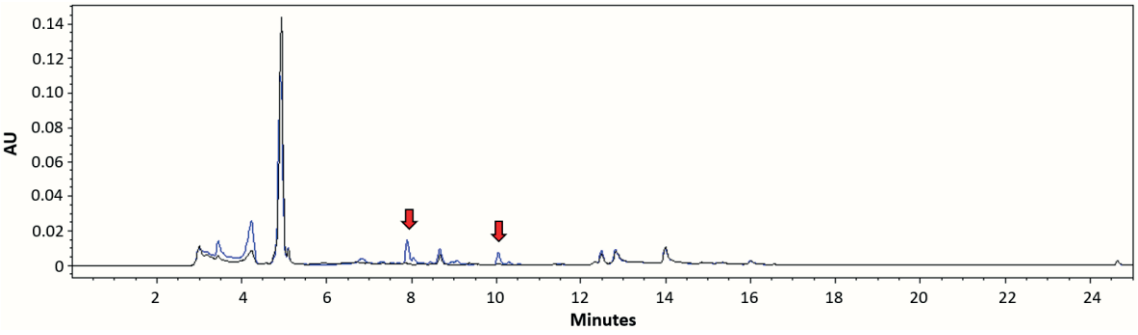

Figure 46. HPLC analysis of ABD-3001 in GL261 cell extracts. Black: GL261 cell extract without prior treatment with ABD-3001; **blue**: GL261 cell extract with prior 2 h-treatment of the culture with 100 µM ABD-3001. Red arrows point at the main eluting peaks corresponding to the drug (those peaks that only appear in the extract of the culture incubated with ABD-3001). AU: absorbance units.

Then, an experiment was performed in order to assess whether the same peaks observed in the cell culture treated with ABD-3001 also appeared in a mouse tissue sample treated with the drug. Specifically, liver slices from control mice were directly treated with different amounts of ABD-3001 and analyzed by HPLC. The resulting chromatograms are shown together in **Figure 47**. Interestingly, two main eluting peaks appeared at retention times of approximately 8 and 10 min, just as in the cell culture treated with ABD-3001 (**Figure 46**). In fact, the chromatographic profiles are in the two cases highly similar. These peaks were absent in the liver sample without treatment, and their intensity increased proportionally to the amount of ABD-3001 added, suggesting that these peaks indeed correspond to the drug. Importantly, the peak observed in **Figure 45**, corresponding to DIMATE alone, should not be used for the detection and quantification of the drug in tissues, since a peak with the same retention time also appears in the tissue without treatment and, additionally, it does not increase proportionally to the amount of ABD-3001 added. The same happened in the *in vitro* cell culture.

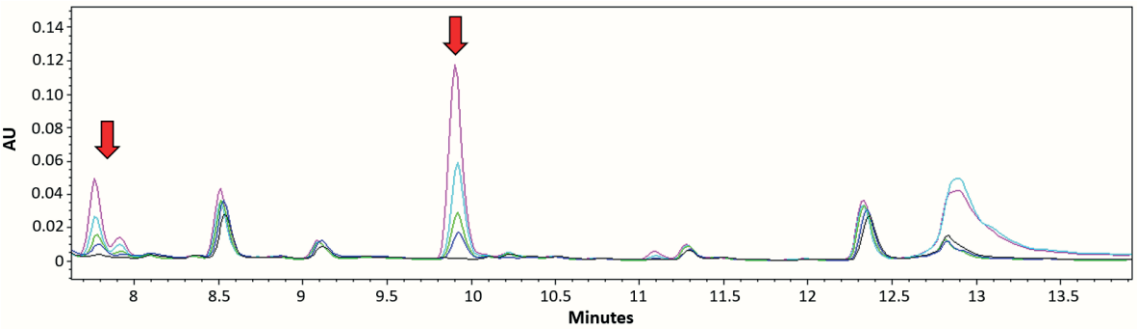

Figure 47. HPLC analysis of control mouse liver treated with different amounts of ABD-3001. Black: liver sample without ABD-3001; **blue**: liver sample treated with 0.5 µg ABD-3001; **green**: liver sample treated with 1 µg ABD-3001; **light blue**: liver sample treated with 2 µg ABD-3001; **pink**: liver sample treated with 4 µg ABD-3001. Red arrows point at the main peaks corresponding to the drug (those peaks that only appear in the samples treated with ABD-3001). AU: absorbance units.

According to the expert opinion of the team of chemists from ABD involved in the synthesis of DIMATE, the peaks with retention times 8 and 10 min observed in the previous figures were likely to be fragments of DIMATE bound to some compound present in the cells, such as GSH. In order to validate this hypothesis, another experiment was performed, consisting on the injection of samples of DIMATE incubated with different amounts of GSH. The chromatogram resulting from the injection of these samples is shown in **Figure 48**, where it can be observed that two peaks appear with retention times near 8 and 10 min, and have an intensity proportional to the amount of GSH used. In addition, the overlapping of this chromatographic profile with those of mouse liver samples untreated and treated with ABD-3001, shown in **Figure 49**, strongly suggests that, indeed, those peaks correspond to DIMATE or fragments of DIMATE bound to GSH present in the cells of the tissue.

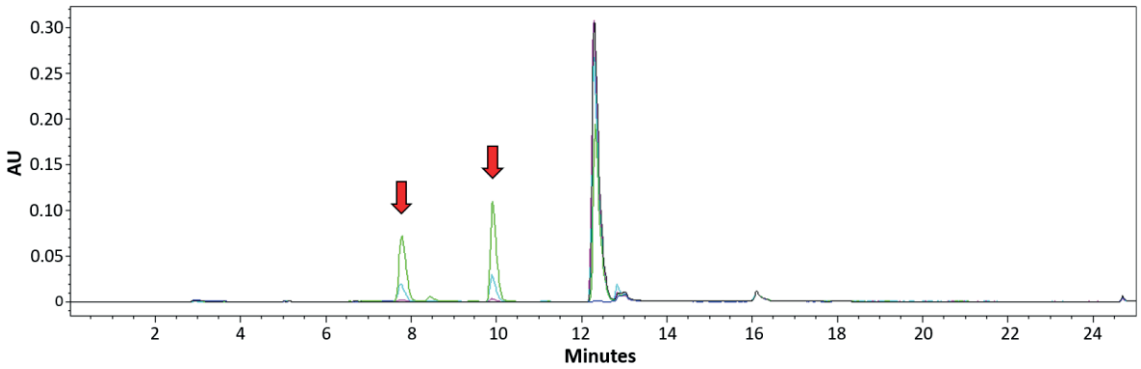

Figure 48. HPLC analysis of samples containing DIMATE incubated with various concentrations of GSH. Black: 100 µM DIMATE alone; **blue**: 100 µM GSH alone; **green**: 100 µM DIMATE incubated with 100 µM GSH for 1 h at 37°C; **light blue**: 100 µM DIMATE incubated with 10 µM GSH for 1 h at 37°C; **pink**: 100 µM DIMATE incubated with 1 µM GSH for 1 h at 37°C. Red arrows point at the peaks corresponding to DIMATE or fragments of DIMATE bound to GSH. AU: absorbance units.

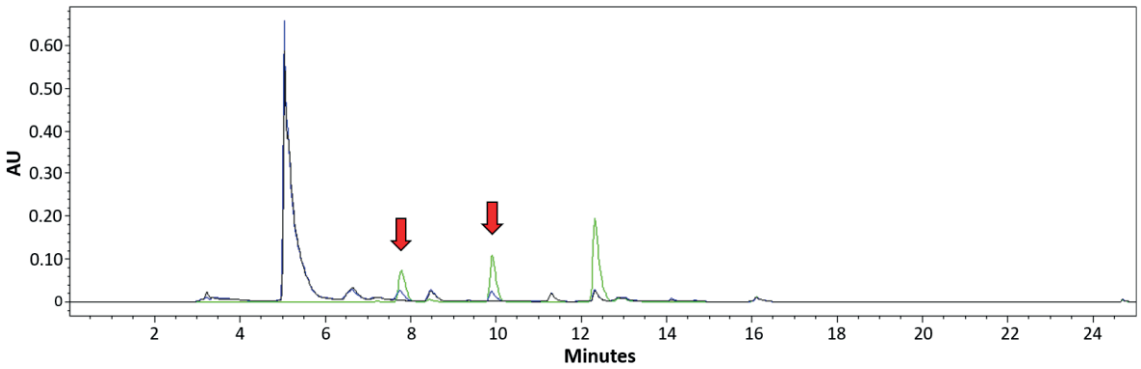

Figure 49. Overlapped HPLC chromatograms of mouse liver treated with ABD-3001 and a sample of DIMATE incubated with GSH. Black: liver sample without ABD-3001; **blue**: liver sample treated with 4 µg ABD-3001; **green**: 100 µM DIMATE incubated with 100 µM GSH for 1 h at 37°C. Red arrows point at the peaks corresponding to DIMATE or presumably fragments of DIMATE bound to GSH. AU: absorbance units.

After all these preliminary tests, the analysis of tissues of mice treated with ABD-3001 in the therapeutic efficacy assays was performed. However, unfortunately, the drug could not be detected in none of the tissues analyzed, including the tumor. Probably, the amount of DIMATE in each tissue after its biodistribution in the animal was below the levels of detection of this HPLC method. Despite it is likely that ABD-3001 reaches the tumor, given the antitumor effect observed in the assays, another detection method should be implemented in order to observe the molecule and perform a proper study of the drug biodistribution.

Although DIMATE could not be detected in the tissues of treated mice, some relevant information could be obtained for these experiments. In summary, these tests allowed us to know that DIMATE is internalized in cells, that the molecule is not likely to remain in its initial molecular form after being internalized, and specifically, that the drug (or its metabolites) binds to cellular GSH. GSH is found in high concentrations in cellular systems and plays a major role as an antioxidant molecule, detoxifying electrophilic compounds such as DIMATE [206]. By binding

to DIMATE, part of the cellular GSH would be unavailable to detoxify other electrophilic compounds occurring naturally, putting the cell at risk for oxidative damage. This mechanism may add to a similar effect resulting from the inhibition of ALDH enzymes.

4.3.4. Analysis of ALDH expression in tissues from mice treated with ABD-3001

The last study performed on samples taken from mice of the therapeutic efficacy assays was the assessment of the expression of different ALDH isoforms in various tissues. **Figure 50** shows the expression levels of ALDH1A1, ALDH1A2 and ALDH1A3 for all the tissues tested, both from an untreated mouse (C1633) and a mouse treated with 5 mg/kg ABD-3001 (C1640). Firstly, it can be observed that ALDH1A3 is mainly detected in the tumor. Other general observations are that the expression of ALDH1A1 and ALDH1A2 is quite higher in the lungs, compared to other tissues, as well as the expression of ALDH1A2 in the kidneys. Regarding to comparisons of specific tissues between treated and untreated mice, three main observations can be made: firstly, ALDH1A1 expression decreases in the tumor when the mouse has been submitted to treatment with 5 mg/kg ABD-3001; secondly, the expression of ALDH1A1 and ALDH1A2 also seems to decrease in the cerebellum of the treated mouse; and lastly, the expression of the three ALDH1A isoforms is clearly lower in the heart of the treated mouse. Thus, there seems to be a downregulation of the expression of ALDH1A enzymes in some tissues after treatment with ABD-3001, including the tumor, which could be related with the antitumor effect of the drug observed in the therapeutic efficacy assays. Since ALDH1A enzymes are the main responsible for the production of RA in the cell, this could also affect the regulation of the expression of other genes that have not been tested in this study and are under the control of RA-inducible promoters.

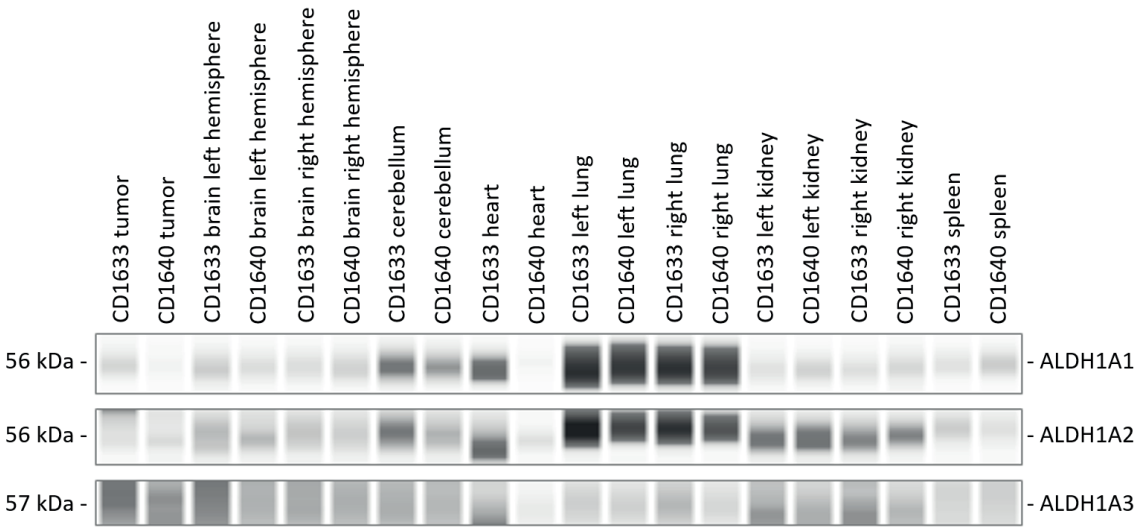

Figure 50. Immunoblot analysis of ALDH1A expression in tissues from mice untreated or treated with ABD-3001. C1633: mouse belonging to the control group of the therapeutic efficacy assays, treated with 5 mg/kg ABD-3000; C1640: mouse belonging to a treated group of the therapeutic efficacy assays, treated with 5 mg/kg ABD-3001. Comparisons here can be made across all tissues for a single isoform, but not in the same tissue for different isoforms, since the different isoforms were tested in different plates, using different primary antibody dilutions and incubation times. The plot was cropped to show the ALDH bands only.

In addition, the expression of ALDH1A enzymes and other isoforms was compared between GL261 cell culture and the tumors of the untreated and treated mice used before, as shown in **Figure 51**. These tumors were originated from GL261 cells, but other non-cancer cells are probably also present in the tumor mass, so the observed expression of ALDHs may not only be due to the GL261 cells present there. The results obtained from the immunoblot analysis seem to indicate that there is a switch in the expression of some ALDH isoforms when GL261 cells go from an *in vitro* culture to an *in vivo* tumor. Specifically, all screened isoforms decrease their expression in the tumor compared to the cells grown *in vitro* except for ALDH1A1, which is clearly increased. This suggests that ALDH1A1 could play a key role in the maintenance of the GL261 tumor *in vivo*. Interestingly, as mentioned above, the expression of this isoform seems to be downregulated when the tumor is treated with ABD-3001. Conversely, the expression levels of the other isoforms tested do not seem to change dramatically between the untreated and treated tumor. Only ALDH3A2 expression may be slightly higher in the treated tumor. These changes in the protein expression may be one of the consequences of DIMATE inhibiting ALDH activity. Specifically, the inhibition of the enzymes involved in RA synthesis could alter the expression of a number of other proteins in the cell.

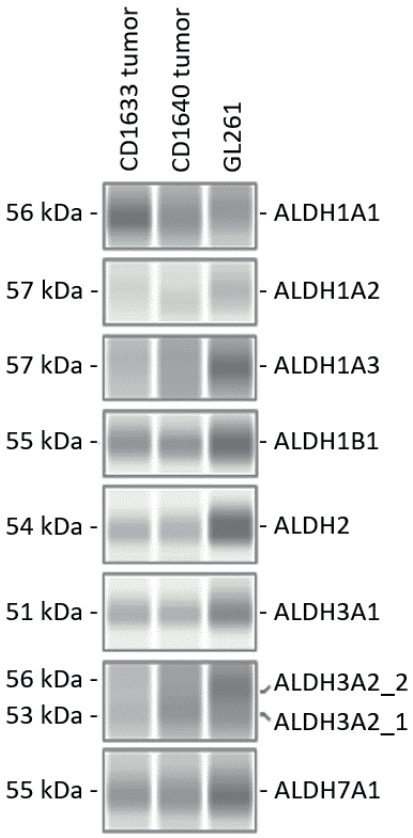

Figure 51. Comparison of ALDH expression between the tumor of an untreated mouse, the tumor of a mouse treated with ABD-3001, and GL261 *in vitro* culture. C1633: mouse belonging to the control group of the therapeutic efficacy assays, treated with 5 mg/kg ABD-3000; C1640: mouse belonging to a treated group of the therapeutic efficacy assays, treated with 5 mg/kg ABD-3001.

GENERAL DISCUSSION

GB, the most common and aggressive type of primary malignant CNS tumor, remains incurable and highly lethal despite decades of extensive research. One of the main factors contributing to treatment failure is the development of chemoresistance towards TMZ, the standard therapeutic agent used currently. In this regard, enzymes belonging to the ALDH superfamily have been reported to be involved in resistance mechanisms, as well as in other important processes related with the maintenance of the CSC subpopulation of the tumor, cell proliferation, differentiation via RA generation, apoptosis, immune evasion, etc. Consequently, ALDH inhibition has emerged as a growing area of research for cancer treatment in recent years. In the present thesis, some compounds synthesized by the biotechnology company ABD were studied as novel potential drugs for the treatment of GB, namely DIMATE, ABD0099, ABD0171, and a lipidic nanoemulsion of DIMATE named ABD-3001.

1. Several isoforms, specifically ALDH1A3, were expressed in GB cell lines as assessed by a capillary-based immunoassay

The expression of ALDH isoforms was first assessed in a panel of GB cell lines. Remarkably, ALDH1A3 was highly expressed in all the GB cell lines tested, except for T98G. This finding aligns with previous reports highlighting the significance of ALDH1A3 in GB. ALDH1A3 has been implicated in the transformation of proneural GSCs to mesenchymal GSCs, which correlates with higher invasiveness, spreading, resistance to therapy and lower overall survival in GB patients [145]–[149].

Importantly, ALDH1A3 has also been directly related to TMZ resistance, as well as ALDH1A1 [136], [137], [139]. However, according to the results obtained in the cytotoxicity assays, there seems not to exist a direct relationship between the expression levels of these ALDH isoforms and resistance to TMZ. Probably, this is due to the fact that TMZ resistance is mediated by other factors, such as the *MGMT* status, which has not been assessed in this thesis and is well known to be a key contributor to chemoresistance against this drug [46]–[48]. Whereas the EC_{50} values of TMZ are in the mM range for almost all the GB cell lines tested, the EC_{50} values of the ALDH inhibitors fall within the low micromolar range, indicating that these compounds are three orders of magnitude more potent than the standard of care itself.

2. *ALDH* knockout in a human GB cell line identified ALDH as a valid drug target

The importance of ALDHs as a viable drug target in GB was further validated through the knockout of several *ALDH* genes in the human GB cell line A172. The enzymatic activity with hexanal and RAL was highly reduced in the KO cell line, and the growth rate of the cells at the exponential phase and their migration capacity were hampered. Most likely, this is directly

related with the fact that RAL elimination and RA production in the KO cell line are strongly reduced. In addition, the KO cell line was shown to be more sensitive to the standard of care TMZ and also to CP, another FDA-approved anticancer drug. These results align well with those reported by Wu *et al*. [138], who demonstrated that ALDH1A3-KO GB cells were significantly more sensitive to TMZ treatment compared to their wild type counterpart. Furthermore, these results also support the results obtained in the synergy assays, and justify why the implementation of ALDH inhibitors could be a suitable approach to enhance the efficacy of the standard of care TMZ. DIMATE, ABD-3001, ABD0099 and ABD0171 were also tested in the KO cell line, but unexpectedly, these cells were not more resistant than the wild type cells. This suggests that these compounds probably have other target molecules apart from ALDHs, leading to off-target effects.

3. Liposome-based nanoparticles with encapsulated DIMATE (ABD-3001) were suitable for drug delivery

Firstly, the characterization of ABD-3001 by cryo-TEM and DLS revealed that these nanoparticles show a spherical morphology and are monodisperse with a diameter below 200 nm, which are features that could make them suitable for drug delivery purposes, although their nearly neutral zeta potential could be a risk factor promoting particle aggregation. In fact, nanoparticles with an average size up to 200 nm have been shown to be efficiently transported transcellularly via intranasal route [203], which is the route utilized in the *in vivo* experiments conducted in this thesis. The intranasal route offers some advantages: the nose is easily accessible, highly vascularized, it allows for lower doses of drug due to minimal first pass metabolism, and importantly, it circumvents the BBB and allows drug delivery directly to the brain, which is one of the main issues in GB management. However, this route presents challenges such as irritation of the nasal cavity and mucociliary clearance, which can be addressed by using nanoparticles, which have been increasingly explored in preclinical studies for the treatment of GB [211]. In addition, analysis of DIMATE release also reinforces the need of its encapsulation for therapeutic purposes, since these experiments suggested that the drug is hydrolyzed in a time-dependent manner in aqueous buffer.

Among the different types of nanoparticles, liposomes have emerged as the most established drug delivery vehicles, with numerous clinical products available to date. However, there is still no FDA-approved clinical liposomal product for the treatment of CNS pathologies. In general, lipid nanocarriers have been considered the most promising treatment strategy for brain cancers due to their ability to cross the BBB [212] and, indeed, some liposomal formulations

have been tested with promising results against GB in preclinical stages of research [213]. Some advantages of liposomes are their high biocompatibility, non-immunogenicity and, remarkably, their ability to encapsulate a wide array of drugs, both hydrophilic and hydrophobic [189], [214]. This is especially relevant for the development of the so-called combination therapies, which are currently arising as a standard practice for cancer treatment. These therapies have yielded enhanced response and survival compared with single-agent therapies for preclinical and clinical investigations [193].

4. Combination treatments with ALDH inhibitors in addition to TMZ demonstrated synergistic effects

In general, monotherapies based on the usage of a single drug often fail to achieve tumor regression. However, combining two or more drugs with distinct mechanisms of action and directed to different molecular targets can synergistically enhance the chances of eradicating the tumor. In this sense, nanoparticles such as liposomes could deliver multiple therapeutic agents at the same time and site, maintaining the optimized synergistic drug ratio in a single carrier all the way up to intracellular uptake by the target cancer cell [193]. In the case of GB, given the high level of tumor heterogeneity and the complexity of the mechanisms that drive development, progression and invasion, combination therapies should probably be the main focus of research from now on. We postulate that the combination of the current standard of care TMZ with ALDH inhibitors could be an encouraging approach, given the important roles of ALDHs in the maintenance and resistance mechanisms of GSCs.

According to some studies on other cancer types [185]–[187], DIMATE would act by causing the accumulation of toxic aldehydes in the cell as a consequence of ALDH inhibition, leading to cell death by apoptosis. In fact, DIMATE, as well as ABD0099 and ABD0171, were proven here to inhibit the cellular ALDH activity in extracts of the human GB cell line A172 and the murine GB cell line GL261. ALDH inhibition was analyzed using both hexanal and RAL as substrates. The inhibition of the reaction with RAL, which is the physiological substrate of the ALDH1A isoforms, could be of particular interest for pharmacological purposes, since the product of the reaction, RA, is a key molecule in the regulation of wide variety of signaling pathways related with cell proliferation, differentiation, cell cycle arrest and apoptosis, among others [84], [102], [103]. In any case, the inhibition of the cellular ALDH activity could be the reason why combination therapies of these compounds with TMZ show synergy in the two GB cell lines mentioned above. It is reported that TMZ, apart from exerting cytotoxicity by causing DNA damage, also contributes to cell death by generating ROS [136]–[138]. These ROS can cause lipid peroxidation,

resulting in the production of toxic aldehydes that further lead to protein and DNA damage, ultimately triggering cell apoptosis. Thus, inhibition of ALDHs by DIMATE, ABD0099 or ABD0171 would prevent detoxification of harmful aldehydes generated by the action of TMZ. Consistent with this theory, synergy was observed in the treatment of A172 cells with TMZ plus DIMATE, which was the most potent compound at inhibiting the ALDH activity with RAL. Similarly, in GL261, the most synergistic combination was that of TMZ with ABD0171, which was the most potent compound at inhibiting ALDH activity with hexanal. Furthermore, in support of the proposed theory, this thesis demonstrated that TMZ and ALDH inhibitors promoted cell death through apoptosis and led to the accumulation of ROS in the cells. Thus, these combination therapies could improve the efficacy of TMZ, suggesting that ALDH inhibitors should be further explored in the field of GB treatment.

5. Intranasal administration of ABD-3001 exerted an antitumor effect by decreasing the rate of tumor growth

Regarding the *in vivo* studies performed in this thesis, tolerability and therapeutic efficacy assays with ABD-3001 were carried out in a murine immunocompetent GL261 GB model. On the one hand, tolerability assays in healthy mice revealed that ABD-3001 displayed some degree of toxicity at the dose of 5 mg/kg, as evidenced by a slight but statistically significant weight loss during the time of treatment, and also by necropsies. This could be due to the drug reaching healthy tissues and also due to the affection of other metabolic processes by the inhibition of off-target proteins, as suggested above. On the other hand, therapeutic efficacy assays with different doses of ABD-3001 on GB-bearing mice showed that, in spite of the toxicity, the drug exerted an antitumor effect by decreasing the rate of tumor growth compared to untreated controls. Toxicity could be mitigated by lowering the dose of ABD-3001, and this allowed the lifespan of treated mice to be extended. Probably, the intranasal administration route and the properties of ABD-3001 nanoparticles allow for the drug to properly reach the tumor and be internalized by cells. We hypothesize, based on the results of the *in vitro* studies, that the reduction of the tumor growth rate could be due to the inhibition of ALDHs and the consequent death of cancer cells by accumulation of ROS and toxic aldehydes, as well as due to the reduction of RA levels, which could lead to impaired cell proliferation and affection of oncogenic signaling pathways. Another potential factor that could be involved in the antitumor effect of ABD-3001 is the enhancement of the immune response against the tumor. It has been reported that RA promotes the induction, function and stability of regulatory T (Treg) cells, which are known to infiltrate in the tumor and maintain immunological self-tolerance [139]–[144]. The inhibition of ALDH1A enzymes could lead to a reduction of RA levels, which in turn could hamper the function

of Treg cells and facilitate the attack of the immune system against the tumor. Nevertheless, the results obtained in these assays clearly suggest that ABD-3001, which has already shown promising results in other cancer types and is currently in clinical phase I for the treatment of AML, could also be a promising drug candidate for the treatment of GB.

Further experiments have provided confirmation that DIMATE is internalized in GL261 cells as well as in tissues of mice treated with ABD-3001 nanoparticles. Interestingly, we found out that DIMATE binds to cellular GSH. This could impair the natural detoxifying function of GSH [206] and have the same effect as the inhibition of ALDH enzymes, regarding the accumulation of damaging electrophilic compounds in the cell. Additionally, we observed changes in the expression of certain ALDHs in the tissues of mice following treatment with ABD-3001. Specifically, the expression of ALDH1A1 and ALDH1A2 decreased in the cerebellum, and all three ALDH1A isoforms exhibited decreased expression in the heart. Notably, ALDH1A1 showed the most significant downregulation in the tumor, which may contribute to the observed decrease in tumor growth rate during the therapeutic efficacy assays and reinforces the idea that the growth of the tumor might be slowed down due to the lack of RA production in the cells. Furthermore, it is worth noting that ALDH1A1 expression is highly increased in the tumor compared to the GL261 cell culture. All this suggests that ALDH1A1 is probably a key enzyme for the maintenance and growth of the GL261 tumor.

6. Summary

The compounds DIMATE, ABD-3001, ABD0099 and ABD0171, developed by the biotechnology company ABD, have demonstrated their ability to inhibit the cellular ALDH activity, displayed high cytotoxicity in a panel of GB cell lines as monotherapies, exhibited synergy when combined with TMZ, and induced the intracellular accumulation of ROS, which is likely to be the reason why cells undergo apoptosis after treatment with the compounds. Furthermore, the knockout of multiple *ALDH* genes in a human GB cell line evidence the importance of these enzymes in processes such as cell proliferation, migration and resistance to various anticancer drugs. The compound ABD-3001, specifically, when tested in a murine immunocompetent GB model, showed efficacy in reducing the rate of tumor growth compared to control mice, thereby potentially extending the lifespan of treated mice. Also, treatment with this drug induced changes in the ALDH expression pattern of several tissues. All in all, the *in vitro* and *in vivo* experiments performed in the present thesis shed some light in the relevance of ALDHs in GB and show how ALDH inhibition could be a promising new pharmacological approach for the treatment of this lethal and incurable disease.

CONCLUSIONS

1. Cryo-TEM analysis revealed that ABD-3001 nanoparticles, encapsulating DIMATE, exhibited a spherical morphology with an average diameter of 30 nm.

2. The monodispersity of ABD-3001 nanoparticles in solution was confirmed under both storage (4°C in saline solution) and physiological conditions, as indicated by the PdI values obtained through DLS. However, their greater hydrodynamic diameter compared to cryo-TEM analysis and their nearly neutral zeta potential suggest that these nanoparticles could form aggregates, especially under physiological conditions.

3. HPLC analysis showed that approximately 70% of DIMATE encapsulated in ABD-3001 nanoparticles was released within the first 4 hours, regardless of pH (pH 5.0 or pH 7.0). In addition, DIMATE seemed to be hydrolyzed with time, slightly to a larger extent at pH 7.0 as compared to pH 5.0.

4. ALDH1A3 showed high expression in all the GB cell lines tested except for T98G, whereas ALDH1A1 and ALDH1A2 showed the highest expression in LN229 and A172.

5. ALDH inhibitors, DIMATE, ABD-3001, ABD0099 and ABD0171, demonstrated cytotoxicity in the low micromolar range against the GB cell lines tested, and were approximately three orders of magnitude more potent than the standard of care TMZ. There was not a direct relationship between ALDH1A expression and the cytotoxicity of the compounds tested.

6. DIMATE, ABD0099 and ABD0171 at 15 µM effectively inhibited ALDH activity with hexanal substrate in cellular extracts of A172 and GL261, being ABD0171 the most potent inhibitor. Furthermore, all three compounds also inhibited RAL dehydrogenase activity in A172 cell extracts in a concentration-dependent manner, with DIMATE displaying the highest potency.

7. In terms of absolute values, A172 cell extracts exhibited higher ALDH activity than GL261 cell extracts, either using hexanal or RAL as a substrate.

8. The combination of TMZ and DIMATE demonstrated synergistic effects against A172 cells, whereas combination of TMZ with the other inhibitors only resulted in an additive effect. Conversely, TMZ combinations with ABD-3001, ABD0099 and ABD0171 displayed

synergistic effects against GL261, whereas the combination with DIMATE resulted in an additive effect in this cell line.

9. Both TMZ and ALDH inhibitors induced apoptosis rather than necrosis as monotherapies in A172 and GL261 cell lines.

10. Treatment with TMZ and all ALDH inhibitors led to ROS accumulation in GL261 cells, while only ABD-3001 induced ROS accumulation in A172 cells at the tested concentrations.

11. A172 KO exhibited decreased expression levels of various ALDH isoforms at both mRNA and protein levels compared to A172 WT cells. Accordingly, ALDH activity with hexanal was significantly reduced and RAL dehydrogenase activity was completely abolished in the KO cell line.

12. A172 KO cells exhibited slower growth compared to A172 WT cells, with an approximate increase of 12 hours in the doubling time during the exponential phase.

13. Migration capacity was hampered in A172 KO cells as compared to A172 WT cells.

14. A172 KO cell line showed increased sensitivity towards RAL, TMZ and CP compared to the WT cell line. A172 KO cells were also slightly more sensitive to ALDH inhibitors (except for ABD0099) than A172 WT cells, suggesting that these compounds were probably not selective for ALDHs and have other target molecules in the cell.

15. Administration of ABD-3001 *in vivo* at doses above 2.5 mg/kg resulted in certain toxicity, leading to organ damage and increased weight loss in treated mice. This issue could be addressed by lowering the dose of ABD-3001 to 1.5 mg/kg.

16. ABD-3001 demonstrated an antitumor effect in GB-bearing mice at different doses, slowing down the rate of tumor growth compared to that of control mice. Particularly, at the dose of 1.5 mg/kg, the lifespan of mice treated with ABD-3001 could be extended.

17. GL261 cells and mice tissues treated directly with ABD-3001 were able to internalize DIMATE. However, upon internalization, DIMATE underwent changes and did not

remain in its original form. The HPLC analysis revealed that the whole DIMATE molecule and/or hydrolyzed fragments of DIMATE bound to GSH.

18. Treatment of GB-bearing mice with ABD-3001 altered the expression of some ALDH isoforms in various organs as assessed by a capillary-based immunoassay. Specifically, ALDH1A1 expression decreased in the tumor, ALDH1A1 and ALDH1A2 expression decreased in the cerebellum, and the expression of the three ALDH1A isoforms decreased in the heart. These findings suggest a downregulation of ALDH enzymes after ABD-3001 treatment.

19. The expression levels of the majority of ALDH isoforms are higher in GL261 cells than in the GL261 tumor, with the exception of ALDH1A1, which is clearly increased on the tumor. This suggests that ALDH1A1 may play crucial roles in the development and maintenance of GL261 tumors.

BIBLIOGRAPHY

[1] H. Sung *et al.*, "Global Cancer Statistics 2020: GLOBOCAN Estimates of Incidence and Mortality Worldwide for 36 Cancers in 185 Countries," *CA Cancer J Clin*, vol. 71, no. 3, pp. 209–249, May 2021, doi: 10.3322/caac.21660.

[2] K. Szklener, M. Mazurek, M. Wieteska, M. Wacławska, M. Bilski, and S. Mańdziuk, "New Directions in the Therapy of Glioblastoma," *Cancers (Basel)*, vol. 14, no. 21, Nov. 2022, doi: 10.3390/cancers14215377.

[3] S. Brandner and Z. Jaunmuktane, "Neurological update: gliomas and other primary brain tumours in adults," *J Neurol*, vol. 265, no. 3, pp. 717–727, Mar. 2018, doi: 10.1007/s00415-017-8652-3.

[4] S. Gritsch, T. T. Batchelor, and L. N. Gonzalez Castro, "Diagnostic, therapeutic, and prognostic implications of the 2021 World Health Organization classification of tumors of the central nervous system," *Cancer*, vol. 128, no. 1, pp. 47–58, Jan. 2022, doi: 10.1002/cncr.33918.

[5] D. N. Louis *et al.*, "The 2021 WHO classification of tumors of the central nervous system: A summary," *Neuro Oncol*, vol. 23, no. 8, pp. 1231–1251, Aug. 2021, doi: 10.1093/neuonc/noab106.

[6] Y. H. Byun and C.-K. Park, "Classification and Diagnosis of Adult Glioma: A Scoping Review," *Brain & Neurorehabilitation*, vol. 15, no. 3, 2022, doi: 10.12786/bn.2022.15.e23.

[7] C. McKinnon, M. Nandhabalan, S. A. Murray, and P. Plaha, "Glioblastoma: Clinical presentation, diagnosis, and management," *BMJ*, vol. 374, Jul. 2021, doi: 10.1136/bmj.n1560.

[8] N. Sanai, A. Alvarez-Buylla, and M. S. Berger, "Neural Stem Cells and the Origin of Gliomas," *New England Journal of Medicine*, vol. 8, pp. 811–833, 2005, [Online]. Available: www.nejm.org

[9] F. L. Robertson, M. A. Marqués-Torrejón, G. M. Morrison, and S. M. Pollard, "Experimental models and tools to tackle glioblastoma," *Dis Model Mech*, vol. 12, no. 9, 2019, doi: 10.1242/dmm.040386.

[10] A. Perry and P. Wesseling, "Histologic classification of gliomas," in *Handbook of Clinical Neurology*, 2016, pp. 71–95.

[11] M. Osswald *et al.*, "Brain tumour cells interconnect to a functional and resistant network," *Nature*, vol. 528, no. 7580, pp. 93–98, Dec. 2015, doi: 10.1038/nature16071.

[12] M. Antonelli and P. L. Poliani, "Adult type diffuse gliomas in the new 2021 WHO Classification," *Pathologica*, vol. 114, no. 6, pp. 397–409, Dec. 2022, doi: 10.32074/1591-951X-823.

[13] D. N. Louis *et al.*, “The 2007 WHO classification of tumours of the central nervous system,” *Acta Neuropathol*, vol. 114, no. 2, pp. 97–109, Aug. 2007, doi: 10.1007/s00401-007-0243-4.

[14] A. Perez and J. T. Huse, “The Evolving Classification of Diffuse Gliomas: World Health Organization Updates for 2021,” *Curr Neurol Neurosci Rep*, vol. 21, no. 12, Dec. 2021, doi: 10.1007/s11910-021-01153-8.

[15] T. Komori, “Grading of adult diffuse gliomas according to the 2021 WHO Classification of Tumors of the Central Nervous System,” *Laboratory Investigation*, vol. 102, no. 2, pp. 126–133, Feb. 2022, doi: 10.1038/s41374-021-00667-6.

[16] E. Verdugo, I. Puerto, and M. Á. Medina, “An update on the molecular biology of glioblastoma, with clinical implications and progress in its treatment,” *Cancer Commun*, vol. 42, no. 11, pp. 1083–1111, Nov. 2022, doi: 10.1002/cac2.12361.

[17] S. DeCordova *et al.*, “Molecular Heterogeneity and Immunosuppressive Microenvironment in Glioblastoma,” *Front Immunol*, vol. 11, Jul. 2020, doi: 10.3389/fimmu.2020.01402.

[18] F. B. Furnari *et al.*, “Malignant astrocytic glioma: Genetics, biology, and paths to treatment,” *Genes Dev*, vol. 21, no. 21, pp. 2683–2710, Nov. 2007, doi: 10.1101/gad.1596707.

[19] A. C. Tan, D. M. Ashley, G. Y. López, M. Malinzak, H. S. Friedman, and M. Khasraw, “Management of glioblastoma: State of the art and future directions,” *CA Cancer J Clin*, vol. 70, no. 4, pp. 299–312, Jul. 2020, doi: 10.3322/caac.21613.

[20] F. Liesche-Starnecker *et al.*, “Immunohistochemically characterized intratumoral heterogeneity is a prognostic marker in human glioblastoma,” *Cancers (Basel)*, vol. 12, no. 10, pp. 1–17, Oct. 2020, doi: 10.3390/cancers12102964.

[21] D. Friedmann-Morvinski, “Glioblastoma Heterogeneity and Cancer Cell Plasticity,” *Crit Rev Oncog*, vol. 19, no. 5, pp. 327–336, 2014.

[22] S. Jankowska, M. Lewandowska, M. Masztalewicz, L. Sagan, P. Nowacki, and E. Urasińska, “Molecular classification of glioblastoma based on immunohistochemical expression of EGFR, PDGFRA, NF1, IDH1, p53 and PTEN proteins,” *Polish Journal of Pathology*, vol. 72, no. 1, pp. 1–10, 2021, doi: 10.5114/pjp.2021.106439.

[23] S. H. Soomro, L. R. Ting, Y. Y. Qing, and M. Ren, “Molecular biology of glioblastoma: Classification and mutational locations,” *J Pak Med Assoc*, vol. 67, no. 9, pp. 1410–1414, 2017.

[24] R. G. W. Verhaak *et al.*, “Integrated Genomic Analysis Identifies Clinically Relevant Subtypes of Glioblastoma Characterized by Abnormalities in PDGFRA, IDH1, EGFR, and NF1,” *Cancer Cell*, vol. 17, no. 1, pp. 98–110, Jan. 2010, doi: 10.1016/j.ccr.2009.12.020.

[25] S. Grochans *et al.*, “Epidemiology of Glioblastoma Multiforme–Literature Review,” *Cancers (Basel)*, vol. 14, no. 10, May 2022, doi: 10.3390/cancers14102412.

[26] N. Grech, T. Dalli, S. Mizzi, L. Meilak, N. Calleja, and A. Zrinzo, “Rising Incidence of Glioblastoma Multiforme in a Well-Defined Population,” *Cureus*, May 2020, doi: 10.7759/cureus.8195.

[27] O. Rominiyi, A. Vanderlinden, S. J. Clenton, C. Bridgewater, Y. Al-Tamimi, and S. J. Collis, “Tumour treating fields therapy for glioblastoma: current advances and future directions,” *Br J Cancer*, vol. 124, no. 4, pp. 697–709, Feb. 2021, doi: 10.1038/s41416-020-01136-5.

[28] Q. T. Ostrom, H. Gittleman, G. Truitt, A. Boscia, C. Kruchko, and J. S. Barnholtz-Sloan, “CBTRUS statistical report: Primary brain and other central nervous system tumors diagnosed in the United States in 2011-2015,” *Neuro Oncol*, vol. 20, pp. iv1–iv86, Oct. 2018, doi: 10.1093/neuonc/noy131.

[29] R. C. Gimple, S. Bhargava, D. Dixit, and J. N. Rich, “Glioblastoma stem cells: lessons from the tumor hierarchy in a lethal cancer,” *Genes Dev*, vol. 33, pp. 591–609, 2019, doi: 10.1101/gad.324301.

[30] M. Jiménez-Alcázar *et al.*, “Dianhydrogalactitol overcomes multiple temozolomide resistance mechanisms in glioblastoma,” *Mol Cancer Ther*, vol. 20, no. 6, pp. 1029–1038, Jun. 2021, doi: 10.1158/1535-7163.MCT-20-0319.

[31] B. Obermeier, R. Daneman, and R. M. Ransohoff, “Development, maintenance and disruption of the blood-brain barrier,” *Nat Med*, vol. 19, no. 12, pp. 1584–1596, Dec. 2013, doi: 10.1038/nm.3407.

[32] B. Auffinger, D. Spencer, P. Pytel, A. U. Ahmed, and M. S. Lesniak, “The role of glioma stem cells in chemotherapy resistance and glioblastoma multiforme recurrence,” *Expert Rev Neurother*, vol. 15, no. 7, pp. 741–752, Jul. 2015, doi: 10.1586/14737175.2015.1051968.

[33] J. V. R. Cruz *et al.*, “Obstacles to Glioblastoma Treatment Two Decades after Temozolomide,” *Cancers (Basel)*, vol. 14, no. 13, Jul. 2022, doi: 10.3390/cancers14133203.

[34] M. Y. Ali *et al.*, “Radioresistance in glioblastoma and the development of radiosensitizers,” *Cancers (Basel)*, vol. 12, no. 9, pp. 1–29, Sep. 2020, doi: 10.3390/cancers12092511.

[35] Z. Chen, X. Wei, L. Shen, H. Zhu, and X. Zheng, “20(S)-ginsenoside-Rg3 reverses temozolomide resistance and restrains epithelial-mesenchymal transition progression in glioblastoma,” *Cancer Sci*, vol. 110, no. 1, pp. 389–400, Jan. 2019, doi: 10.1111/cas.13881.

[36] R. O. Mirimanoff *et al.*, “Radiotherapy and temozolomide for newly diagnosed glioblastoma: Recursive partitioning analysis of the EORTC 26981/22981-NCIC CE3 phase III randomized trial,” *Journal of Clinical Oncology*, vol. 24, no. 16, pp. 2563–2569, Jun. 2006, doi: 10.1200/JCO.2005.04.5963.

[37] R. Stupp *et al.*, “Radiotherapy plus Concomitant and Adjuvant Temozolomide for Glioblastoma,” *New England Journal of Medicine*, vol. 352, no. 10, pp. 987–996, 2005, [Online]. Available: www.nejm.org

[38] R. Stupp *et al.*, “Effects of radiotherapy with concomitant and adjuvant temozolomide versus radiotherapy alone on survival in glioblastoma in a randomised phase III study: 5-year analysis of the EORTC-NCIC trial,” *Lancet Oncology*, pp. 459–466, 2009.

[39] S. Jiapaer, T. Furuta, S. Tanaka, T. Kitabayashi, and M. Nakada, “Potential strategies overcoming the temozolomide resistance for glioblastoma,” *Neurol Med Chir (Tokyo)*, vol. 58, no. 10, pp. 405–421, 2018, doi: 10.2176/nmc.ra.2018-0141.

[40] S. Y. Lee, “Temozolomide resistance in glioblastoma multiforme,” *Genes Dis*, vol. 3, no. 3, pp. 198–210, Sep. 2016, doi: 10.1016/j.gendis.2016.04.007.

[41] R. Ortiz *et al.*, “Temozolomide: An Updated Overview of Resistance Mechanisms, Nanotechnology Advances and Clinical Applications,” *Curr Neuropharmacol*, vol. 19, no. 4, pp. 513–537, Jun. 2020, doi: 10.2174/1570159x18666200626204005.

[42] A. Rodríguez-Camacho *et al.*, “Glioblastoma Treatment: State-of-the-Art and Future Perspectives,” *Int J Mol Sci*, vol. 23, no. 13, Jul. 2022, doi: 10.3390/ijms23137207.

[43] J. I. L. Bastien, K. A. McNeill, and H. A. Fine, “Molecular characterizations of glioblastoma, targeted therapy, and clinical results to date,” *Cancer*, vol. 121, no. 4, pp. 502–516, Feb. 2015, doi: 10.1002/cncr.28968.

[44] S. A. Grossman *et al.*, “Survival of patients with newly diagnosed glioblastoma treated with radiation and temozolomide in research studies in the United States,” *Clinical Cancer Research*, vol. 16, no. 8, pp. 2443–2449, Apr. 2010, doi: 10.1158/1078-0432.CCR-09-3106.

[45] W. Wick and M. Platten, “Understanding and targeting alkylator resistance in glioblastoma,” *Cancer Discov*, vol. 4, no. 10, pp. 1120–1122, Oct. 2014, doi: 10.1158/2159-8290.CD-14-0918.

[46] J. Feldheim, A. F. Kessler, C. M. Monoranu, R. I. Ernestus, M. Löhr, and C. Hagemann, “Changes of O6-methylguanine DNA methyltransferase (MGMT) promoter methylation in glioblastoma relapse—a meta-analysis type literature review,” *Cancers (Basel)*, vol. 11, no. 12, Dec. 2019, doi: 10.3390/cancers11121837.

[47] A. L. Rivera *et al.*, “MGMT promoter methylation is predictive of response to radiotherapy and prognostic in the absence of adjuvant alkylating chemotherapy for glioblastoma,” *Neuro Oncol*, vol. 12, no. 2, pp. 116–121, Feb. 2010, doi: 10.1093/neuonc/nop020.

[48] K. A. Van Nifterik *et al.*, “Absence of the MGMT protein as well as methylation of the MGMT promoter predict the sensitivity for temozolomide,” *Br J Cancer*, vol. 103, no. 1, pp. 29–35, Jun. 2010, doi: 10.1038/sj.bjc.6605712.

[49] H. Kang *et al.*, “Targeting Glioblastoma Stem Cells to Overcome Chemoresistance: An Overview of Current Therapeutic Strategies,” *Biomedicines*, vol. 10, no. 6, Jun. 2022, doi: 10.3390/biomedicines10061308.

[50] A. Thakur *et al.*, “Glioblastoma: Current Status, Emerging Targets, and Recent Advances,” *J Med Chem*, vol. 65, no. 13, pp. 8596–8685, Jul. 2022, doi: 10.1021/acs.jmedchem.1c01946.

[51] A. Arora and K. Somasundaram, “Glioblastoma vs temozolomide: can the red queen race be won?,” *Cancer Biol Ther*, vol. 20, no. 8, pp. 1083–1090, Aug. 2019, doi: 10.1080/15384047.2019.1599662.

[52] Y. Yan, Z. Xu, S. Dai, L. Qian, L. Sun, and Z. Gong, "Targeting autophagy to sensitive glioma to temozolomide treatment," *Journal of Experimental and Clinical Cancer Research*, vol. 35, no. 1, Feb. 2016, doi: 10.1186/s13046-016-0303-5.

[53] T. Kanzawa, I. M. Germano, T. Komata, H. Ito, Y. Kondo, and S. Kondo, "Role of autophagy in temozolomide-induced cytotoxicity for malignant glioma cells," *Cell Death Differ*, vol. 11, no. 4, pp. 448–457, Apr. 2004, doi: 10.1038/sj.cdd.4401359.

[54] A. J. Manea and S. K. Ray, "Regulation of autophagy as a therapeutic option in glioblastoma," *Apoptosis*, vol. 26, no. 11–12, pp. 574–599, Dec. 2021, doi: 10.1007/s10495-021-01691-z.

[55] J. E. Simpson and N. Gammoh, "The impact of autophagy during the development and survival of glioblastoma: Role of autophagy in glioblastoma," *Open Biol*, vol. 10, no. 9, Sep. 2020, doi: 10.1098/rsob.200184.

[56] Z. Hu *et al.*, "A Potential Mechanism of Temozolomide Resistance in Glioma–Ferroptosis," *Front Oncol*, vol. 10, Jun. 2020, doi: 10.3389/fonc.2020.00897.

[57] M. Zhang, Q. Lei, X. Huang, and Y. Wang, "Molecular mechanisms of ferroptosis and the potential therapeutic targets of ferroptosis signaling pathways for glioblastoma," *Front Pharmacol*, vol. 13, Nov. 2022, doi: 10.3389/fphar.2022.1071897.

[58] S. Zhuo *et al.*, "Emerging role of ferroptosis in glioblastoma: Therapeutic opportunities and challenges," *Front Mol Biosci*, vol. 9, Aug. 2022, doi: 10.3389/fmolb.2022.974156.

[59] M. D. Friedman, D. S. Jeevan, M. Tobias, R. Murali, and M. Jhanwar-Uniyal, "Targeting cancer stem cells in glioblastoma multiforme using mTOR inhibitors and the differentiating agent all-trans retinoic acid," *Oncol Rep*, vol. 30, no. 4, pp. 1645–1650, Oct. 2013, doi: 10.3892/or.2013.2625.

[60] M. Jackson, F. Hassiotou, and A. Nowak, "Glioblastoma stem-like cells: At the root of tumor recurrence and a therapeutic target," *Carcinogenesis*, vol. 36, no. 2, pp. 177–185, 2014, doi: 10.1093/carcin/bgu243.

[61] Q. Xie, S. Mittal, and M. E. Berens, "Targeting adaptive glioblastoma: An overview of proliferation and invasion," *Neuro Oncol*, vol. 16, no. 12, pp. 1575–1584, Dec. 2014, doi: 10.1093/neuonc/nou147.

[62] D. Nassar and C. Blanpain, "Cancer Stem Cells: Basic Concepts and Therapeutic Implications," *Annual Review of Pathology: Mechanisms of Disease*, vol. 11, pp. 47–76, May 2016, doi: 10.1146/annurev-pathol-012615-044438.

[63] S. J. Sundar, J. K. Hsieh, S. Manjila, J. D. Lathia, and A. Sloan, "The role of cancer stem cells in glioblastoma," *Neurosurg Focus*, vol. 37, no. 6, 2014, doi: 10.3171/2014.9.FOCUS14494.

[64] B. Auffinger *et al.*, "Conversion of differentiated cancer cells into cancer stem-like cells in a glioblastoma model after primary chemotherapy," *Cell Death Differ*, vol. 21, no. 7, pp. 1119–1131, 2014, doi: 10.1038/cdd.2014.31.

[65] G. J. Yoshida and H. Saya, "Molecular pathology underlying the robustness of cancer stem cells," *Regen Ther*, vol. 17, pp. 38–50, Jun. 2021, doi: 10.1016/j.reth.2021.02.002.

[66] S. M. Afify and M. Seno, “Conversion of stem cells to cancer stem cells: Undercurrent of cancer initiation,” *Cancers (Basel)*, vol. 11, no. 3, Mar. 2019, doi: 10.3390/cancers11030345.

[67] J. D. Lathia *et al.*, “Distribution of CD133 reveals glioma stem cells self-renew through symmetric and asymmetric cell divisions,” *Cell Death Dis*, vol. 2, no. 9, Sep. 2011, doi: 10.1038/cddis.2011.80.

[68] T. Lapidot *et al.*, “A cell initiating human acute myeloid leukaemia after transplantation into SCID mice,” *Nature*, vol. 367, pp. 645–648, 1994.

[69] M. Al-Hajj, M. S. Wicha, A. Benito-Hernandez, S. J. Morrison, and M. F. Clarke, “Prospective identification of tumorigenic breast cancer cells,” *PNAS*, vol. 100, no. 7, pp. 3983–3988, 2003, [Online]. Available: www.pnas.orgcgidoi10.1073pnas.0530291100

[70] S. K. Singh *et al.*, “Identification of a Cancer Stem Cell in Human Brain Tumors,” *Cancer Res*, vol. 63, pp. 5821–5828, 2003, [Online]. Available: http://aacrjournals.org/cancerres/article-pdf/63/18/5821/2506915/ch1803005821.pdf

[71] G. Muzio, M. Maggiora, E. Paiuzzi, M. Oraldi, and R. A. Canuto, “Aldehyde dehydrogenases and cell proliferation,” *Free Radic Biol Med*, vol. 52, no. 4, pp. 735–746, Feb. 2012, doi: 10.1016/j.freeradbiomed.2011.11.033.

[72] K. Pors and J. S. Moreb, “Aldehyde dehydrogenases in cancer: An opportunity for biomarker and drug development?,” *Drug Discov Today*, vol. 19, no. 12, pp. 1953–1963, Nov. 2014, doi: 10.1016/j.drudis.2014.09.009.

[73] E. Vlashi and F. Pajonk, “Cancer stem cells, cancer cell plasticity and radiation therapy,” *Semin Cancer Biol*, vol. 31, pp. 28–35, Apr. 2015, doi: 10.1016/j.semcancer.2014.07.001.

[74] I. Ma and A. L. Allan, “The Role of Human Aldehyde Dehydrogenase in Normal and Cancer Stem Cells,” *Stem Cell Rev Rep*, vol. 7, no. 2, pp. 292–306, Jun. 2011, doi: 10.1007/s12015-010-9208-4.

[75] A. Moretti, J. Li, S. Donini, R. W. Sobol, M. Rizzi, and S. Garavaglia, “Crystal structure of human aldehyde dehydrogenase 1A3 complexed with NAD+ and retinoic acid,” *Sci Rep*, vol. 6, Oct. 2016, doi: 10.1038/srep35710.

[76] J. J. Duan, J. Cai, Y. F. Guo, X. W. Bian, and S. C. Yu, “ALDH1A3, a metabolic target for cancer diagnosis and therapy,” *Int J Cancer*, vol. 139, no. 5, pp. 965–975, Sep. 2016, doi: 10.1002/ijc.30091.

[77] M. Hassn Mesrati, A. B. Behrooz, A. Y Abuhamad, and A. Syahir, “Understanding Glioblastoma Biomarkers: Knocking a Mountain with a Hammer,” *Cells*, vol. 9, no. 5, May 2020, doi: 10.3390/cells9051236.

[78] R. W. Storms *et al.*, “Isolation of primitive human hematopoietic progenitors on the basis of aldehyde dehydrogenase activity,” *PNAS*, vol. 96, pp. 9118–9123, 1999, [Online]. Available: www.pnas.org.

[79] J. W. Park *et al.*, “ATP-binding Cassette Transporters Substantially Reduce Estimates of ALDH-positive Cancer Cells based on Aldefluor and AldeRed588 Assays,” *Sci Rep*, vol. 9, no. 1, Dec. 2019, doi: 10.1038/s41598-019-42954-9.

[80] H. Tomita, K. Tanaka, T. Tanaka, and A. Hara, “Aldehyde dehydrogenase 1A1 in stem cells and cancer,” *Oncotarget*, vol. 7, no. 10, pp. 11018–11032, 2016, [Online]. Available: www.impactjournals.com/oncotarget/

[81] L. Zhou *et al.*, “Identification of cancer-type specific expression patterns for active aldehyde dehydrogenase (ALDH) isoforms in ALDEFLUOR assay,” *Cell Biol Toxicol*, vol. 35, no. 2, pp. 161–177, Apr. 2019, doi: 10.1007/s10565-018-9444-y.

[82] J. J. Duan, J. Cai, L. Gao, and S. C. Yu, “ALDEFLUOR activity, ALDH isoforms, and their clinical significance in cancers,” *J Enzyme Inhib Med Chem*, vol. 38, no. 1, 2023, doi: 10.1080/14756366.2023.2166035.

[83] C. A. Morgan, B. Parajuli, C. D. Buchman, K. Dria, and T. D. Hurley, “N,N-diethylaminobenzaldehyde (DEAB) as a substrate and mechanism-based inhibitor for human ALDH isoenzymes,” *Chem Biol Interact*, vol. 234, pp. 18–28, Jun. 2015, doi: 10.1016/j.cbi.2014.12.008.

[84] P. Marcato, C. A. Dean, C. A. Giacomantonio, and P. W. K. Lee, “Aldehyde dehydrogenase its role as a cancer stem cell marker comes down to the specific isoform,” *Cell Cycle*, vol. 10, no. 9, pp. 1378–1384, May 2011, doi: 10.4161/cc.10.9.15486.

[85] H. Feng, Y. Liu, X. Bian, F. Zhou, and Y. Liu, “ALDH1A3 affects colon cancer in vitro proliferation and invasion depending on CXCR4 status,” *Br J Cancer*, vol. 118, no. 2, pp. 224–232, Jan. 2018, doi: 10.1038/bjc.2017.363.

[86] J. S. Moreb *et al.*, “The enzymatic activity of human aldehyde dehydrogenases 1A2 and 2 (ALDH1A2 and ALDH2) is detected by Aldefluor, inhibited by diethylaminobenzaldehyde and has significant effects on cell proliferation and drug resistance,” *Chem Biol Interact*, vol. 195, no. 1, pp. 52–60, Jan. 2012, doi: 10.1016/j.cbi.2011.10.007.

[87] S. Singh *et al.*, “Aldehyde dehydrogenases in cellular responses to oxidative/ electrophilicstress,” *Free Radic Biol Med*, vol. 56, pp. 89–101, Mar. 2013, doi: 10.1016/j.freeradbiomed.2012.11.010.

[88] K. Biserova, A. Jakovlevs, R. Uljanovs, and I. Strumfa, “Cancer stem cells: Significance in origin, pathogenesis and treatment of glioblastoma,” *Cells*, vol. 10, no. 3, pp. 1–20, Mar. 2021, doi: 10.3390/cells10030621.

[89] A. M. Bleau *et al.*, “PTEN/PI3K/Akt Pathway Regulates the Side Population Phenotype and ABCG2 Activity in Glioma Tumor Stem-like Cells,” *Cell Stem Cell*, vol. 4, no. 3, pp. 226–235, Mar. 2009, doi: 10.1016/j.stem.2009.01.007.

[90] M. Cojoc, K. Mäbert, M. H. Muders, and A. Dubrovska, “A role for cancer stem cells in therapy resistance: Cellular and molecular mechanisms,” *Semin Cancer Biol*, vol. 31, pp. 16–27, Apr. 2015, doi: 10.1016/j.semcancer.2014.06.004.

[91] V. Vasiliou and D. W. Nebert, “Analysis and update of the human aldehyde dehydrogenase (ALDH) gene family,” *Hum Genomics*, vol. 2, no. 2, pp. 138–143, 2005, [Online]. Available: http://www.aldh.org

[92] R. Lindahl and H. Weiner, “Aldehyde Dehydrogenases and Their Role in Carcinogenesis,” *Crit Rev Biochem Mol Biol*, vol. 27, pp. 283–335, 1992.

[93] D. V. Nadkarni and L. M. Sayre, “Structural Definition of Early Lysine and Histidine Adduction Chemistry of 4-Hydroxynonenal,” *Chem Res Toxicol*, vol. 8, pp. 284–291, 1996.

[94] P. J. Brooks and J. A. Theruvathu, “DNA adducts from acetaldehyde: Implications for alcohol-related carcinogenesis,” *Alcohol*, vol. 35, no. 3, pp. 187–193, Apr. 2005, doi: 10.1016/j.alcohol.2005.03.009.

[95] J. S. Rodríguez-Zavala, L. F. Calleja, R. Moreno-Sánchez, and B. Yoval-Sánchez, “Role of Aldehyde Dehydrogenases in Physiopathological Processes,” *Chem Res Toxicol*, vol. 32, no. 3, pp. 405–420, Mar. 2019, doi: 10.1021/acs.chemrestox.8b00256.

[96] D. A. Korasick and J. J. Tanner, “Impact of missense mutations in the ALDH7A1 gene on enzyme structure and catalytic function,” *Biochimie*, vol. 183, pp. 49–54, Apr. 2021, doi: 10.1016/j.biochi.2020.09.016.

[97] S. A. Marchitti, C. Brocker, D. Stagos, and V. Vasiliou, “Non-P450 aldehyde oxidizing enzymes: the aldehyde dehydrogenase superfamily,” *Expert Opin Drug Metab Toxicol*, vol. 4, no. 6, pp. 697–720, 2008, doi: 10.1517/17425250802102627.

[98] G. Duester, F. A. Mic, and A. Molotkov, “Cytosolic retinoid dehydrogenases govern ubiquitous metabolism of retinol to retinaldehyde followed by tissue-specific metabolism to retinoic acid,” *Chem Biol Interact*, vol. 143–144, pp. 201–210, 2003, [Online]. Available: www.elsevier.com/locate/chembioint

[99] N. Y. Kedishvili, “Retinoic acid synthesis and degradation,” *Subcell Biochem*, vol. 81, pp. 127–161, Nov. 2016, doi: 10.1007/978-94-024-0945-1_5.

[100] R. Pequerul *et al.*, “Structural and kinetic features of aldehyde dehydrogenase 1A (ALDH1A) subfamily members, cancer stem cell markers active in retinoic acid biosynthesis,” *Arch Biochem Biophys*, vol. 681, Mar. 2020, doi: 10.1016/j.abb.2020.108256.

[101] K. Niederreither, J. Vermot, B. Schuhbaur, P. Chambon, and P. Dollé, “Retinoic acid synthesis and hindbrain patterning in the mouse embryo,” *Development*, vol. 127, pp. 75–85, 2000.

[102] R. K. T. Kam, Y. Deng, Y. Chen, and H. Zhao, “Retinoic acid synthesis and functions in early embryonic development,” *Cell Biosci*, vol. 2, no. 1, Mar. 2012, doi: 10.1186/2045-3701-2-11.

[103] R. Suzuki *et al.*, “Identification of RALDH-3, a novel retinaldehyde dehydrogenase, expressed in the ventral region of the retina,” *Mech Dev*, vol. 98, pp. 37–50, 2000, [Online]. Available: www.elsevier.com/locate/modo

[104] V. Vasiliou, D. C. Thompson, C. Smith, M. Fujita, and Y. Chen, “Aldehyde dehydrogenases: From eye crystallins to metabolic disease and cancer stem cells,” *Chem Biol Interact*, vol. 202, no. 1–3, pp. 2–10, Feb. 2013, doi: 10.1016/j.cbi.2012.10.026.

[105] J. S. Rodríguez-Zavala, A. Allali-Hassani, and H. Weiner, “Characterization of E. coli tetrameric aldehyde dehydrogenases with atypical properties compared to other aldehyde dehydrogenases,” *Protein Science*, vol. 15, no. 6, pp. 1387–1396, Jun. 2006, doi: 10.1110/ps.052039606.

[106] K. Shortall, A. Djeghader, E. Magner, and T. Soulimane, “Insights into Aldehyde Dehydrogenase Enzymes: A Structural Perspective,” *Front Mol Biosci*, vol. 8, May 2021, doi: 10.3389/fmolb.2021.659550.

[107] J. Farrés, T. T. Y. Wang, S. J. Cunningham, and H. Weiner, “Investigation of the Active Site Cysteine Residue of Rat Liver Mitochondrial Aldehyde Dehydrogenase by Site-Directed Mutagenesis,” *Biochemistry*, vol. 34, pp. 2592–2598, 1995.

[108] S. L. Bradbury and W. B. Jakoby, “Ordered binding of substrates to yeast aldehyde dehydrogenase,” *Journal of Biological Chemistry*, vol. 246, no. 6, pp. 1834–1840, Mar. 1971, doi: 10.1016/s0021-9258(18)62384-1.

[109] E. M. Valenzuela-Soto and R. A. Muñoz-Clares, “Betaine-aldehyde dehydrogenase from leaves of Amaranthus hypochondriacus L. exhibits an iso ordered bi bi steady state mechanism,” *Journal of Biological Chemistry*, vol. 268, no. 32, pp. 23818–23824, 1993.

[110] V. Koppaka *et al.*, “Aldehyde dehydrogenase inhibitors: A comprehensive review of the pharmacology, mechanism of action, substrate specificity, and clinical application,” *Pharmacol Rev*, vol. 64, no. 3, pp. 520–539, 2012, doi: 10.1124/pr.111.005538.

[111] N. E. Sládek, “Human aldehyde dehydrogenases: Potential pathological, pharmacological, and toxicological impact,” *J Biochem Mol Toxicol*, vol. 17, no. 1, pp. 7–23, 2003, doi: 10.1002/jbt.10057.

[112] E. E. Blatter, D. P. Abriola, and R. Pietruszko, “Aldehyde dehydrogenase. Covalent intermediate in aldehyde dehydrogenation and ester hydrolysis,” *Biochemical Journal*, vol. 282, pp. 353–360, 1992.

[113] Z. Chen, J. Zhang, and J. S. Stamler, “Identification of the enzymatic mechanism of nitroglycerin bioactivation,” *PNAS*, vol. 99, no. 12, pp. 8306–8311, 2002, [Online]. Available: www.pnas.orgcgidoi10.1073pnas.122225199

[114] K. Sydow *et al.*, “Central role of mitochondrial aldehyde dehydrogenase and reactive oxygen species in nitroglycerin tolerance and cross-tolerance,” *Journal of Clinical Investigation*, vol. 113, no. 3, pp. 482–489, Feb. 2004, doi: 10.1172/JCI200419267.

[115] B. C. Jackson, D. C. Thompson, G. Charkoftaki, and V. Vasiliou, “Dead enzymes in the aldehyde dehydrogenase gene family: Role in drug metabolism and toxicology,” *Expert Opin Drug Metab Toxicol*, vol. 11, no. 12, pp. 1839–1847, Dec. 2015, doi: 10.1517/17425255.2016.1108406.

[116] J. V. Jester, “Corneal Crystallins and the Development of Cellular Transparency,” *Semin Cell Dev Biol*, vol. 19, no. 2, pp. 82–93, 2008.

[117] T. Estey, M. Cantore, P. A. Weston, J. F. Carpenter, J. M. Petrash, and V. Vasiliou, “Mechanisms involved in the protection of UV-induced protein inactivation by the corneal crystallin ALDH3A1,” *Journal of Biological Chemistry*, vol. 282, no. 7, pp. 4382–4392, Feb. 2007, doi: 10.1074/jbc.M607546200.

[118] N. Lassen *et al.*, “Multiple and additive functions of ALDH3A1 and ALDH1A1: cataract phenotype and ocular oxidative damage in ALDH3A1 (-/-)/ALDH1A1(-/-) knock-out mice,” *Journal of Biological Chemistry*, vol. 282, no. 35, pp. 25668–25676, 2007, [Online]. Available: http://www.jbc.org

[119] N. Lassen *et al.*, "Antioxidant function of corneal ALDH3A1 in cultured stromal fibroblasts," *Free Radic Biol Med*, vol. 41, no. 9, pp. 1459–1469, Nov. 2006, doi: 10.1016/j.freeradbiomed.2006.08.009.

[120] A. Pappa, C. Chen, Y. Koutalos, A. J. Townsend, and V. Vasiliou, "ALDH3A1 protects human corneal epithelial cells from ultraviolet- and 4-hydroxy-2-nonenal-induced oxidative damage," *Free Radic Biol Med*, vol. 34, no. 9, pp. 1178–1189, May 2003, doi: 10.1016/S0891-5849(03)00070-4.

[121] L. Uma, J. Hariharan, Y. Sharma, and D. Balasubramanian, "Corneal Aldehyde Dehydrogenase Displays Antioxidant Properties," *Exp Eye Res*, vol. 63, no. 1, pp. 117–120, 1996.

[122] V. Vasiliou, A. Pappa, and T. Estey, "Role of human aldehyde dehydrogenases in endobiotic and xenobiotic metabolism," *Drug Metab Rev*, vol. 36, no. 2, pp. 279–299, 2004, doi: 10.1081/DMR-120034001.

[123] P. Marcato *et al.*, "Aldehyde dehydrogenase activity of breast cancer stem cells is primarily due to isoform ALDH1A3 and its expression is predictive of metastasis," *Stem Cells*, vol. 29, no. 1, pp. 32–45, Jan. 2011, doi: 10.1002/stem.563.

[124] C. Ginestier *et al.*, "Retinoid signaling regulates breast cancer stem cell differentiation," *Cell Cycle*, vol. 8, no. 20, pp. 3297–3302, 2009.

[125] M. Ying *et al.*, "Regulation of glioblastoma stem cells by retinoic acid: Role for Notch pathway inhibition," *Oncogene*, vol. 30, no. 31, pp. 3454–3467, Aug. 2011, doi: 10.1038/onc.2011.58.

[126] N. Bushue and Y. J. Y. Wan, "Retinoid pathway and cancer therapeutics," *Adv Drug Deliv Rev*, vol. 62, no. 13, pp. 1285–1298, Oct. 2010, doi: 10.1016/j.addr.2010.07.003.

[127] J. S. Moreb, D. A. Ucar-Bilyeu, and A. Khan, "Use of retinoic acid/aldehyde dehydrogenase pathway as potential targeted therapy against cancer stem cells," *Cancer Chemother Pharmacol*, vol. 79, no. 2, pp. 295–301, Feb. 2017, doi: 10.1007/s00280-016-3213-5.

[128] X. Xu *et al.*, "Aldehyde dehydrogenases and cancer stem cells," *Cancer Lett*, vol. 369, no. 1, pp. 50–57, Dec. 2015, doi: 10.1016/j.canlet.2015.08.018.

[129] B. Mezquita and C. Mezquita, "Two opposing faces of retinoic acid: Induction of stemness or induction of differentiation depending on cell-type," *Biomolecules*, vol. 9, no. 10, Oct. 2019, doi: 10.3390/biom9100567.

[130] M. Poturnajova, Z. Kozovska, and M. Matuskova, "Aldehyde dehydrogenase 1A1 and 1A3 isoforms – mechanism of activation and regulation in cancer," *Cell Signal*, vol. 87, Nov. 2021, doi: 10.1016/j.cellsig.2021.110120.

[131] R. Januchowski, K. Wojtowicz, and M. Zabel, "The role of aldehyde dehydrogenase (ALDH) in cancer drug resistance," *Biomedicine and Pharmacotherapy*, vol. 67, no. 7, pp. 669–680, Sep. 2013, doi: 10.1016/j.biopha.2013.04.005.

[132] N. E. Sládek, R. Kollander, L. Sreerama, and D. T. Kiang, "Cellular levels of aldehyde dehydrogenases (ALDH1A1 and ALDH3A1) as predictors of therapeutic responses to cyclophosphamide-based chemotherapy of breast cancer: A retrospective study," *Cancer*

Chemother Pharmacol, vol. 49, no. 4, pp. 309–321, 2002, doi: 10.1007/s00280-001-0412-4.

[133] K. Honoki *et al.*, "Possible involvement of stem-like populations with elevated ALDH1 in sarcomas for chemotherapeutic drug resistance," *Oncol Rep*, vol. 24, no. 2, pp. 501–505, 2010, doi: 10.3892/or_00000885.

[134] G. Vassalli, "Aldehyde dehydrogenases: Not just markers, but functional regulators of stem cells," *Stem Cells Int*, vol. 2019, 2019, doi: 10.1155/2019/3904645.

[135] L. Prasmickaite *et al.*, "Aldehyde dehydrogenase (ALDH) activity does not select for cells with enhanced aggressive properties in malignant melanoma," *PLoS One*, vol. 5, no. 5, 2010, doi: 10.1371/journal.pone.0010731.

[136] A. Schäfer *et al.*, "Aldehyde dehydrogenase 1A1-a new mediator of resistance to temozolomide in glioblastoma," *Neuro Oncol*, vol. 14, no. 12, pp. 1452–1464, Dec. 2012, doi: 10.1093/neuonc/nos270.

[137] W. Wu, J. Schecker, S. Würstle, F. Schneider, M. Schönfelder, and J. Schlegel, "Aldehyde dehydrogenase 1A3 (ALDH1A3) is regulated by autophagy in human glioblastoma cells," *Cancer Lett*, vol. 417, pp. 112–123, Mar. 2018, doi: 10.1016/j.canlet.2017.12.036.

[138] W. Wu *et al.*, "Lipid Peroxidation Plays an Important Role in Chemotherapeutic Effects of Temozolomide and the Development of Therapy Resistance in Human Glioblastoma," *Transl Oncol*, vol. 13, no. 3, Mar. 2020, doi: 10.1016/j.tranon.2020.100748.

[139] B. Aramini and V. Masciale, "Editorial: Aldehyde dehydrogenase in clinical settings: Potential biomarker and therapeutic target in solid tumors," *Front Med (Lausanne)*, vol. 9, Oct. 2023, doi: 10.3390/biom11101423.

[140] A. Tanaka and S. Sakaguchi, "Regulatory T cells in cancer immunotherapy," *Cell Res*, vol. 27, no. 1, pp. 109–118, Jan. 2017, doi: 10.1038/cr.2016.151.

[141] F. Bayati, M. Mohammadi, M. Valadi, S. Jamshidi, A. M. Foma, and E. Sharif-Paghaleh, "The Therapeutic Potential of Regulatory T Cells: Challenges and Opportunities," *Front Immunol*, vol. 11, Jan. 2021, doi: 10.3389/fimmu.2020.585819.

[142] S. S. Dinavahi, C. G. Bazewicz, R. Gowda, and G. P. Robertson, "Aldehyde Dehydrogenase Inhibitors for Cancer Therapeutics," *Trends Pharmacol Sci*, vol. 40, no. 10, pp. 774–789, Oct. 2019, doi: 10.1016/j.tips.2019.08.002.

[143] C. G. Bazewicz, S. S. Dinavahi, T. D. Schell, and G. P. Robertson, "Aldehyde dehydrogenase in regulatory T-cell development, immunity and cancer," *Immunology*, vol. 156, no. 1, pp. 47–55, Jan. 2019, doi: 10.1111/imm.13016.

[144] K. C. Galvin *et al.*, "Blocking retinoic acid receptor-α enhances the efficacy of a dendritic cell vaccine against tumours by suppressing the induction of regulatory T cells," *Cancer Immunology, Immunotherapy*, vol. 62, no. 7, pp. 1273–1282, Jul. 2013, doi: 10.1007/s00262-013-1432-8.

[145] P. Mao *et al.*, "Mesenchymal glioma stem cells are maintained by activated glycolytic metabolism involving aldehyde dehydrogenase 1A3," *Proc Natl Acad Sci U S A*, vol. 110, no. 21, pp. 8644–8649, May 2013, doi: 10.1073/pnas.1221478110.

[146] C. Gan *et al.*, "The predominant expression of cancer stem cell marker ALDH1A3 in tumor infiltrative area is associated with shorter overall survival of human glioblastoma," *BMC Cancer*, vol. 20, no. 1, Jul. 2020, doi: 10.1186/s12885-020-07153-0.

[147] T. Vasilogiannakopoulou, C. Piperi, and A. G. Papavassiliou, "Impact of Aldehyde Dehydrogenase Activity on Gliomas," *Trends Pharmacol Sci*, vol. 39, no. 7, pp. 605–609, Jul. 2018, doi: 10.1016/j.tips.2018.04.001.

[148] I. Nakano, "Stem cell signature in glioblastoma: Therapeutic development for a moving target," *J Neurosurg*, vol. 122, no. 2, pp. 324–330, Feb. 2015, doi: 10.3171/2014.9.JNS132253.

[149] K. Ganser *et al.*, "Patient-individual phenotypes of glioblastoma stem cells are conserved in culture and associate with radioresistance, brain infiltration and patient prognosis," *Int J Cancer*, vol. 150, no. 10, pp. 1722–1733, May 2022, doi: 10.1002/ijc.33950.

[150] P. Cheng *et al.*, "FOXD1-ALDH1A3 signaling is a determinant for the self-renewal and tumorigenicity of mesenchymal glioma stem cells," *Cancer Res*, vol. 76, no. 24, pp. 7219–7230, Dec. 2016, doi: 10.1158/0008-5472.CAN-15-2860.

[151] Z. Chen *et al.*, "USP9X deubiquitinates ALDH1A3 and maintains mesenchymal identity in glioblastoma stem cells," *Journal of Clinical Investigation*, vol. 129, no. 5, pp. 2043–2055, May 2019, doi: 10.1172/JCI126414.

[152] K. E. Sullivan, K. Rojas, R. A. Cerione, I. Nakano, and K. F. Wilson, "The stem cell/cancer stem cell marker ALDH1A3 regulates the expression of the survival factor tissue transglutaminase, in mesenchymal glioma stem cells," *Oncotarget*, vol. 8, no. 14, pp. 22325–22343, 2017, [Online]. Available: www.impactjournals.com/oncotarget

[153] M. V. Liberti and J. W. Locasale, "The Warburg Effect: How Does it Benefit Cancer Cells?," *Trends Biochem Sci*, vol. 41, no. 3, pp. 211–218, Mar. 2016, doi: 10.1016/j.tibs.2015.12.001.

[154] M. E. McLean *et al.*, "The Expanding Role of Cancer Stem Cell Marker ALDH1A3 in Cancer and Beyond," *Cancers (Basel)*, vol. 15, no. 2, p. 492, Jan. 2023, doi: 10.3390/cancers15020492.

[155] G. Li *et al.*, "ALDH1A3 induces mesenchymal differentiation and serves as a predictor for survival in glioblastoma," *Cell Death Dis*, vol. 9, no. 12, Dec. 2018, doi: 10.1038/s41419-018-1232-3.

[156] J. Branter, S. Basu, and S. Smith, "Tumour treating fields in a combinational therapeutic approach," *Oncotarget*, vol. 9, no. 93, pp. 36631–36644, 2018, [Online]. Available: www.oncotarget.com

[157] R. Stupp *et al.*, "Maintenance therapy with tumor-Treating fields plus temozolomide vs temozolomide alone for glioblastoma a randomized clinical trial," *J Am Med Assoc*, vol. 314, no. 23, pp. 2535–2543, Dec. 2015, doi: 10.1001/jama.2015.16669.

[158] B. Huang, X. Li, Y. Li, J. Zhang, Z. Zong, and H. Zhang, "Current Immunotherapies for Glioblastoma Multiforme," *Front Immunol*, vol. 11, Mar. 2021, doi: 10.3389/fimmu.2020.603911.

[159] I. Khan, S. Mahfooz, E. B. Elbasan, B. Karacam, M. N. Oztanir, and M. A. Hatiboglu, "Targeting Glioblastoma: The Current State of Different Therapeutic Approaches," *Curr Neuropharmacol*, vol. 19, no. 10, pp. 1701–1715, Jan. 2021, doi: 10.2174/1570159x19666210113152108.

[160] W. Huang, Z. Hao, F. Mao, and D. Guo, "Small Molecule Inhibitors in Adult High-Grade Glioma: From the Past to the Future," *Front Oncol*, vol. 12, Jun. 2022, doi: 10.3389/fonc.2022.911876.

[161] H. Liu *et al.*, "Therapeutic strategies of glioblastoma (GBM): The current advances in the molecular targets and bioactive small molecule compounds," *Acta Pharm Sin B*, vol. 12, no. 4, pp. 1781–1804, Apr. 2022, doi: 10.1016/j.apsb.2021.12.019.

[162] A.-S. Sevastre *et al.*, "Glioblastoma pharmacotherapy: A multifaceted perspective of conventional and emerging treatments (Review)," *Exp Ther Med*, vol. 22, no. 6, Oct. 2021, doi: 10.3892/etm.2021.10844.

[163] R. B. Kargbo, "Discovery of Selective Aldehyde Dehydrogenase Inhibitors for the Treatment of Cancer," *ACS Med Chem Lett*, Feb. 2023, doi: 10.1021/acsmedchemlett.2c00543.

[164] C. A. Morgan and T. D. Hurley, "Development of a high-throughput in vitro assay to identify selective inhibitors for human ALDH1A1," *Chem Biol Interact*, vol. 234, pp. 29–37, Jun. 2015, doi: 10.1016/j.cbi.2014.10.028.

[165] M. L. Thomas *et al.*, "Citral reduces breast tumor growth by inhibiting the cancer stem cell marker ALDH1A3," *Mol Oncol*, vol. 10, no. 9, pp. 1485–1496, Nov. 2016, doi: 10.1016/j.molonc.2016.08.004.

[166] R. Bista, D. W. Lee, O. B. Pepper, D. O. Azorsa, R. J. Arceci, and E. Aleem, "Disulfiram overcomes bortezomib and cytarabine resistance in Down-syndrome-associated acute myeloid leukemia cells," *Journal of Experimental and Clinical Cancer Research*, vol. 36, no. 1, pp. 1–14, Feb. 2017, doi: 10.1186/s13046-017-0493-5.

[167] G. K. Rekha and N. E. Sladek, "Inhibition of human class 3 aldehyde dehydrogenase, and sensitization of tumor cells that express significant amounts of this enzyme to oxazaphosphorines, by the naturally occurring compound gossypol," *Adv Exp Med Biol*, vol. 414, pp. 133–146, 1996.

[168] G. Fournet, G. Martin, and G. Quash, "α,β-Acetylenic Amino Thiolester Inhibitors of Aldehyde Dehydrogenases 1&3: Suppressors of Apoptogenic Aldehyde Oxidation and Activators of Apoptosis," *Curr Med Chem*, vol. 20, pp. 527–533, 2013.

[169] M. Khanna *et al.*, "Discovery of a novel class of covalent inhibitor for aldehyde dehydrogenases," *Journal of Biological Chemistry*, vol. 286, no. 50, pp. 43486–43494, Dec. 2011, doi: 10.1074/jbc.M111.293597.

[170] J. Kim *et al.*, "Targeting aldehyde dehydrogenase activity in head and neck squamous cell carcinoma with a novel small molecule inhibitor," *Oncotarget*, vol. 8, no. 32, pp. 52345–52356, 2017, [Online]. Available: www.impactjournals.com/oncotarget/

[171] A. I. M. Ibrahim *et al.*, "Expansion of the 4-(Diethylamino)benzaldehyde Scaffold to Explore the Impact on Aldehyde Dehydrogenase Activity and Antiproliferative Activity in

Prostate Cancer," *J Med Chem*, vol. 65, no. 5, pp. 3833–3848, Mar. 2022, doi: 10.1021/acs.jmedchem.1c01367.

[172] B. C. Huddle *et al.*, "Structure-Based Optimization of a Novel Class of Aldehyde Dehydrogenase 1A (ALDH1A) Subfamily-Selective Inhibitors as Potential Adjuncts to Ovarian Cancer Chemotherapy," *J Med Chem*, vol. 61, no. 19, pp. 8754–8773, Oct. 2018, doi: 10.1021/acs.jmedchem.8b00930.

[173] Z. Omran, "Novel Disulfiram Derivatives as ALDH1a1-Selective Inhibitors," *Molecules*, vol. 27, no. 2, Jan. 2022, doi: 10.3390/molecules27020480.

[174] S. M. Yang *et al.*, "Discovery of Orally Bioavailable, Quinoline-Based Aldehyde Dehydrogenase 1A1 (ALDH1A1) Inhibitors with Potent Cellular Activity," *J Med Chem*, vol. 61, no. 11, pp. 4883–4903, Jun. 2018, doi: 10.1021/acs.jmedchem.8b00270.

[175] D. H. Overstreet, D. J. Knapp, G. R. Breese, and I. Diamond, "A selective ALDH-2 inhibitor reduces anxiety in rats," *Pharmacol Biochem Behav*, vol. 94, no. 2, pp. 255–261, Dec. 2009, doi: 10.1016/j.pbb.2009.09.004.

[176] B. Wang, C. D. Buchman, L. Li, T. D. Hurley, and S. O. Meroueh, "Enrichment of chemical libraries docked to protein conformational ensembles and application to aldehyde dehydrogenase 2," *J Chem Inf Model*, vol. 54, no. 7, pp. 2105–2116, Jul. 2014, doi: 10.1021/ci5002026.

[177] B. Parajuli, M. L. Fishel, and T. D. Hurley, "Selective ALDH3A1 inhibition by benzimidazole analogues increase mafosfamide sensitivity in cancer cells," *J Med Chem*, vol. 57, no. 2, pp. 449–461, Jan. 2014, doi: 10.1021/jm401508p.

[178] B. Parajuli, T. M. Georgiadis, M. L. Fishel, and T. D. Hurley, "Development of selective inhibitors for human aldehyde dehydrogenase 3A1 (ALDH3A1) for the enhancement of cyclophosphamide cytotoxicity," *ChemBioChem*, vol. 15, no. 5, pp. 701–712, Mar. 2014, doi: 10.1002/cbic.201300625.

[179] E. L. M. Gelardi *et al.*, "A selective competitive inhibitor of aldehyde dehydrogenase 1A3 hinders cancer cell growth, invasiveness and stemness in vitro," *Cancers (Basel)*, vol. 13, no. 2, pp. 1–20, Jan. 2021, doi: 10.3390/cancers13020356.

[180] E. L. M. Gelardi *et al.*, "Curcumin-based-fluorescent probes targeting ALDH1A3 as a promising tool for glioblastoma precision surgery and early diagnosis," *Commun Biol*, vol. 5, no. 1, Dec. 2022, doi: 10.1038/s42003-022-03834-7.

[181] J. Li *et al.*, "A specific inhibitor of ALDH1A3 regulates retinoic acid biosynthesis in glioma stem cells," *Commun Biol*, vol. 4, no. 1, Dec. 2021, doi: 10.1038/s42003-021-02949-7.

[182] L. Quattrini *et al.*, "Imidazo[1,2- a]pyridine derivatives as aldehyde dehydrogenase inhibitors: Novel chemotypes to target glioblastoma stem cells," *J Med Chem*, vol. 63, no. 9, pp. 4603–4616, May 2020, doi: 10.1021/acs.jmedchem.9b01910.

[183] J. Park *et al.*, "Regulation of bioenergetics through dual inhibition of aldehyde dehydrogenase and mitochondrial complex i suppresses glioblastoma tumorspheres," *Neuro Oncol*, vol. 20, no. 7, pp. 954–965, Jun. 2018, doi: 10.1093/neuonc/nox243.

[184] H. H. Park *et al.*, "Combinatorial therapeutic effect of inhibitors of aldehyde dehydrogenase and mitochondrial complex i, and the chemotherapeutic drug,

temozolomide against glioblastoma tumorspheres," *Molecules*, vol. 26, no. 2, Jan. 2021, doi: 10.3390/molecules26020282.

[185] G. Venton *et al.*, "Aldehyde dehydrogenases inhibition eradicates leukemia stem cells while sparing normal progenitors," *Blood Cancer J*, vol. 6, no. 9, 2016, doi: 10.1038/BCJ.2016.78.

[186] M. Pérez-Alea *et al.*, "ALDH1A3 is epigenetically regulated during melanocyte transformation and is a target for melanoma treatment," *Oncogene*, vol. 36, no. 41, pp. 5695–5708, Oct. 2017, doi: 10.1038/onc.2017.160.

[187] R. Rebollido-Rios *et al.*, "Dual disruption of aldehyde dehydrogenases 1 and 3 promotes functional changes in the glutathione redox system and enhances chemosensitivity in nonsmall cell lung cancer," *Oncogene*, vol. 39, no. 13, pp. 2756–2771, Mar. 2020, doi: 10.1038/s41388-020-1184-9.

[188] A. Barzegar Behrooz, Z. Talaie, and A. Syahir, "Nanotechnology-Based Combinatorial Anti-Glioblastoma Therapies: Moving from Terminal to Treatable," *Pharmaceutics*, vol. 14, no. 8, Aug. 2022, doi: 10.3390/pharmaceutics14081697.

[189] D. Petrenko *et al.*, "Temozolomide Efficacy and Metabolism: The Implicit Relevance of Nanoscale Delivery Systems†," *Molecules*, vol. 27, no. 11, Jun. 2022, doi: 10.3390/molecules27113507.

[190] N. Nordin *et al.*, "In vitro cytotoxicity and anticancer effects of citral nanostructured lipid carrier on MDA MBA-231 human breast cancer cells," *Sci Rep*, vol. 9, no. 1, Dec. 2019, doi: 10.1038/s41598-018-38214-x.

[191] H. Fasehee, A. Ghavamzadeh, K. Alimoghaddam, S.-H. Ghaffari, and S. Faghihi, "A Comparative Cytotoxic Evaluation of Disulfiram Encapsulated PLGA Nanoparticles on MCF-7 Cells," *Int J Hematol Oncol Stem Cell Res*, vol. 5, no. 2, 2017.

[192] G. Martin, A. Gaudin, and M. A. Irujo Gallardo, "Nanocapsule lipidique comprenant au moins un composé aminothiolester ou un de ses dérivés pharmaceutiquement acceptable," 2022.

[193] S. Gurunathan, M. H. Kang, M. Qasim, and J. H. Kim, "Nanoparticle-mediated combination therapy: Two-in-one approach for cancer," *Int J Mol Sci*, vol. 19, no. 10, Oct. 2018, doi: 10.3390/ijms19103264.

[194] N. Montegiove, E. Calzoni, C. Emiliani, and A. Cesaretti, "Biopolymer Nanoparticles for Nose-to-Brain Drug Delivery: A New Promising Approach for the Treatment of Neurological Diseases," *J Funct Biomater*, vol. 13, no. 3, Sep. 2022, doi: 10.3390/jfb13030125.

[195] F. A. Bruinsmann *et al.*, "Nasal drug delivery of anticancer drugs for the treatment of glioblastoma: Preclinical and clinical trials," *Molecules*, vol. 24, no. 23, Nov. 2019, doi: 10.3390/molecules24234312.

[196] S. Perriot *et al.*, "Human Induced Pluripotent Stem Cell-Derived Astrocytes Are Differentially Activated by Multiple Sclerosis-Associated Cytokines," *Stem Cell Reports*, vol. 11, no. 5, pp. 1199–1210, Nov. 2018, doi: 10.1016/j.stemcr.2018.09.015.

[197] A. Ianevski, L. He, T. Aittokallio, and J. Tang, “SynergyFinder: A web application for analyzing drug combination dose-response matrix data,” *Bioinformatics*, vol. 33, no. 15, pp. 2413–2415, Aug. 2017, doi: 10.1093/bioinformatics/btx162.

[198] C. I. Bliss, “The toxicity of poisons applied jointly,” *Annals of Applied Biology*, vol. 26, no. 3, pp. 585–615, 1939.

[199] S. Sołobodowska, J. Giebułtowicz, R. Wolinowska, and P. Wroczyński, “Contribution of ALDH1A1 isozyme to detoxification of aldehydes present in food products,” *Acta Pol Pharm*, vol. 69, no. 6, pp. 1380–1383, 2012.

[200] M. A. Kane, N. Chen, S. Sparks, and J. L. Napoli, “Quantification of endogenous retinoic acid in limited biological samples by LC/MS/MS,” *Biochemical Journal*, vol. 388, pp. 363–369, 2005.

[201] M. Domínguez *et al.*, “Synthesis of apocarotenoids by acyclic cross metathesis and characterization as substrates for human retinaldehyde dehydrogenases,” *Tetrahedron*, vol. 74, no. 21, pp. 2567–2574, May 2018, doi: 10.1016/j.tet.2018.03.050.

[202] R. Jiménez *et al.*, “Inhibitors of aldehyde dehydrogenases of the 1A subfamily as putative anticancer agents: Kinetic characterization and effect on human cancer cells,” *Chem Biol Interact*, vol. 306, pp. 123–130, Jun. 2019, doi: 10.1016/j.cbi.2019.04.004.

[203] R. G. Madane and H. S. Mahajan, “Curcumin-loaded nanostructured lipid carriers (NLCs) for nasal administration: design, characterization, and in vivo study,” *Drug Deliv*, vol. 23, no. 4, pp. 1326–1334, May 2016, doi: 10.3109/10717544.2014.975382.

[204] Y. Wu, H. Kram, J. Gempt, F. Liesche-Starnecker, W. Wu, and J. Schlegel, “ALDH1-Mediated Autophagy Sensitizes Glioblastoma Cells to Ferroptosis,” *Cells*, vol. 11, no. 24, Dec. 2022, doi: 10.3390/cells11244015.

[205] R. Pequerul, S. Porté, X. Parés, M. Pérez-Alea, and J. Farrés, “Production, Purification, and Fluorometric Activity Assay of Human Aldehyde Dehydrogenases,” *Bio Protoc*, vol. 12, no. 17, Sep. 2022, doi: 10.21769/BioProtoc.4505.

[206] J. D. Hayes and L. I. McLellan, “Glutathione and glutathione-dependent enzymes represent a co-ordinately regulated defence against oxidative stress,” *Free Radic Res*, vol. 31, no. 4, pp. 273–300, 1999, doi: 10.1080/10715769900300851.

[207] S. Wang *et al.*, “ALDH1A3 serves as a predictor for castration resistance in prostate cancer patients,” *BMC Cancer*, vol. 20, no. 1, May 2020, doi: 10.1186/s12885-020-06899-x.

[208] E. Grimley *et al.*, “Aldehyde dehydrogenase inhibitors promote DNA damage in ovarian cancer and synergize with ATM/ATR inhibitors,” *Theranostics*, vol. 11, no. 8, pp. 3540–3551, 2021, doi: 10.7150/THNO.51885.

[209] J. W. Park, K.-H. Jung, J. H. Lee, S. H. Moon, Y. S. Cho, and K.-H. Lee, “Inhibition of aldehyde dehydrogenase 1 enhances the cytotoxic effect of retinaldehyde on A549 cancer cells,” *Oncotarget*, vol. 8, no. 59, pp. 99382–99393, 2017, [Online]. Available: www.impactjournals.com/oncotarget

[210] J. L. Blaize *et al.*, “Differential Regulation of Retinoic Acid Metabolism in Fanconi Anemia,” *bioRxiv [Preprint]*, 2023, doi: 10.1101/2023.04.06.535759.

[211] D. E. Morales and S. Mousa, “Intranasal delivery in glioblastoma treatment: prospective molecular treatment modalities,” *Heliyon*, vol. 8, no. 5, May 2022, doi: 10.1016/j.heliyon.2022.e09517.

[212] H. Nsairat *et al.*, “Lipid nanostructures for targeting brain cancer,” *Heliyon*, vol. 7, no. 9, Sep. 2021, doi: 10.1016/j.heliyon.2021.e07994.

[213] W. Alshaer *et al.*, “Encapsulation of echinomycin in cyclodextrin inclusion complexes into liposomes:: In vitro anti-proliferative and anti-invasive activity in glioblastoma,” *RSC Adv*, vol. 9, no. 53, pp. 30976–30988, 2019, doi: 10.1039/c9ra05636j.

[214] P. P. Deshpande, S. Biswas, and V. P. Torchilin, “Current trends in the use of liposomes for tumor targeting,” *Nanomedicine*, vol. 8, no. 9, pp. 1509–1528, 2013, doi: 10.2217/nnm.13.118.

ANNEX

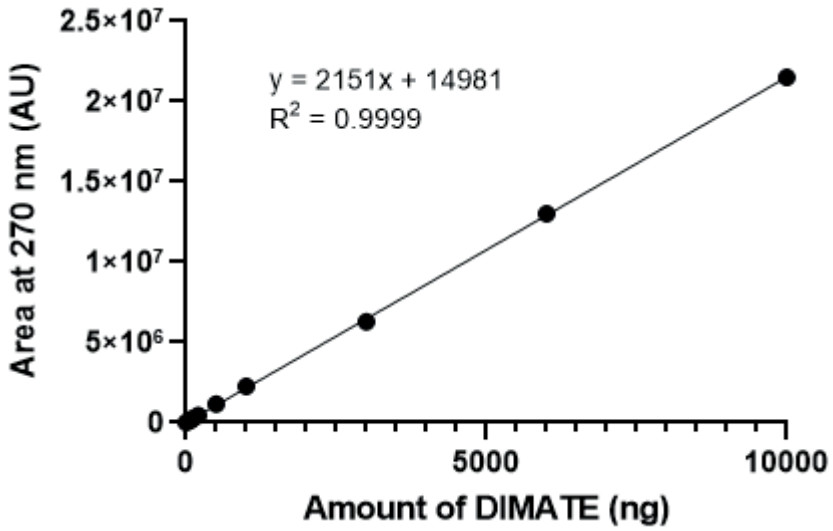

Annex 1.1. Calibration curve for DIMATE analyzed by HPLC. Peak areas at 270 nm were plotted against twelve different amounts of DIMATE. Experimental values were fit to a simple linear regression using GraphPad software. AU: absorbance units.

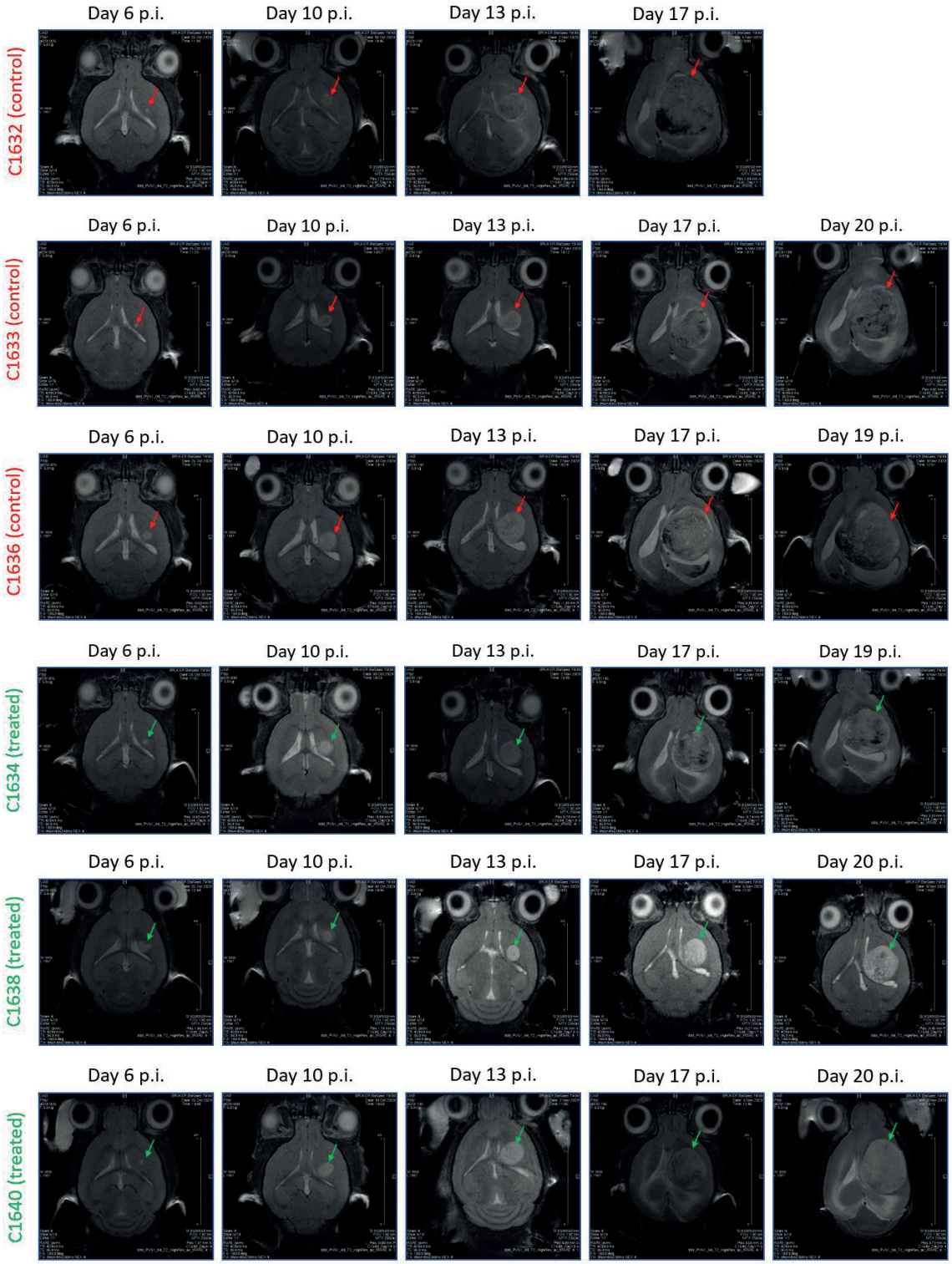

Annex 1.2. MRI of the tumors of GB-bearing mice during the therapeutic efficacy assay with 5 mg/kg ABD-3001. Mice C1632, C1633, and C1636, belonging to the control group (**red**), were treated with 5 mg/kg ABD-3000, whereas mice C1634, C1638, and C1640, belonging to the treated group (**green**), were treated with 5 mg/kg ABD-3001. Arrows point at the tumor. Day p.i.: day post-implantation.

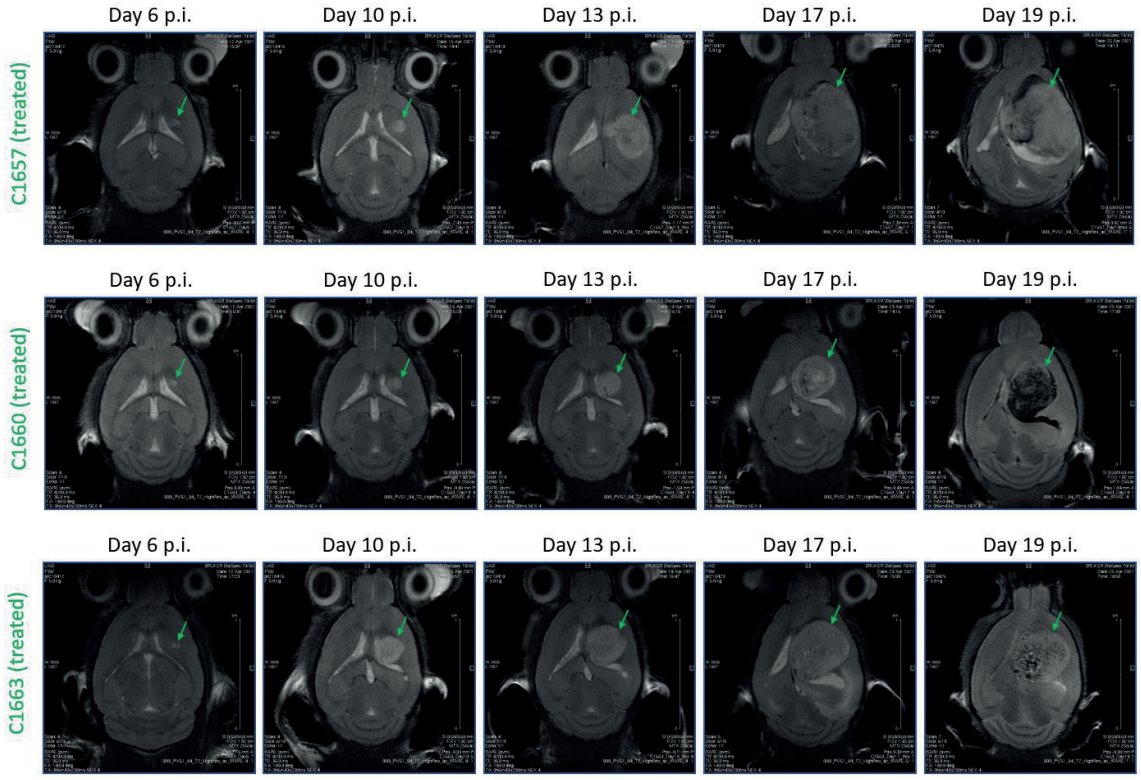

Annex 1.3. MRI of the tumors of GB-bearing mice during the therapeutic efficacy assay with 2.5 mg/kg ABD-3001. Mice C1657, C1660, and C1663, belonging to the treated group, were treated with 2.5 mg/kg ABD-3001. Arrows point at the tumor. Day p.i.: day post-implantation.